공학박사 학위논문

Conversion of biomass-derived feedstocks to chemicals over heterogeneous catalyst supported on 3D porous structure

3차원 다공성 구조에 담지된 불균일계 촉매를 이용한 바이오매스 유래 원료로부터 화합물질 생산기술

2014년 8월

서울대학교 대학원

화학생물공학부

에너지환경화학융합기술전공

박대성

Abstract

Conversion of biomass-derived feedstocks to chemicals over heterogeneous catalyst supported on 3D porous structure

Dae Sung Park

Chemical Convergence for Energy and Environment

School of Chemical and Biological Engineering

The Graduate School

Seoul National University

Biomass can be an alternative energy source to fossil fuels, because it can serve as a sustainable and renewable carbon source which can be converted to fuels and chemicals. Biomass is very abundant source, and its energy production can reduce the emissions of CO_2 gas compared to the use of fossil fuels. The catalytic processing of biomass derived feedstocks is similar with the catalytic reaction of petroleum feedstocks. However, the different contents and properties of the compounds in biomass comparing with fossil fuels require to develope the newly designed solid catalysts. In this study, the three-dimensionally opened porous material is suggested to one of the good candidate catalysts which is widely appicable in the conversion of biomass derived feedstocks. The effect of 3D structured-catalyst on the conversion of biomass is deeply demonstrated through several reactions, such as dehydration in gas- and liquid phase, and hydrolytic hydrogenations in three

parts. Firstly, the advantage of the 3D carbon material on the deactivation by coking is discussed in gas-phase dehydration of glycerol. Secondly, the enhancement of mass transfer on the 3D porous catalyst is quantitatively calculated by kinetic study for liquid-phase dehydration of n-butanol to di-n-butyl ether. Finally, the accessibility of the large molecules to the catalyst is discussed by the hydrolytic hydrogenation of lignocellulose over Pt supported on 3D mesoporous carbon. Details are as follows:

Supported heteropoly acid catalysts are frequently employed in the dehydration of glycerol to acrolein because of their high activity. However, they are easily deactivated by coke that can become deposited on the catalyst surface. We studied on a technique that significantly reduces coke formation by capturing coke precursors in a Pd lattice. The Pd-added $H_3PW_{12}O_{40}$/C catalyst (Pd-PWC) shows a stable catalytic activity and the amount of deposited coke is reduced to about 40 %, compared to catalysts without Pd addition. The results show that the palladium lattice on the carbon support is easily loosened, and coking precursors are incorporated into the Pd lattice under the reaction conditions employed. Moreover, on the developed 3D open porous catalyst, the pore plugging by coke is significantly reduced inside the pores, resulting in enhancing the catalytic stability.

The production of di-n-butyl-ether (DNBE), for use as a blending agent in diesel fuel, is very attractive because the n-butanol can be readily produced by the fermentation of bio-derivatives. The dehydration of n-butanol is known to show diffusion-limited characteristics on porous catalysts, such as zeolites or mesoporous supported catalysts. In order to overcome this limitation, we synthesized 3D open porous catalyst. The quantitative values are calculated by kinetic study to investigate the effect of 3D pore structures on the mass transfer limitation reaction. The catalyst shows the best performance among the catalysts (2D and 1D porous catalysts) at various temperatures (453, 473, and 493 K). The extent of catalytic performance enhancement is quantified by

calculating the effectiveness factor (η) based on kinetics data. The η values for PW/ESS, PW/SBA, and PW/mi-S are determined to be 0.83, 0.63 and 0.52, respectively.

The conversion of lignocellulose is a crucial topic. However, the fact that cellulose consisted of lignocellulose being not soluble in polar solvents makes it difficult to convert into value-added chemicals. A strategy to overcome this drawback is the use of mesoporous carbon which enhances the affinity between the cellulose and the catalyst through its abundant functional groups and large uniform pores. The 3D mesoporous carbon (CNE) is developed, inspired by an Echinometra Mathae to enhance the interaction between the catalyst and the non-soluble reactant. In the hydrolytic hydrogenation of cellulose, abundant oxygen groups of CNE facilitate the access of cellulose to the surface of the catalyst and the open pore structure permits cello-oligomers to effectively diffuse to the active sites inside the pore. The highly dispersed Pt performs dual roles of hydrolysis by in-situ generating protons from H_2 or water as well as effective hydrogenation. The Pt/CNE catalyst shows a 80 % yield of hexitol, which is the best performance reported to date. In direct conversion of hardwood powder, the Pt/CNE also shows the good performance to produce the sugar alcohols (23 % yield).

Keywords: Three-dimensional porous materials, glycerol, lignocelluloses, platinum, heteropoly acid, mass transfer

Student Number: 2010-30805

Contents

List of Tables

List of Figures

Chapter 1. Introduction

1.1 Biomass for alternative source to fossil fuels

The fossil fuels such as oil, coal, and natural gas have been supplied to the various industries as an energy source to convert liquid fuels or chemicals. It provides above 70 % of the world's energy source [1]. Unfortunately, the reserves of fossil fuels are progressively diminished, and they bring about the environmental problems such as global warming and pollution [2]. In this respect, biomass can serve a sustainable and renewable energy source for carbon which can be used to fuels and chemicals [3-7]. Biomass is very abundant source containing in, e.g., corn stover, starch, grasses, wood, vegetable oil, etc. Moreover, energy production from biomass can reduce greenhouse gas emissions compared to the use of fossil fuels, because the produced carbon dioxide can be consumed during regrowth of biomass (Figure 1-1) [8-9].

The resources from biomass is classified to three groups as follows; woody biomass (lignocellulose), amorphous sugars (starch and glucose), and triglycerides (vegetable oil). These feedstocks, compared to the hydrocarbons from fossil fuels, have quite different properties, such as low volatility, high oxygen to carbon ratio, and large molecular size and weight. Therefore, the challenging point for biomass conversion is how to remove oxygen from the feedstocks for high energy efficiency [10-12]. In this respect, it is very important to develop the novel-structured catalysts which have the ability of removing oxygen and accessibility of the large molecules

in a reaction medium, such as water and organic solvent.

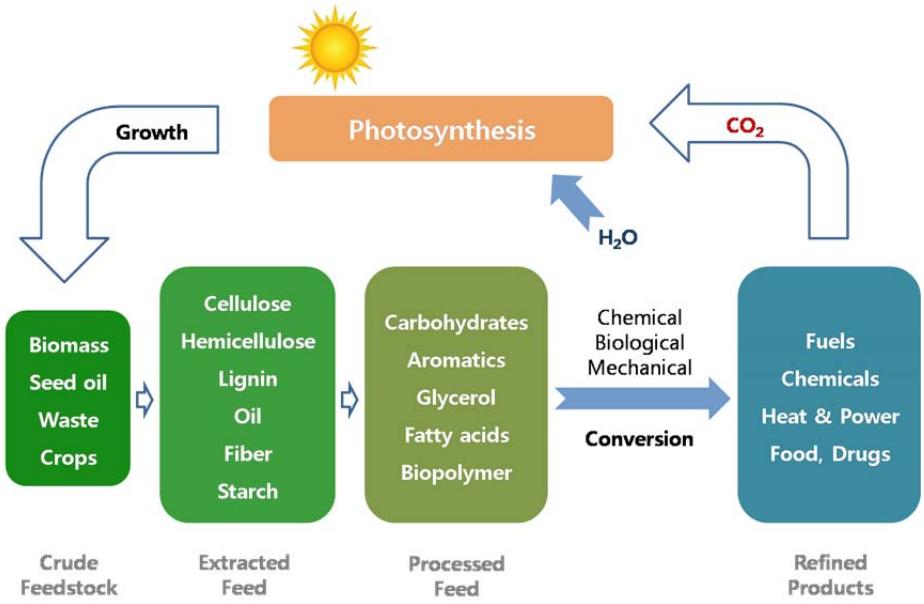

Figure 1-1. Processing of the biomass feedstocks to fuels and chemicals in a sustainable energy production. Adapted from Chheda *et al* [9].

1.2 Catalytic processing in biomass conversion

It is possible to produce a various value-added chemicals from biomass-derived feedstocks via catalytic reaction as shown in Figure 1-2. The conversion of biomas-derived feedstocks to valuable chemicals is occurred by the sequential and/or coupling of various reactions, such as dehydration, hydrolysis, reforming, hydrogenolysis, hydrogenation, aldol condensation, isomerization, and selective oxidation. Generally, the various reactions occur at different reaction conditions, temperature and pressure, compared to the conversion of petroleum feedstocks [13-18]. Figure 1-3 shows a diagram of reaction conditions for the catalytic conversion of petroleum and biomass-derived feedstocks [9]. Petroleum processes are converted at temperatures higher than 673 K in vapor phase, however, the biomass-derived feedstocks are treated at lower temperature in the mainly liquid phase. This is due to the thermal stability of the biomass-derived compounds is lower than that of petroleum compounds. The different reaction conditions and characteristics of the compounds from biomass-derived feedstocks lead to requirement a new designed solid catalyst that is not applicable for petroleum conversion by catalytic reaction. It is known that the homogeneous catalysts and enzymes are not suitable for the processing of bio-derived feedstocks [19-21].

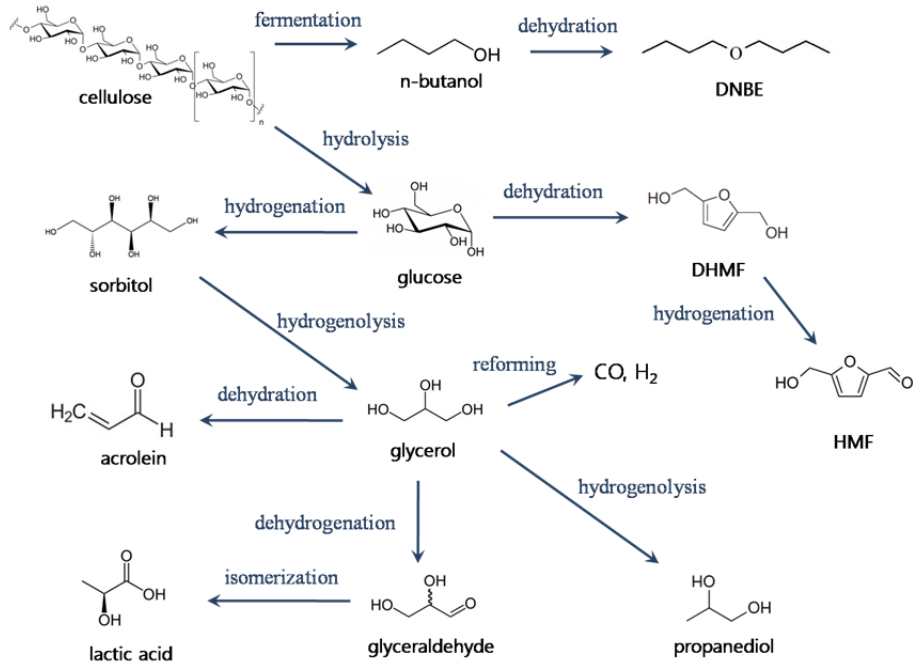

Figure 1-2. Reaction routes for the production of value-added chemicals from the conversion of biomass-derived feedstocks.

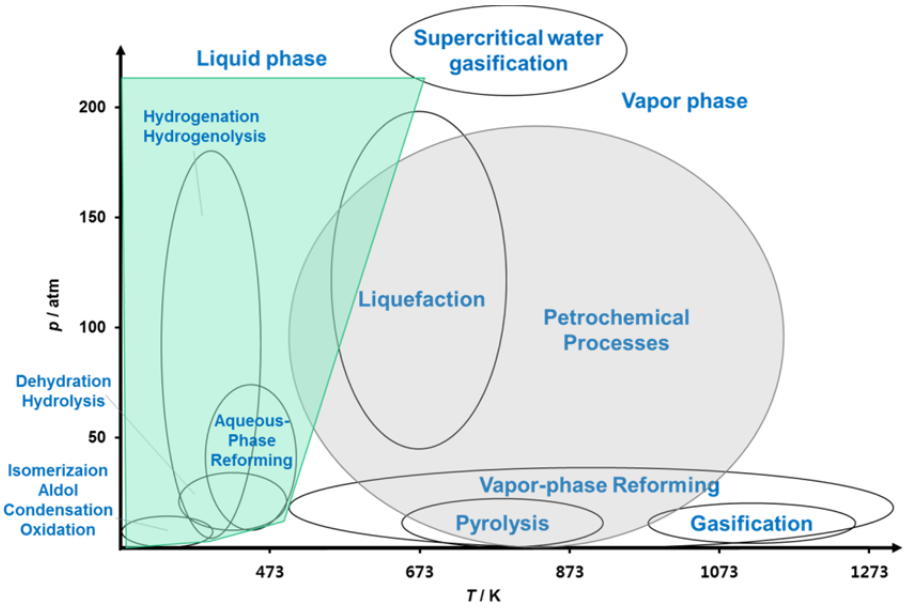

Figure 1-3. Diagram of approximate reaction conditions for the catalytic processing of petroleum versus biomass-derived carbohydrates. Adapted from Chheda *et al* [9].

1.3 Design of solid catalysts for biomass conversion

As mentioned above, the conversion of biomass-derived chemicals is required a special solid catalysts. Owing to the structural and chemical properties, the solid catalyst should be prepared with considering of accessiblitity in novel reaction media and porosity of the catalyst.

The biomass is essential polymeric structure, resulting in less solubility in most polar solvents. Mostly the derived feedstocks have relatively large molecular unit. A less soluble and large molcular reactant brings out a difficulty of accessibility to the catalyst [22]. To improve this problem, several researchers used an ionic solvent or homogeneous catalyst during a reaction. However, the use of ionic liquids cause a production of pollutant chemicals, and the use of homogeneous catalyst have a disadvantage of high cost cased by additional separation process [23-29]. Therefore, the solid catalyst should be prepared for enhancing the acceccibility of less soluble and large molcular reactant in reaction medium. In addition, the catalyst should be resistant to the excess water in the condition of biomass conversion.

The porosity is one of the important factors of solid catalysts for the conversion of biomass. The porous catalyst is necessary to synthesize with high surface area and uniform size of pores. It is known that the active sites are existed inside the pores in porous catalysts [30]. In this respect, the molecular dimensions of the biomass-derived feedstocks have to consider in preparation of the porous catalyst. The various compounds of biomass have large molecular dimensions. For example, beta-glucose has a length of 0.58 nm, and branched or long-chain building blocks are larger than glucose

monomer [31]. Thus, the meso- and macro-sized pores are required for efficient accessibility of reactant to active sites inside the pores [32-38].

In these regards, the carbon materials are very useful for developing a novel catalyst. Carbon is highly resistant to water medium and provides high surface area with low cost. The pore structure of the mesoporous carbon is easily controlled by various synthetic methods [39-41]. Moreover, recently, the abundant hydroxyl groups on the carbon enhance the affinity of the bio-derived molecules by excess electron from pi interaction with the linked-oxygen groups. In this study, for design a novel catalyst in biomass conversion, the carbon material is used for the support of catalysts. Additionally, several challenging points in conversion of various biomass-derived feedstocks are improved with a designed 3D mesoporous materials.

1.4 Target reactions over 3D structured catlayst

1.4.1 Dehydration of glycerol to acrolein

Among the various catalytic reactions, in this study, dehydration and sequential hydrolysis – hydrogenation reactions are investigated to show the effect of the 3D porous materials on the conversion of various biomass-derived feedstocks. Dehydration is an important reaction in the field of sugar and polyol chemistry. This is a typical reaction which reduces the O/C ratio in biomass-derived feedstocks. Among them, the glycerol, propanetriol, is an important bio-derived chemical selected for one of the top 12 biomass-derived building blocks. It can be used as a feedstock to produce various value-added chemicals, such as acrolein, propylene glycol, and syn gas by dehydration, hydrogenolysis, and reforming [42,43]. By transesterification of vegetable oil with methanol, the biodiesel is produced, and 10 wt% of glycerol is also simultaneously produced as a byproduct. As increasing the use of biodiesel, the production of glycerol is on the increase, resulting in diminish of the price of glycerol [44]. Therefore, the production of value-added chemicals from glycerol by catalytic process is a challengeble process in biomass industry. Among the possible transformation of glycerol, dehydration of glycerol to acrolein is one of the most vigorously researched reactions. Acrolein can be used for an intermediate to the production of acrylic acid and polyesters, and directly used for the feedstocks in cosmetic, solvent, and agricultural industries [45-47]. Although the dehydration of glycerol to acrolein has been deeply studied in previous reports, the problem of severe deactivation by coking is still for the challenging point.

1.4.2 Hydrolytic hydrogenation of lignocellulose to sugar alcohols

Lignocellulose is the most abount source of biomass, contained in wood, grasses, and plants. Lignocellulose is composed of cellulose, hemicelluloses, and lignin. Among them, cellulose is a major component containing about 50 %, and it is composed of numerous beta-glucose by beta-1,4-glycosidic and hydrogen bonds. The production of glucose from the hydrolysis of cellulose is a primary step to produce the various value-added chemicals or building blocks by sequential reaction [9]. Unfortunatly, cellulose is not soluble in most solvents, and very large moluclar due to polymerized units. It should be noted that the hydrolysis of cellulose is hardly reacted on conventional solid acid catalyst, such as zeolite, heteropolyacid, and aluminosilicate due to the low accessibility.

1.4.3 Dehydration of n-butanol to di-n-butyl ether

Dehydration of n-butanol to di-n-butyl ether (DNBE) is also an important process, because the DNBE has been used for a blending agent to improve the quality of the fuel. Recently, with increasing use of biodiesel, the linear ether, such as DNBE, is widely used to improve the fuel efficiency and to reduce the exhaust gases. From the fermentation of waste sources of biomass, the n-butanol can be produced easily [48-50]. The DNBE via dehydration of n-butanol is generally produced with high activity using a homogeneous catalyst, such as sulfuric acid, however the use of sulfuric acid results in the problems of reactor corrosion and production of toxious byproduct. And this reaction is well known be a mass transfer controlled reaction due to long-

chain molecules [51,52].

In these reactions, a new designed catalyst is required for the better catalytic performance. We suggests that the 3-dimensionally porous materials to improve the catalytic performance. Over the 3D porous catalysts, it is respected to reduce the deactivation problems by coking. Both the problems of the mass transfer limitation and accessibility can be improved by the using of the 3D porous catalyst.

1.5 Objectives

This thesis mainly focuses on the preparation of the 3D mesoporous catalysts which are widely applicable to the conversion of various biomass-derived feedstocks. The effect of 3D structured-catalyst on the conversion of biomass is deeply demonstrated through several reactions, such as dehydration in gas and liquid-phase, and hydrolytic hydrogenations.

At first, the advantage of the carbon material with 3D structure on the deactivation by coking is discussed in gas-phase dehydration of glycerol. Pd-C phase captured a coking in Pd lattice is introduced and the 3D porous carbon is developed to prevent the pore-plugging in Chapter 2.

Secondly, the accessibility of the large molecules to the catalyst is discussed by the hydrolytic hydrogenation of lignocellulose over Pt supported on 3D mesoporous carbon in Chapter 3. Through the sequential reactions of cellulose, the reaction pathway to produce the sugar alcohols from cellulose is demonstrated using developed 3D structured catalyst.

Finally, the enhancement of mass transfer on the 3D porous catalyst is quantitatively calculated by kinetic study for liquid-phase dehydration of n-butanol in Chapter 4. The effect of 3D opened-structure on diffusion limited reaction is investigated by calculation of effectiveness factor comparing with 1D and 2D porous catalysts.

Chapter 2. Development of the coke-resistant catalysts for the dehydration of glycerol to acrolein; Coke capturing by Pd-C phase & 3D mesoporous carbon

2.1 Introduction

The synthesis of value-added chemicals by the catalytic conversion of bio-sustainable resources is a challenging issue inchemistry. Among the derivative feedstocks that are from biomass, glycerol has attracted interest in recent years owing to its mass production as a byproduct of biodiesel. Glycerol can be converted into various value-added chemicals by using catalytic processes, such as hydrogenolysis, oxidation, esterification, and dehydration. In particular, the catalytic dehydration of glycerol into acrolein represents an important reaction in this field because acrolein is in the synthesis of various intermediates in the chemical and agricultural industries [46]. The preparation of acrolein from glycerol can be achieved by a two-step dehydration procedure using acid catalysts, such as sulfuric acid, zeolite, sulfated zirconia, and supported heteropolyacid catalysts. Homogeneous acid catalysts, such as sulfuric acid, have been widely used in dehydration reactions and have shown high activity. However, they are highly toxic, cause corrosionin reactors, and require proper disposal after use [53,54]. Therefore, the development of a solid-acid catalyst for the dehydration of

glycerol, which is based on the biomass-derived feedstock, is a challenging research area [46].

Solid-acid catalysts that have been developed until now all have the major drawback of catalytic deactivation owing to extensive coke deposition on the catalyst surface during the reaction, although they typically show a high initial yield. According to previous reports, most acid catalysts lead to the deposition of large amounts of coke onto the catalyst surface after only a few hours. Thus, this drawback must be overcome for applying these catalysts to industrial processes [47, 55-58]. It was reported that coke was produced as the result of the oligomerization of glycerol and the side-reactions between products, such as, acrolein, acetaldehyde, and acetol, and the polymerization of acrolein [59, 60]. Metal oxides that have acidic properties can convert the intermediate into undesired products through oxidation and hydrogenation side-reactions. Therefore, on solid-acid catalysts, it is difficult to decrease the considerable amounts of coke formed apart from decreasing the acidity of the catalyst. Alhanash et al. [61] prepared heteropoly caesium salts of platinum-group metals to investigate the inhibition of coke formation. They showed that a supply of hydrogen led to inhibition of the formation of unsaturated hydrocarbons, and coking was decreased after the reaction. However, this solution for decreasing the amount of deactivation required an additional supply of oxygen or hydrogen and the active sites were not preserved owing to the deposition of coke.

To further investigate the synthesis of coking-resistant catalysts for use in the dehydration of glycerol, herein, we report the preparation of a self-inclusive catalyst that was protected by palladium for capturing the coke precursors. Unlike previous reports,[62-64] this method allowed the catalytic

activity to be maintained against the deposition of coke by using palladium nanoparticles without the need for an additional gas flow. We also decreased the amount of coke that was deposited onto the catalyst surface without reducing the acidic sites. Palladiumis known to interact with elements, such as carbon, hydrogen, and oxygen, then produce new phases that result inthe expansion of the Pd lattice [65-67]. Previously, the incorporation of gas-phase carbon into palladium occurred on small sized metallic Pd (below 5 nm) by using heating processes, owing to the fcc structure. These results showed the formation of an interstitial solid solution of 13−15% carbon in Pd with a Pd-lattice expansion of 2.8 % [68, 69]. Importantly, the catalytic stability was increased in the case of a catalyst with the formula Pd-$H_3PW_{12}O_{40}$/C (Pd-PWC). To investigate the synergetic effects between Pd and the support, Pd-$H_3PW_{12}O_{40}$/SiO_2 (Pd-PWS) was investigated as a catalyst and the results were compared with a typical carbon-supported catalyst.

2.2 Experimental

2.2.1 Preparation of catalysts

The supported heteropoly acid catalysts were prepared by an impregnation method using 12 tungstophosphoric acid n-hydrate ($H_3PW_{12}O_{40} \cdot nH_2O$, Junsei Chemical Co. Ltd., GR). Tungstophosphoric acid (PW, 20 wt.%) was loaded onto two supports, one with activated carbon and one with aerosil 200 (SiO_2), in MeOH and deionized water, respectively. Palladium (1 wt.%) was added to the supported PW catalysts by the incipient wetness impregnation method by using palladium chloride (99 %, Aldrich) as the precursor. After drying at 80 ^oC for 12 h, the catalysts were obtained by calcination at 300 ^oC for 3 h and were heat-treated in-situ at 260 ^oC for 2 h in an atmosphere of hydrogen before the test reaction. The supported PWs on activated carbon and aerosil 200 were referred to as PWC and PWS, and the Pd-added catalysts as Pd-PWC and Pd-PWS, respectively.

In order to confirm the effect of 3D porous carbon on the deactivation of catalyst by coke, the various carbon materials were used for the support, such as, AC, CMK-3, and CNE (Carbon Nano Echinometra). The 3D carbon, CNE, was synthesized by a hard template method using phenol-formaldehyde resin. The synthesis of phenolic resin was performed according to the method of Yan Meng et al [39]. To synthesize the 3-dimensionally opened porous silica, we modified a previously reported synthetic method which uses a microwave reactor. ESS was prepared by a water-in-oil microemulsion process in a hydrothermal reactor. Tetraethyl orthosilicate (2.5 g) was dissolved in cyclohexane (30 mL) and pentanol (1.5

mL). A solution of cetylpyridinium bromide (1 g) and urea (0.6 g) in water (30 mL) was then added to the solution. The mixed solution was reacted at 393 K for 4 h in an autoclave with vigorous stirring. After the reaction, the suspension was slowly cooled to room temperature and the product was isolated by centrifugation. The resulting material was centrifuged with a mixture of deionized water and acetone (1:1 volume ratio) three times. The obtained precipitate was dried at room temperature for 24 h, and the dried material was calcined at 823 K (rampingrate of 1 K min^{-1}) for 6 h in an atmosphere of air. ESS which was used as hard template and resol precursors were mixed and centrifuged at 10000 rpm for 50 min. Excess resin was removed and the solid product was dried at room temperature in air. The resulting sample was aged at 373 K in air and carbonized at 1173 K for 3 h in a flow of N_2. The ESS carbon composite was etched for 24 h using HF, followed by filtering and drying at room temperature in air.

2.2.2 Characterization

The lattice expansion of Pd was examined by X-ray diffraction (XRD; D-Max2500-PC, Rigaku) by using CuKa as the radiation source in the range 2θ = 10–80 ^{o} with a scan rate of 4 ^{o} min^{-1} at 50 kV and 100 mA. The particle sizes and d-spacing values of Pd were confirmed by high-resolution TEM (HR-TEM; JEM 3010-JEOL, 300 kV). The SEM images were obtained by means of a Carl Zeiss SUPRA 55VP field-emission scanning electron microscope. To investigate any changes in the Pd surface, the samples were examined by X-ray photoelectron spectroscopy (XPS; Sigma Probe, Thermo-VG, UK) with a monochromatic AlKa X-ray source. The binding

energies were corrected for the surface charge by referencing to the C 1s peak of contaminant carbon at 284.5 eV. Thermogravimetric analysis (TGA; SDT Q600, TA instruments) was performed to investigate the amount of coke deposited on the catalysts after the reaction. During the analysis, the temperature was increased from RT to 900 ^{o}C at a rate of 10 ^{o}C min^{-1} in air. Temperature-programmed desorption (TPD) with a MS detector was performed to investigate the properties of the acidic sites. TPD measurements were carried out in a pyrex flow reactor. In each measurement, 0.05 g of catalyst was pre-treated in a reactor at 110 ^{o}C for 1 h in He. Ammonia gas was injected in pulses into the He stream at RT until the catalyst was saturated and the catalyst was pre-treated in a flow of He at 100 ^{o}C before the TPD analysis to remove any weakly adsorbed species. The temperature was increased to 500 ^{o}C at a rate of 5 ^{o}C min^{-1}. The outlet gas was analyzed by on-line MS (VG Sensorlab). To avoid the presence of a peak from water fragmentation, the fragment at m/z=16 was used for the ammonia desorption peak.

2.2.3 Catalytic activity

To investigate the resistance of the Pd-added catalysts to coking, the dehydration of glycerol to produce acrolein was used as a model reaction. The gas-phase dehydration of glycerol was performed in a fixed-bed quartz reactor with an internal diameter of 7 mm at 260 ^{o}C. An aqueous solution of glycerol (10 wt.%) was fed at a rate of 2.1 mL h^{-1} by means of a syringe pump and nitrogen was used as a co-flow gas at a rate of 30 mL min^{-1}. The feed composition was controlled to molar ratios of 40.2 : 58.5 : 1.3

(N_2/H_2O/glycerol). We carried out the catalytic reactions on 0.3 g of catalyst and pretreated the sample at the reaction temperature for 1 h. The product was collected in a cold trap and analyzed by GC (DS6200, Donam instrument) with a capillary column (DB-WAX, 30 m × 0.32 mm × 0.5 mm) and a flame ionization detector (FID). The temperatures of the detector and injector were 300 and 260 ^{o}C, respectively, and the oven temperature was programmed between 45 and 235 ^{o}C. The initial and final temperatures were maintained for 5 min.

2.3 Results and discussion

2.3.1 Diffusion of coke into the palladium lattice

To study the expansion of the Pd lattice by the addition of coke, we examined the changes in the XRD patterns before and after the reaction. Figure 2-1 shows XRD patterns of the Pd-PWC and Pd-PWS catalysts before and after the reaction in the range $2\theta = 10–80^{o}$. No XRD peaks owing to the heteropolyacids (HPAs) were observed, presumably because the HPAs were well-dispersed over the carbon and silica [62]. As shown in Figure 2-1a, the diffraction pattern for palladium in the Pd-PWC catalyst shifted to lower angles after the reaction, which was attributed to the fact that the palladium lattice had expanded and has been incorporated onto the carbon support. From the JCPDS diffraction data, we confirmed the lattice parameters of Pd with respect to fresh and used Pd-PWC catalysts (Pd-PWC (f) and Pd-PWC (u), respectively). The lattice was expanded from 3.89 to 3.99 Å (2.7 %) by PDF# 01-087-0637 and 00-046-1043 in the JCPDS data. This result was consistent with the reported values for lattice expansion owing to the formation of a Pd–coke precursor phase [65, 66]. It was reported that the carbon support assisted the gas-phase atoms in diffusing the subsurface on Pd [70, 71].

Therefore, the palladium lattice, on interacting with the carbon support, was readily expanded by the incorporation of coke under the moderate reaction conditions used herein. However, no change was found for the Pd peaks in any of the silica-supported Pd-PW (Pd-PWS) catalysts. This result indicated that the lattice expansion of Pd only occurred on the carbon

supported catalysts owing to assistance from the carbon support. It has been reported that the lattice expansion of Pd could be caused by hydrogen, oxygen, and carbon under harsh gas-phase conditions [66, 67]. To investigate the possibility of incorporating other atoms into the palladium lattice, XRD analysis was carried out by using catalysts that were treated with gas-phase water (O and H source) in the absence of glycerol (C source; Figure 2-1b) and compared with the used catalyst that had been treated with 10 wt.% glycerol (Figure 2-1a). No significant changes were observed in the Pd peaks for the Pd-PWC and Pd-PWS catalysts after treating with gas-phase water (Figure 2-1 b), which indicated that only coke precursors were incorporated into the Pd lattice under these reaction conditions.

The particle size and lattice expansion of Pd on the Pd-PWC catalysts were examined by TEM and HR-TEM (Figure 2-2). In the TEM images, the crystalline palladium particles were well-dispersed with a uniform size. The statistical histogram showed a narrow range for the Pd distribution in Pd-PWC (f) and in Pd-PWC (u) and a slight change in the average diameter from 4.8 to 5.2 nm after the reaction. The average crystalline size of Pd (111), which was calculated from the XRD patterns by using the Sherrer equation, increased slightly from 4.9 to 5.3 nm after the reaction. The d-spacing values for Pd-PWC, which showed a lattice expansion of Pd in the previous XRD analysis, were calculated from the HR-TEM images. The d-spacing values for Pd nanoparticles of the Pd-PWC changed from 0.2 to 0.22 nm, owing to the capture of coke by the Pd lattice. This result was consistent with the XRD analysis.

2.3.2 Characterization of the surface properties and active sites

XPS analysis was carried out to investigate changes in the surface properties of Pd-PWC in terms of capturing coke in the Pd lattice. Figure 2-3 shows the state of the Pd 3d (5/2) core level before and after the reaction. The metallic Pd peak was observed at 335.3 eV and the oxidation-state peak was located above 336 eV. The Pd 3d state appeared as two peaks in the Pd-PW system because, during the heat treatment, palladium was slightly oxidized on the surface but not in the bulk sample. The intensity of the metallic Pd^0 peak decreased and the Pd_{ox} peak that appeared at above 336 eV increased significantly after the reaction. D. Teschner et al.[72] concluded that the peak increase was due to the surface state of the carbon modified Pd–C surface phase. They also reported that the presence of the adsorbates gave rise to a surface state at a similar energy and referred to this as an adsorbate-induced surface core–level shift. Therefore, the increased Pd_{ox} peak intensity could be attributed to the formation of a Pd–coke precursor phase by the diffusion of coke into the Pd lattice during the reaction. These XPS results were not evident in the case of the Pd-PWS catalyst. The results of a Pd 3d oxidation state on Pd-PWS are shown in Figure 2-4. Unlike Pd-PWC, the area ratio of the Pd/Pd_{ox} phases increased [73, 74]. The metallic peak of Pd was observed as 335.3 eV on the silica support, and the oxidation state peak appeared at above 336 eV. Palladium is known to show easy redox transformation $Pd^{2+} \leftrightarrow Pd^0$ and $H_3PW_{12}O_{40}$ also have redox properties in reactions or under conditions of heat-treatment. The state of Pd (3d) appeared as two peaks in the Pd-PW system, because palladium was slightly oxidized on surface not on bulk during the heat-treatment of Pd-PWS.

During the reaction, Pd was re-reduced gradually, due to the redox transformation of HPA by H^+ donating for dehydration [72-74]. Therefore, the intensity of the Pd_{ox} peak was reduced after the reaction. The XPS data of W 4f on Pd-PWC before and after the reaction is shown in Figure 2-5. Based on this result, we concluded that heteropoly acid was not changed by interactions and decomposition after the reaction. Table 1 shows data related to the surface atomic percent of carbon (from coke and the carbon support), oxygen, and tungsten in the catalysts and the area ratio of Pd/Pd_{ox} that was calculated from the deconvolution data from XPS analysis. As shown in Table 2-1, the atomic ratio of carbon on the surface of the Pd-PWS almost doubled after the reaction. In addition, the surface ratios of oxygen and tungsten decreased after the reaction. This result indicated that the majority of the coke that was produced was located on the catalyst surface or sub-surface after the reaction, which resulted in the deposition of coke on the active sites of PW. On the other hand, the rate of increase in C and the decrease in O and W for Pd-PWC was smaller than that for Pd-PWS. In addition, the Pd/Pd_{ox} ratio showed the lowest value in the case of the Pd-PWC catalyst, thereby indicating that Pd had become more-strongly bound to the surface than before the reaction owing to the formation of a Pd–coke precursor phase [75].

The number of active sites on the acid catalysts was estimated by NH_3-TPD analysis. Figure 2-6 shows TPD profiles for Pd-PWC and Pd-PWS catalysts before and after the reaction with their corresponding deconvolution profiles. The total amount of acidic sites on the catalyst is listed in Table 2-2. Three peaks with respect to acidic strength were observed in the fresh supported $H_3PW_{12}O_{40}$ (HPW) catalysts. The total amount of

acidic HPW that was supported on silica was higher than the amount of supported on activated carbon, although the carbon support had a larger surface area than the silica. This result implied that HPW interacted with carbon more-strongly than with silica and that the strong interaction induced a decrease in the amount of acidic sites owing to the high basicity of the support by the dehydroxylation of Keggin polyanions ($[PW_{12}O_{40}]^{3-}$) [81, 82]. Kapustin et al.[83] studied the interaction of HPW with various supports and found that the relative strength was silica < alumina < carbon. As shown in the deconvolution profiles of Pd-PWS and Pd-PWC, HPW had three peaks as the weakly (about 200 ^{o}C), medium (200–300 ^{o}C), and strongly acidic sites (over 300 ^{o}C), and the relative amount of strongly acidic sites on Pd-PWC was larger than that on Pd-PWS. After the reaction, the acidic amounts had decreased on Pd-PWS, except for the amount of strongly acidic sites at above 300 ^{o}C [76, 77]. This result was thought to be due to the deposition of coke on the active sites. However, the acidic characteristics of the Pd-PWC catalyst were retained after the reaction, thereby indicating that most of the active sites were retained after the reaction. The coke was primarily deposited on the weakly acidic sites during the reaction, which implied that the Brønsted acid sites on the Pd-PWC catalyst were more dominant in the reaction than the Lewis acid sites. Cerqueira et al.[84] found that the effect of coke on the acidic properties of the Lewis acid sites was more strong than on the Brønsted acid sites. Quantitative analysis (Table 2-2) showed that the total number of active sites of Pd-PWS had decreased to 48% after the reaction, and the amount of Pd-PWC had decreased to 26 %. This result could be attributed to the incorporation of coke in the Pd lattice, which resulted in the inhibition of the deposition of coke on the active sites of the

catalyst.

2.3.3 Coking resistance in the formation of the Pd–C phase for the dehydration of glycerol

To elucidate the effect of Pd and the carbon support on coking resistance, we used the catalytic dehydration of glycerol into acrolein as a model reaction. Figure 2-7 shows the activity of PWC and PWS before and after the addition of Pd. Glycerol conversion decreased rapidly in both cases owing to severe deactivation by coking. After 8 h, PWC showed 38 % conversion of glycerol and PWS showed 54 % conversion. This difference was due to the larger number of acidic sites on silica support compared to the carbon support. However, after the addition of Pd, the trends were quite different. The catalytic stability of PWC increased significantly, while, for PWS, the change was negligible. The Pd-PWC sample showed 87 % conversion of glycerol whereas the activity of Pd-PWS was 55 % after 8 h. Nitrogen adsorption–desorption analysis was performed to examine the physical properties of the catalysts (Table 2-2). The surface areas of the catalysts showed large differences depending on the support. The catalyst that was supported on activated carbon showed a much-larger surface area than that on the silica support. However, the catalytic activity and the deactivation trend for glycerol dehydration did not correlate with the external surface properties. Both of the PWS and PWC catalysts were easily deactivated, although their initial conversions of glycerol were 100 %. After the reaction, the surface areas of the catalysts had been decreased by coke deposition (Table 2-2). Interestingly, Pd addition to the PWC catalyst was

able to prevent coking much more successfully compared to PWS. Pd-PWC (f) showed a high surface area, and about 80 % of the specific area was due to the microporosity of the activated carbon. After the reaction, the surface area decreased dramatically from 1.03×10^3 to 272 $m^2 g^{-1}$, and Pd-PWC (u) was mainly composed of non-micropores (Table 2-2). Thus, the micropores of the Pd-PWC catalyst became blocked (pore-plugging) during the reaction. The selectivities for glycerol dehydration on Pd-PWC are shown in Figure 2-8. Acrolein, the main product, was produced with a selectivity of above 70 % after 2 h, and this selectivity was maintained for 8 h. This value was analogous to the previous reported use of solely supported heteropoly acid catalysts. The initial selectivity for acrolein was 68 %, because time was required for the reaction to reach a steady-state.

The reason for such an enhanced catalytic activity could be as follows: During the reaction, coke precursors that were produced by the reactants were captured in the Pd lattice owing to the loosening of the Pd lattice by the carbon support on Pd-PWC. This loosening resulted in the inhibition of coke depositionon the active sites in the heteropoly acid catalyst. The reason for the decreased conversion after 6 h was that an insufficient amount of Pd had been added (1 wt.% of the total catalyst weight). Seriani et al.[71] reported that the carbon species were inserted into Pd in hexagonal six-layer fcc-like forms, like Pd_6C. Saturation of the Pd_6C structure by coke did not permit the insertion of additional carbon species.

Next, we carried out the reaction with different wt.% of Pd in the Pd-PWC catalyst. When 3 wt.% of Pd was added to the PWC catalyst, lattice expansion was observed by XRD (Figure 2-9); however, the stability of the catalyst was not higher than that of the 1 wt.% of the Pd added PWC catalyst,

owing to the side-reactions that occurred with surplus Pd, such as dehydrogenation [80]. An increase in the dehydrogenation activity was also observed on 1 wt.% Pd-PWC (Figure 2-10), and 0.1 wt.% of Pd addition to the PWC catalyst did not show any capturing effect. Consequently, the 1 wt.% Pd-PWC catalyst showed the highest stability in the dehydration of glycerol among the catalysts tested (0.1, 1, and 3 wt.% Pd-PWC). To remove the coke on the catalysts, it was necessary to find optimum conditions for the effective regeneration of the used catalyst. The oxidation temperature of deposited coke was determined by TGA-DSC analysis (Figure 2-11a). Fresh Pd-PWC catalyst showed one large exothermic peak at 550 ^{o}C, which was mainly due to the oxidation of the carbon support, and the used Pd-PWC showed a small additional peak in the temperature range 300–400 ^{o}C that was due to the oxidation of coke [78]. Based on this result, the minimum temperature for the regeneration was determined to be 300 ^{o}C. The used catalysts were regenerated at 400 ^{o}C for 2 h in O_2 and at 350 ^{o}C in a flow of steam, and their activity is shown in Figure 2-11b. After regeneration at 400 ^{o}C (O_2), the used Pd-PWC showed a low conversion of glycerol, which was due to the decomposition of the active sites on the heteropoly acid. In case of the catalyst that was treated at 350 ^{o}C (steam treatment), 88% of glycerol conversion was obtained; however, the activity rapidly decreased after 2 h. Although the used Pd-PWC catalyst showed good initial performance after regeneration, heteropoly acid appeared to decompose during the reaction [84, 85]. This result also implied that Pd had no remaining beneficial effect once its lattices were irreversibly saturated with a coke precursor. Figure 2-11c shows two types of Pd particles, lattice-expanded Pd particles and original particles, which indicated that the incorporation of coke into the Pd lattice

was not completely removed during regeneration. The Pd–C phase is known to be the most-stable phase among the atoms that were incorporated (oxygen, hydrogen, and carbon) into the Pd lattice, and it is designated as a "metastable Pd_6C phase". However, at above 600 ^oC, the Pd_6C phase decomposed and changed into a graphitic carbon (layer) on the Pd surface [65, 66, 71]. Consequently, we were not able to completely remove the coke while maintaining activity. This topic is a very important issue and more-detailed research is currently underway.

The activity of Pd-PWS was lower than that of PWS after 8 h, which indicated that the addition of Pd had a negative effect on coking in the case of the silica-supported catalysts. To confirm this result, we carried out TGA analysis of the fresh and used catalysts. The catalytic performance at much-longer time-on-stream of the Pd-PWS and PWS catalysts is shown in Figures 2-12 and 2-13. As seen in Figure 2-12, the conversion of glycerol on Pd-PWC gradually decreased after 6 h, and the activity showed a 40 % conversion after 16 hrs for the reaction. In the case of the PWC catalyst, the activity rapidly decreased to 45 % of conversion within 5 h, and showed a 30 % conversion after 16 h. Although the stability of the Pd-PWC catalyst was better than PWC for up to 16 h, it was necessary to perform more studies related to the optimum amount of added-Pd and a more-detailed catalyst design to develop a more-stable Pd-PWC catalyst.

The amount of coke produced was estimated by TGA analysis (Figure 2-14) [77, 78]. We also calculated the amounts of coke deposited, based on a comparison of the weight change between the fresh and used catalysts. Table 2-3 shows the amount of coke deposited on the catalysts. Before Pd addition, the amounts of coke were 5.4 and 6.3 % for PWS and PWC, respectively.

These values indicated that the coke that had been deposited on the catalysts had been oxidized into CO_x during the TGA analysis in air. In the case of PWS, the amount of coke increased to 10 % after the addition of Pd. However, for Pd-PWC, the amount of coke decreased to 3.8 %, owing to the capture effect that was conferred by the added Pd. As discussed above, produced coke from gas-phase reactants was diffused into the Pd lattice, which was loosened by the carbon support. As a result, the amount of coke on Pd-PWC was reduced. However, in the case of Pd-PWS, palladium exerted its effect based on its dehydrogenation activity [79, 80].

As shown in Figure 2-10-1, the selectivities for acetone, acetaldehyde, and 1-propanal for the Pd-PWC catalyst were higher than that for the PWC catalyst, while Pd-PWC showed a lower value for acetol selectivity than that of the PWC catalyst. After 6 h, the difference in the selectivity of the by-products between Pd-PWC and PWC was not significant (Figure 2-10-2), because the Pd was gradually deactivated by the insertion of the coke precursors. Importantly, we observed that the hydro/dehydrogenation activity of PWC on glycerol conversion was enhanced by the addition of Pd. Herein, we propose a mechanism that explains the effect of Pd on the characteristics of coke on the carbon- and silica-supported catalysts. Figure 2-15 shows a proposed mechanism for the effect of the Pd–coke precursor phase on different supports. It is well-known that coke is produced during the creation of C=C double bonds from gas-phase glycerol by dehydrogenation [55, 56, 60]. The expansion of the Pd lattice by a Pd–coke precursor phase occurred more easily on a carbon support, owing to a loosening of the lattice. Therefore, Pd captured the coke precursors inside its lattice, which only led to a reduction in the amount of deposited coke on the carbon supported acid

catalysts. However, Pd was also able to produce coke from saturated hydrocarbons, owing to its dehydrogenation activity, which had a negative effect on catalytic deactivation by coking on a silica support.

2.3.4 Effect of pore structure on the deactivation by coke deposition

To confirm the effect of pore structure of carbon support, the 3D mesoporous carbon and hexagonal porous carbon (CMK-3) were additionally prepared, and used for the supports. By nanocasting a replica method, the 3D mesoporous carbon was successfully synthesized as shown in Figure 2-16. The carbon material was shaped with fibrous sphere and the pores was developed in three dimensionally manner. It was denominated to CNE (Carbon Nano Echinometra) because of looking like a sea urchin, Echinometra Mathae. Each sphere particle has a uniform size of 450 – 500 nm. These unique structure was expected to prevent a problem which is a pore blocking by coke deposition. Using the various carbons the PW supported on carbon catalysts, PW/AC, PW/CMK-3 and PW/CNE, were prepared by incipient wetness impregnation method. In order to examine the pore structure, N_2 adsorption-desorption analysis of the three catalysts was carried out and the results were shown in Figure 2-17 and Table 2-4. The pore diameters in each catalyst were 1 nm for PW/AC and 3-4 nm for PW/CMK-3 and PW/CNE. In the Langmuir isotherm curves, the PW/CMK-3 and PW/CNE showed a similar hysteresis loop, a characteristic of the mesoporous structure. The surface area of the PW/CNE was the smallest among the other PW catalysts. As shown in Figure 2-18, the

heteropoly acid (PW) was not observed in TEM images due to the active sites were highly dispersed on the carbon materials which have large surface area above 1,000 $m^2 g^{-1}$. The catalytic activity tests of the three catalysts were carried out in a same reaction condition with the results in Figure 2-12 in order to confirm the effect of pore structure on stability. From the results (Figure 2-19), it should be noted that the PW supported on mesoporous carbon catalysts showed better stability than PW/AC catalyst. And PW/CNE catalyst showed the best stability among the other catalysts including the Pd-PW/AC catalyst. The amount of coke deposition of the used catalysts after reaction for 8 h was listed in Table 2-4. The amount of coke deposited on PW/AC was lower than the other catalyst, because the catalyst was severe deactivated in a 8 h reaction time, resulting in less adsorption of glycerol. Although the amount of coke deposited on PW/CNE was larger than the PW/AC, the catalytic stability was significantly proved during a reaction. This result means that the active sites were retained by pore blocking in the opened 3D mesoporous catalyst, although the coke was severly deposition on the catalyst. Therefore, the 3D mesoporous material is expected to good candidate for the catalyst in the conversion of biomass-derived feedstocks which shows a severe deactivation of catalyst by coking.

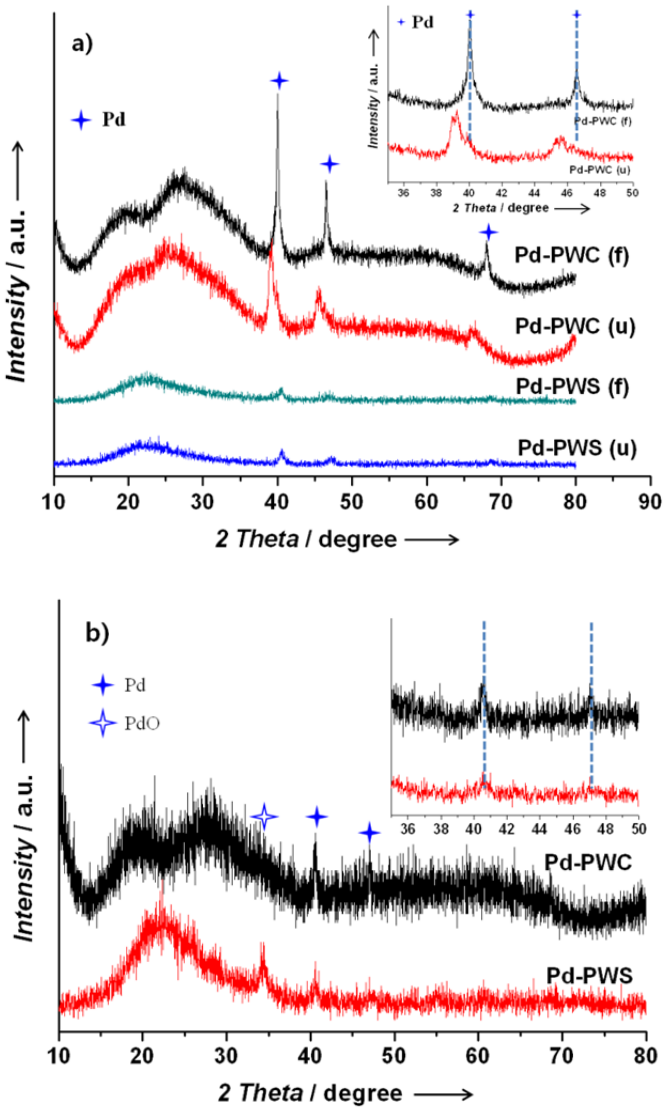

Figure 2-1. a) XRD patterns of Pd-PW catalysts that were supported on carbon and silica in the range $2\theta = 10{-}80^{o}$; b) XRD patterns of Pd-PWC and Pd-PWS that were treated with gas-phase water (Pd-PWS (f): Pd-$H_3PW_{12}O_{40}/SiO_2$, fresh catalyst; Pd-PWC (u): Pd-$H_3PW_{12}O_{40}$/C, used catalyst).

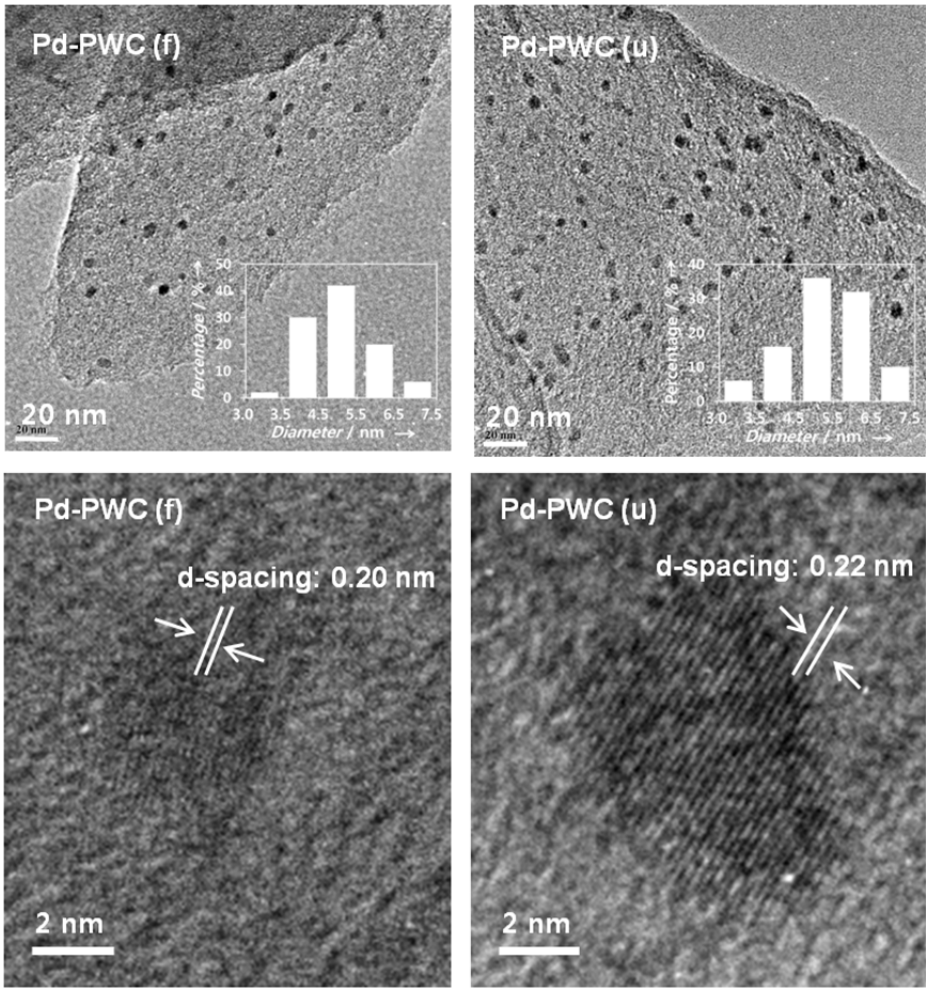

Figure 2-2. TEM and HR-TEM images of the Pd nanoparticles of fresh (Pd-PWC (f)) and used Pd-PWC catalysts (Pd-PWC (u)). Inset: statistical histogram of the size-distribution of Pd.

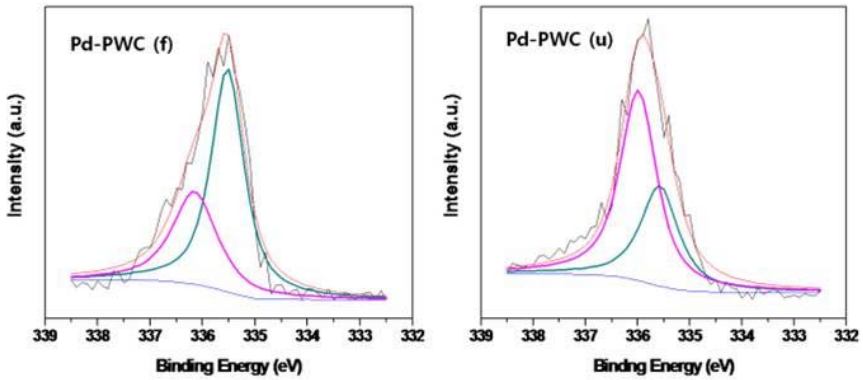

Figure 2-3. XPS spectra of the Pd $3d_{5/2}$ core level of Pd-PWC before and after the reaction. (Deconvolution curve: Pd_{ox} state at 336 eV and Pd^0 state at 335.3 eV)

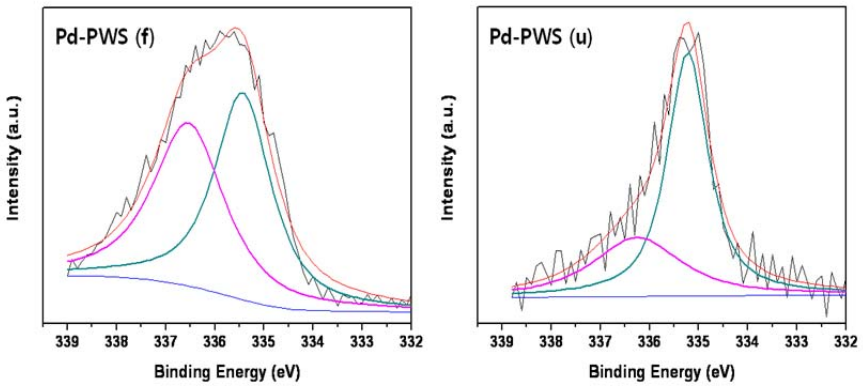

Figure 2-4. The XPS spectra on the Pd $3d_{5/2}$ core level of the Pd-PWS before and after reaction.

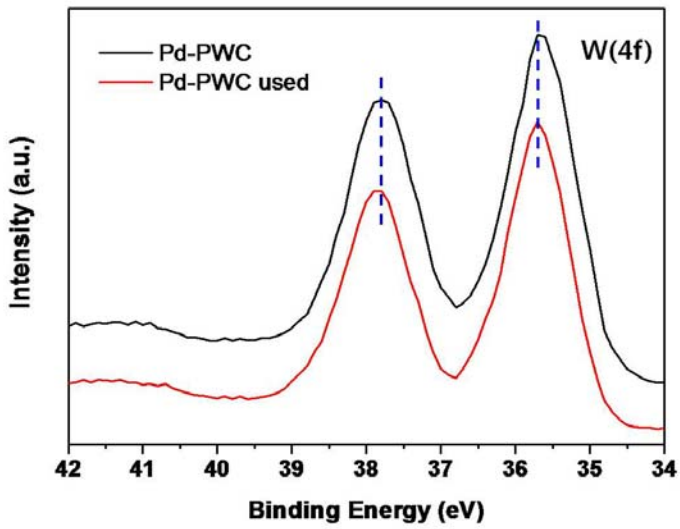

Figure 2-5. The XPS spectras on the W (4f) core level of the Pd-PWC before and after reaction.

Table 2-1. Surface concentration as determined by XPS of Pd-PWS and Pd-PWC catalysts before and after the reactions.

Catalyst	Pd-PWS (fresh)	Pd-PWS (used)	Pd-PWC (fresh)	Pd-PWC (used)
C(%)[a]	14.3	35.4	88.1	88.4
O(%)	81.5	62.8	9.9	7.9
W(%)	2.5	1.5	1.9	1.4
Pd/Pd_{ox}[b]	1.02	1.93	1.76	0.55

[a] Surface atomic percent; different to 100%: Pd, P, trace contaminations

[b] The area ratio of Pd (335.4 eV) to Pd_{ox} (336.2 eV) for deconvolution data

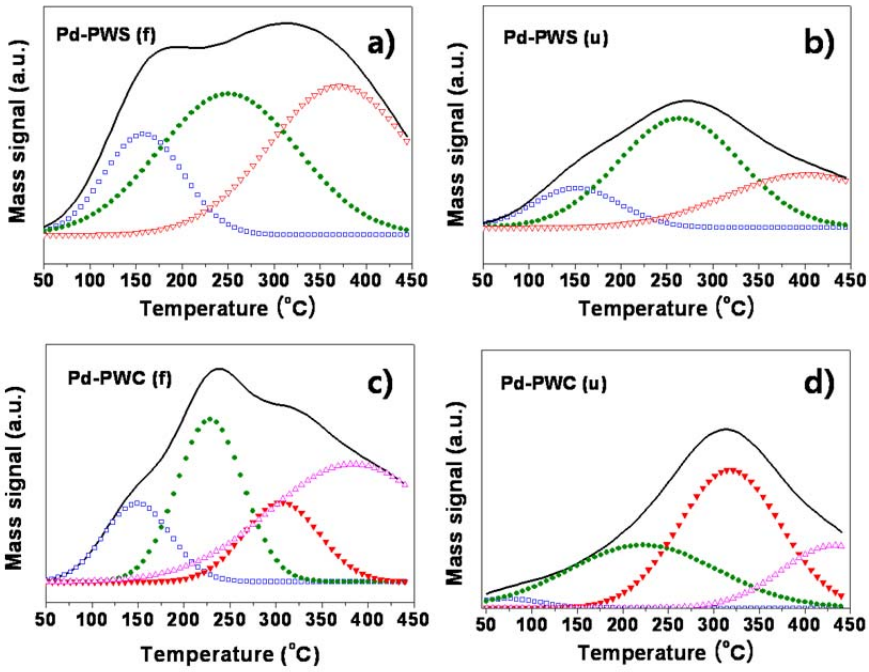

Figure 2-6. NH_3-TPD profiles of Pd-PWC and Pd-PWS before and after the reaction: a) Pd-PWS (f); b) Pd-PWS (u); c) Pd-PWC (f); and d) Pd-PWC (u). Inset: deconvolution profile in the TPD data: weak sites (□), medium sites (▽), strong sites in Pd-PWS (▼ and △) (ratio of the weak, medium, and strong sites of Pd-PWS (f)/Pd-PWC (f): 16.5, 40.3,and 43.2 %/12.5, 25.8, and 61.7 %, respectively).

Table 2-2. Surface area and amount of ammonia adsorbed on the surface of the Pd-PWS and Pd-PWC catalysts before and after the reaction.

Catalyst	Pd-PWS		Pd-PWC	
	fresh	used	fresh	used
BET surface area (m^2/g)	86.6	63.2	1.03×10^3	272.1
Micropore[a] area (m^2/g)	28	13.3	815.1	71
Adsorbed NH_3 (mmol/g)[b]	1.3	0.65	1.1	0.79

[a] Micropore: less than 2 nm sized pores

[b] Amount of adsorbed ammonia on the catalyst calculated by pulse injection of NH_3 with mass detector.

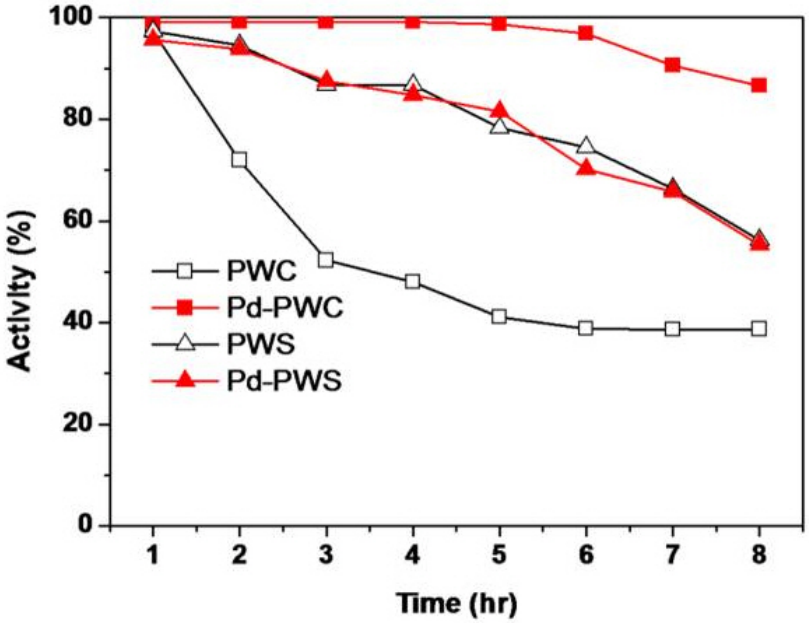

Figure 2-7. Conversion of glycerol into acrolein for various supported PWcatalysts.

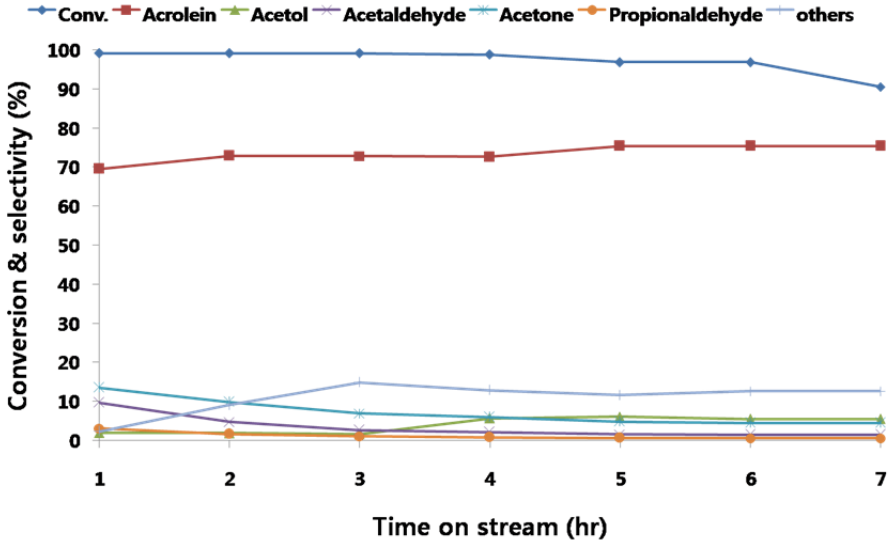

Figure 2-8. Conversion of glycerol and the selectivity for the main products with the Pd-PWC catalyst.

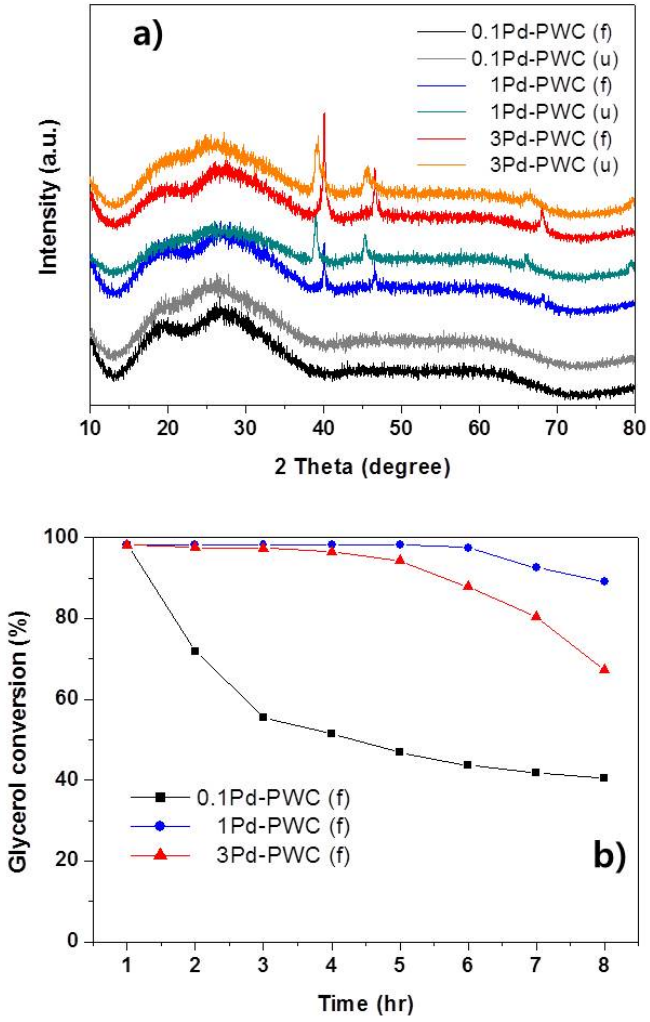

Figure 2-9. XRD patterns and glycerol conversion of the 0.1, 1, and 3 wt% of Pd-added PWC catalysts. a): lattice expansion of Pd after reaction in XRD patterns, b): difference of stability for glycerol conversion between prepared Pd-added PWC catalysts.

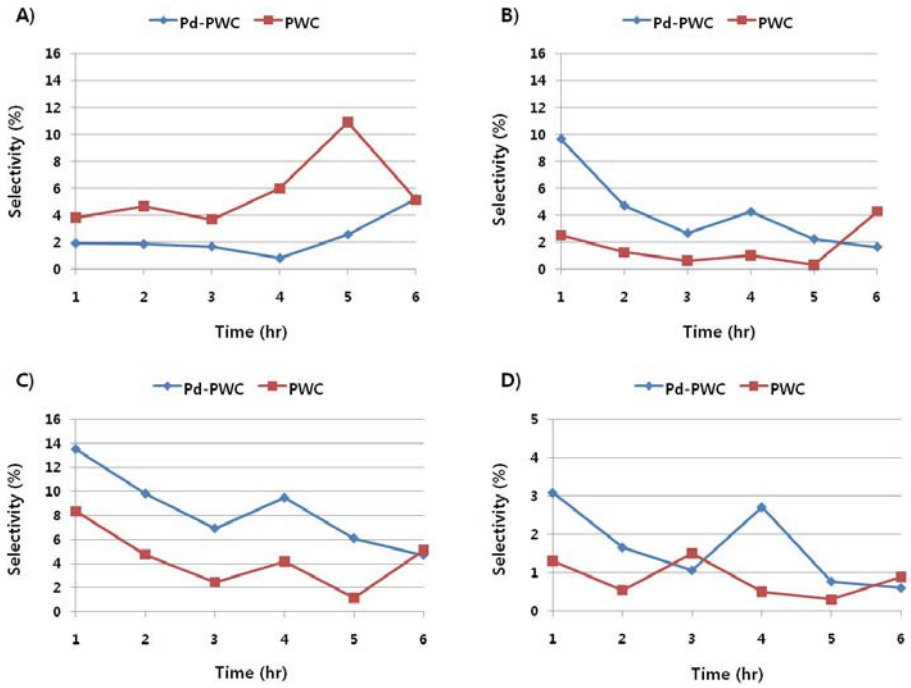

Figure 2-10-1. The selectivity of various by-products for 6 h in the dehydration of glycerol to acrolein. A): acetol, B): acetaldehyde, C): acetone, and D): 1-propanal.

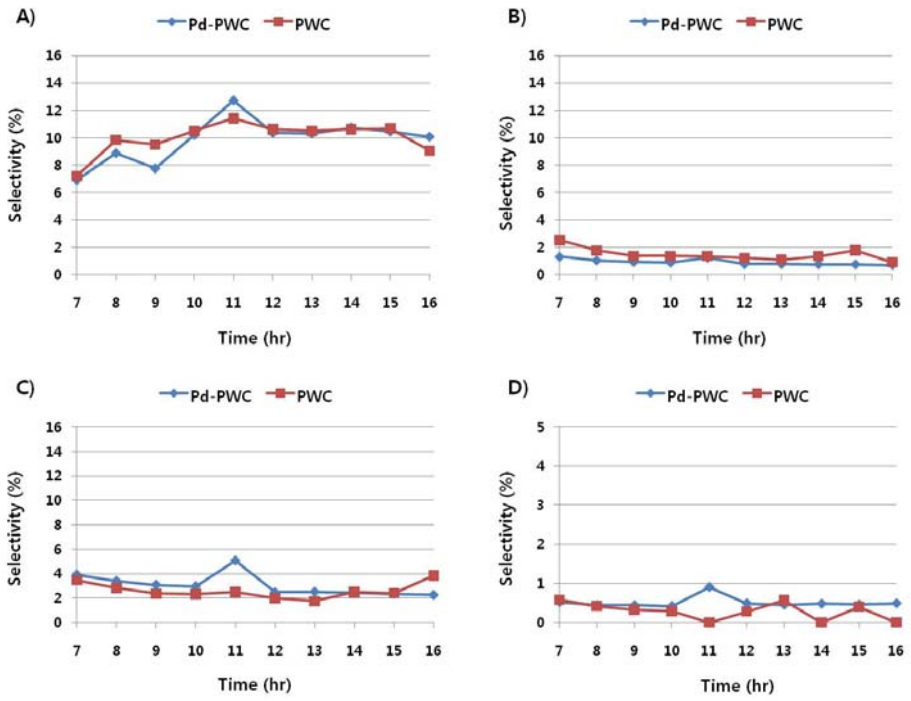

Figure 2-10-2. The selectivity of various by-products after 6 h in the dehydration of glycerol to acrolein. A): acetol, B): acetaldehyde, C): acetone, and D): 1-propanal.

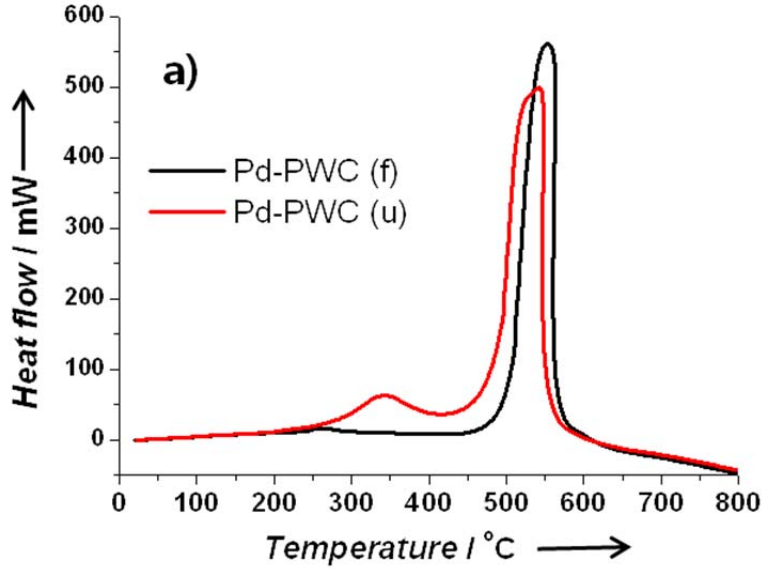
a)
Pd-PWC (f)
Pd-PWC (u)
Heat flow / mW
Temperature / °C
0
100
200
300
400
500
600
700
800

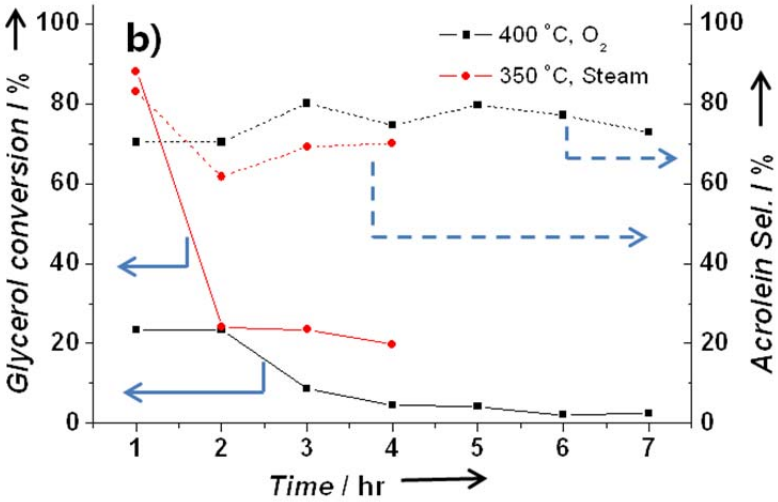
b)
400 °C, O2
350 °C, Steam
Glycerol conversion / %
Acrolein Sel. / %
Time / hr
1
2
3
4
5
6
7
0
20
40
60
80
100

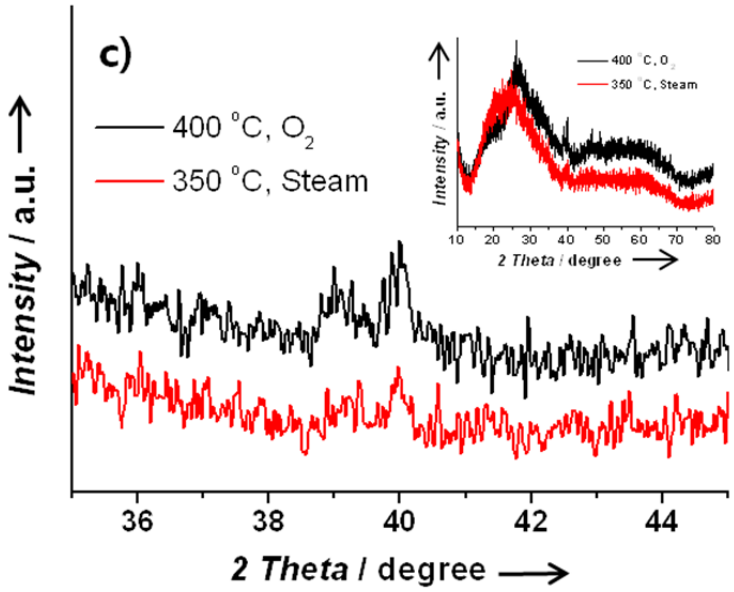

Figure 2-11. a): DSC profiles of Pd-PWC; b) activity of Pd-PWC (u) after regeneration under different conditions; c) XRD patterns of Pd-PWC (u) after regeneration under different conditions. Inset: whole XRD pattern.

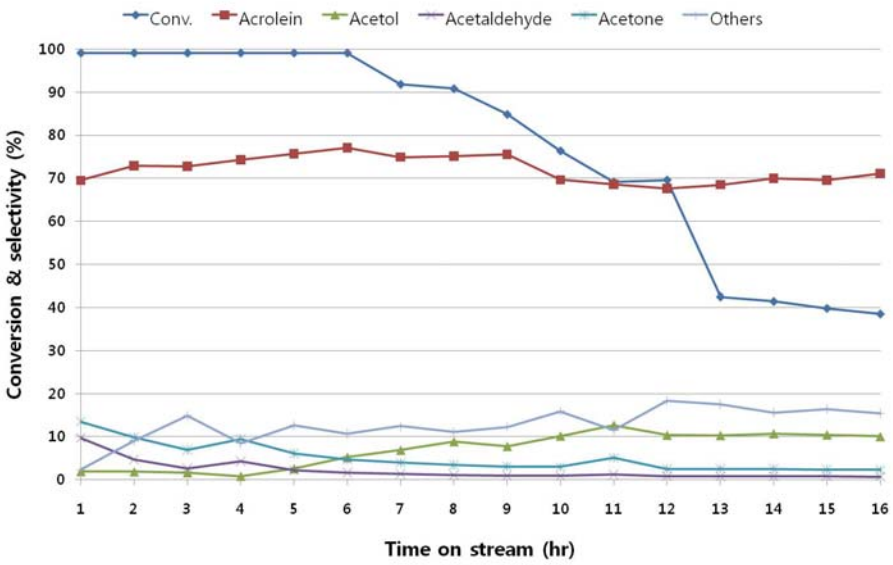

Figure 2-12. Activity test in glycerol dehydration for 16 h TOS of the Pd-PWC catalyst.

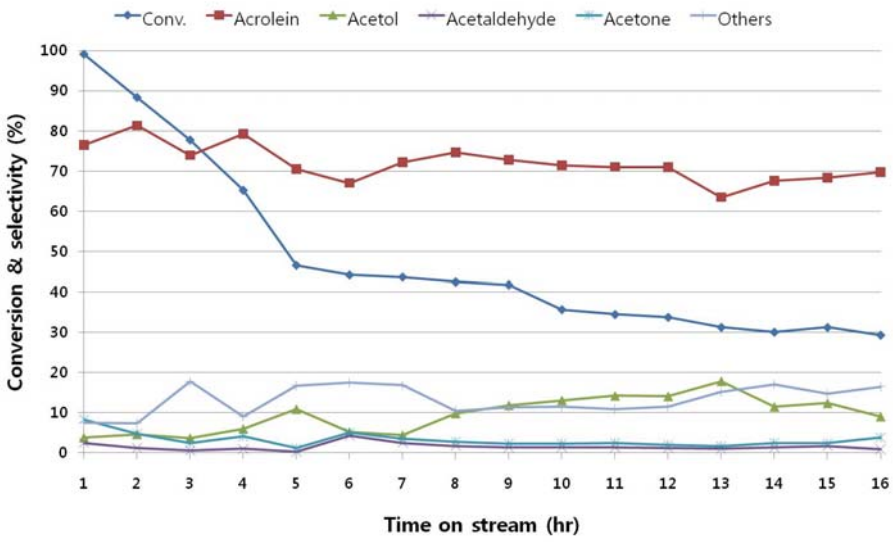

Figure 2-13. Activity test in glycerol dehydration for 16 h TOS of the PWC catalyst.

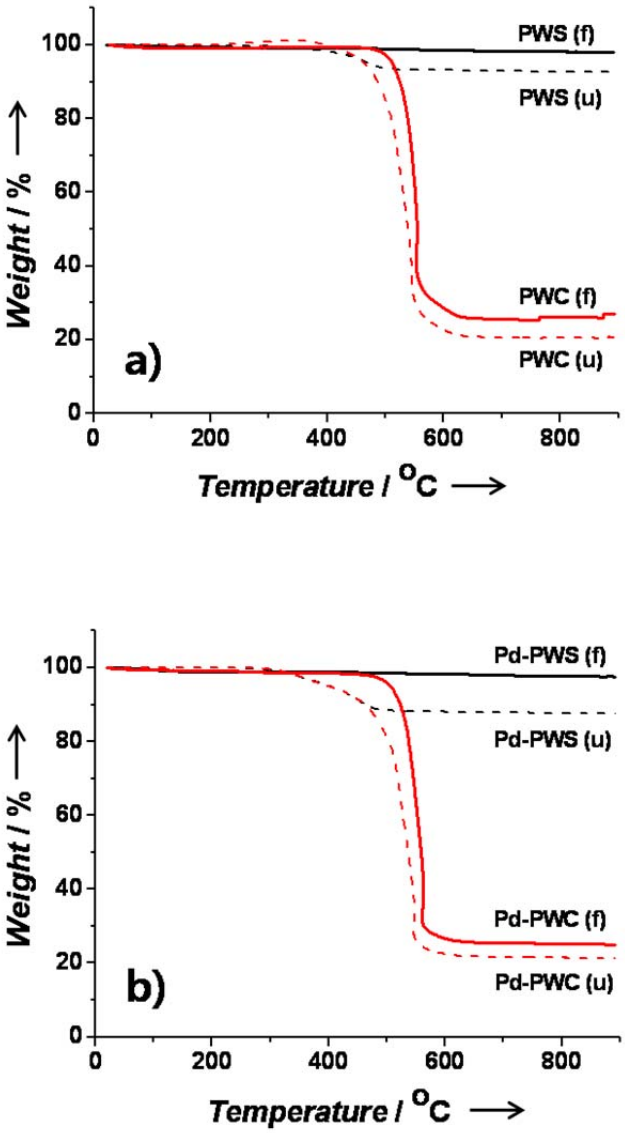

Figure 2-14. Weight change between the fresh and used catalysts, as determined by TGA in a flow of air: a) non-Pd-added catalysts; b) Pd-added catalysts.

Table 2-3. Amount of coke deposited on various catalysts after reaction by TGA analysis.

Catalyst	PWS	Pd-PWS	PWC	Pd-PWC
Cokes (%)[a]	5.4	10	6.3	3.8

[a] Weight percentage of cokes to total weight of catalyst.

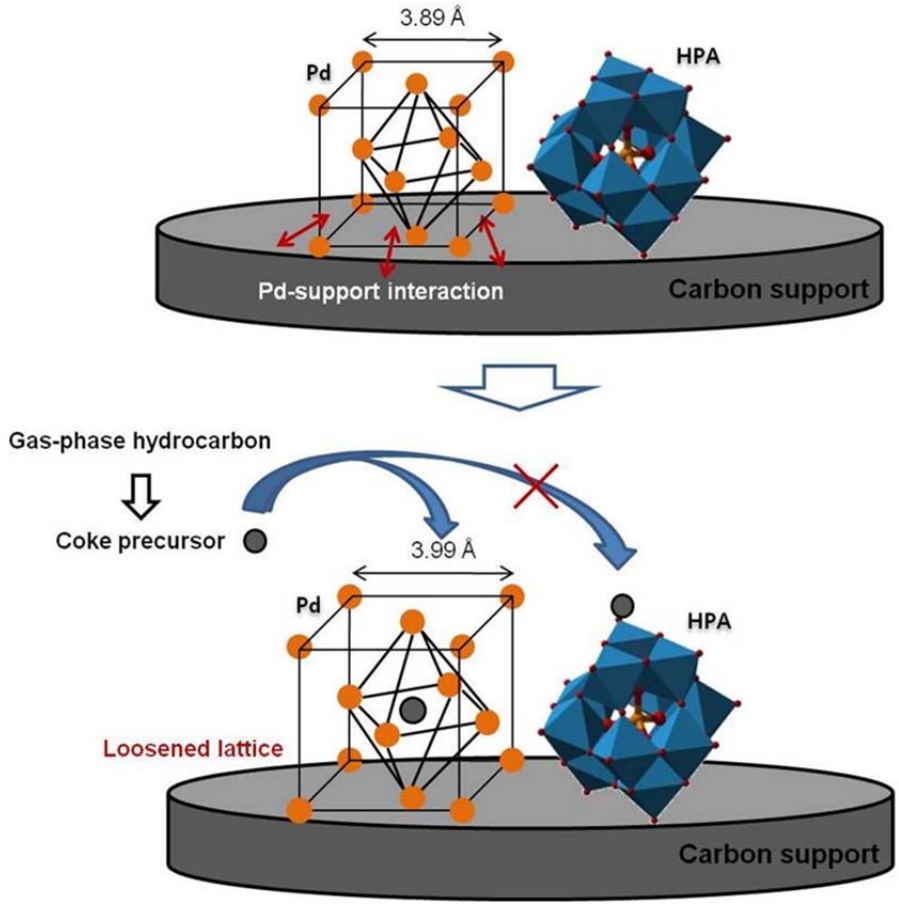

Figure 2-15. Proposed mechanism for coking resistance, as shown by the formationof a Pd–coke precursor phase on different supports for a heteropoly acid.

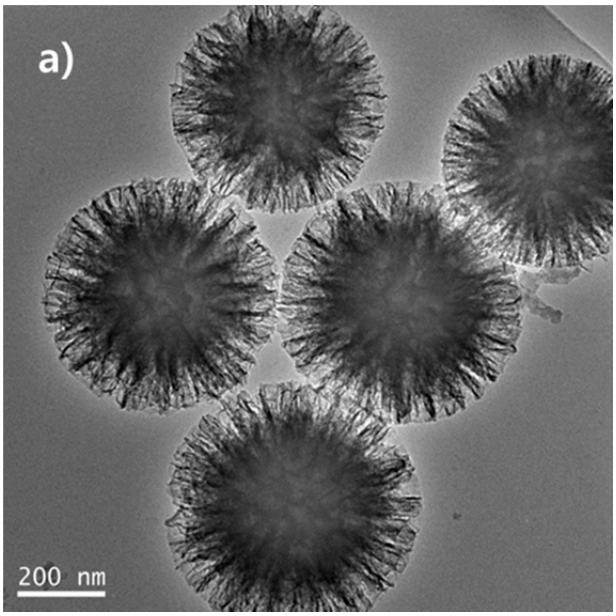

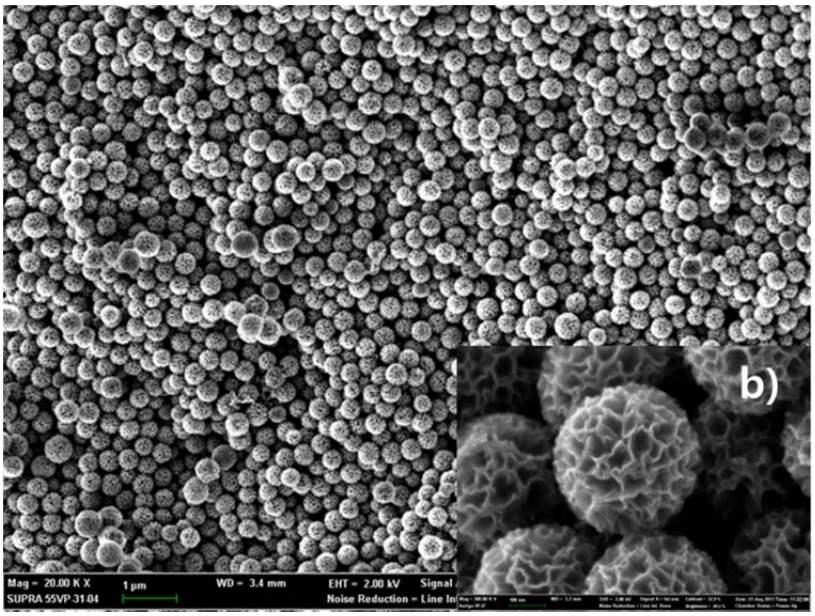

Figure 2-16. a) TEM and b) SEM images of prepared 3D mesoporous carbon (CNE).

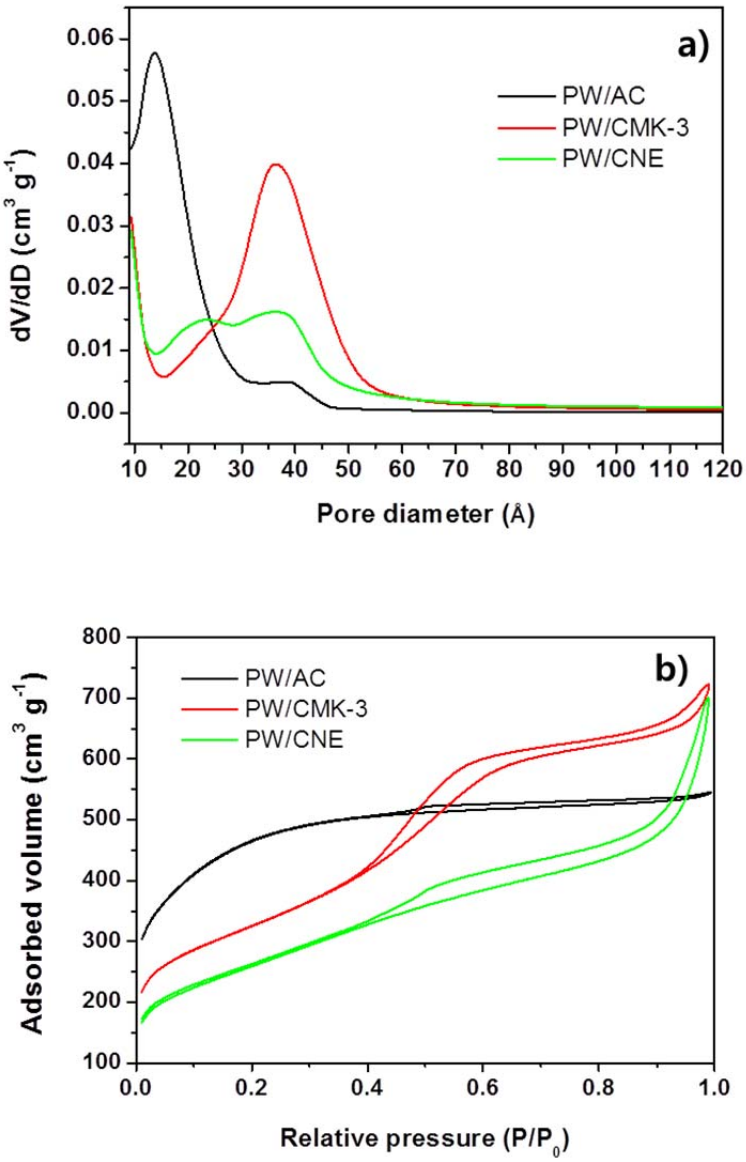

Figure 2-17. a) Pore size distribution and b) isotherm graph of the PW supported on AC, CMK-3 and CNE by N_2 adsorption-desoprtion analysis.

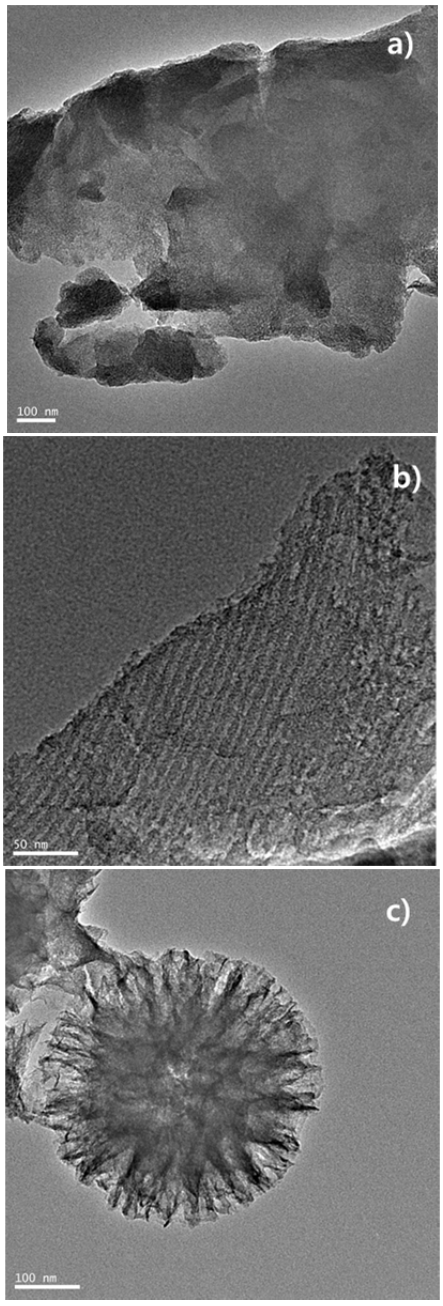

Figure 2-18. TEM images of a)PW/AC, b) PW/CMK-3 and c) PW/CNE.

Table 2-4. BET surface area and amount of coke deposited on various catalysts by N_2 adsorption-desorption analysis and TGA analysis.

Catalyst	PW/AC	PW/CMK-3	PW/CNE
BET area (m^2 g^{-1})	1570.4	1058.8	918.7
Cokes (%)[a]	8	16	11

[a] Weight percentage of cokes to total weight of catalyst.

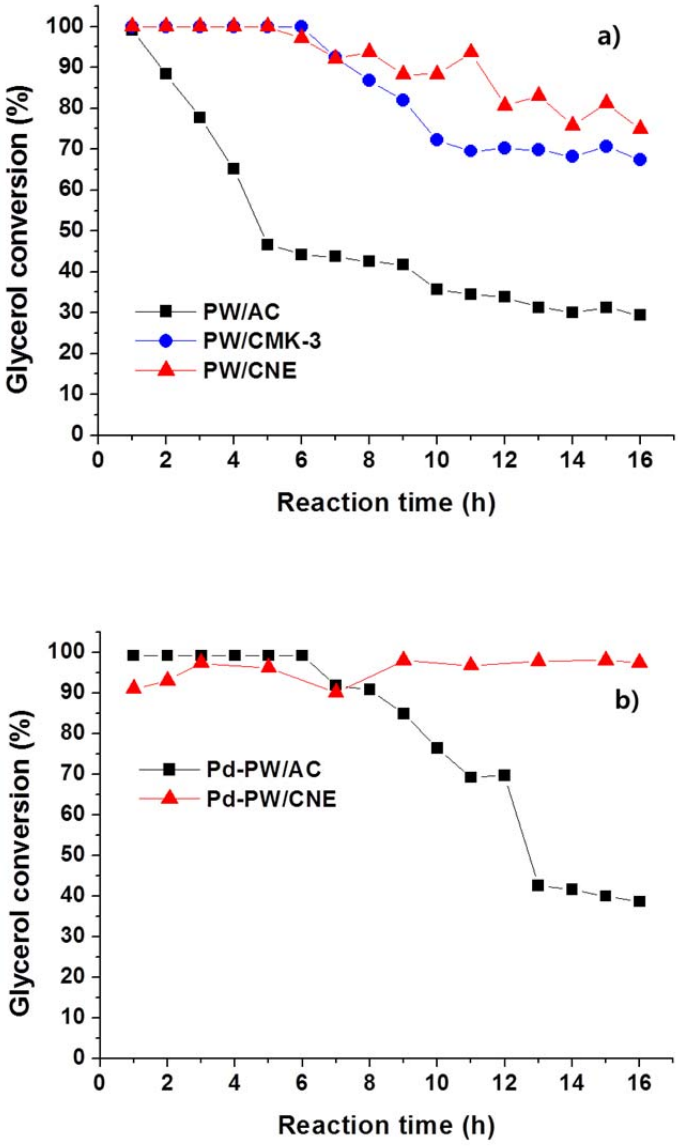

Figure 2-19. Stability test of a) PW/AC, PW/CMK-3 and PW/CNE catalysts comparing with b) Pd-PW/AC and Pd-PW/CNE for 16 h in dehydration of glycerol to acrolein.

Chapter 3. Effect of 3D open-pores on the internal mass transfer in dehydration of n-butanol to di-n-butyl ether (DNBE)

3.1 Introduction

The quality of the fuel being used is an important factor in determining the impact of exhaust gas in the environment and on human health. Low quality fuels emit greater gaseous exhausts that contain higher levels of CO, NO_x, and particulates and make cold starting difficult [86]. One of the most effective ways to improve the quality of a fuel is to add suitable blending agents. Ethers are known to be good blending agents with favorable properties for such use. Branched ethers also enhance the octane rating of gasoline via adding oxygenates, and straight chain primary ethers can improve a diesel fuels cetane number [87-90]. It was observed that linear ethers with more than 9 total atoms showed a good balance of blending cetane number and effectively reduced exhaust gases. Recently, with the increasing use of biodiesel, linear ethers have also attracted interest as a blending agent. Among such possible compounds, di-n-butyl ether can be synthesized from biobutanol or n-butanol derived from fermentation of waste resources of biomass[48-50].

In industry, linear ethers are generally synthesized by the dehydration of a linear alcohol using a homogeneous acid catalyst, such as sulfuric acid. While it shows quite high performance for producing a linear ether, however,

the use of sulfuric acid results in reactor corrosion and the production of toxious by-products, such as alkyl sulfates [87, 91]. Therefore, the development of solid acid catalysts is essential for the large scale production of linear ethers. In previous reports, well-known solid-acid catalysts, such as zeolite, alumina, silica-alumina and heteropoly acids (HPAs) were examined for the dehydration of linear alcohols to produce the corresponding ethers. Based on these reports, it appears that catalytic performance increases with an increase in the desorption peak temperature of ammonia (acid strength) on the acid sites of solid acid catalysts. Another point to be considered is mass transfer due to long-chain molecules in heterogeneous reactions [51]. Zamaraev et al. [52] examined the effect of pore confinement of a catalyst using ZSM-5 and amorphous aluminosilicate in the gas-phase dehydration of n-butanol. The conclusions reached indicate that the concentration of adsorbed reactant decreased the effective energy barrier for ether formation on ZSM-5 (microporous channels with diameter ~ 5.5 Å) in comparison with amorphous aluminosilicate (pores of diameter ~ 50 Å). Attempts have been made to prepare hierarchical structure of catalyst with large surface area, in order to enhance the mass transfer of molecules in heterogeneous reaction, especially on the reaction using long chain molecules. For this reason, various new three-dimensional porous materials have been reported on the fields of catalysis in attempts to enhance the transport of molecules against conventional 2D mesoporous or microporous materials [92-95]. However, in these previous reports, a 3D structure was induced by interconnecting with 1D or 2D porous materials, which limits the access of molecules into fully 3-dimensional structure. Also, the issue of specifically how 3D pores or hierarchical structures enhance the transport of the molecules against

conventional porous materials like 2D meso- and micro-porous materials is not completely understood at present.

In this paper, we report on the design of a heteropoly acid supported on three-dimensionally (3D) opened pore silica with strong acid sites and a mesoporous structure, for use in the dehydration of n-butanol to di-n-butyl ether. The catalyst satisfies the two key factors related to the dehydration of n-butanol, namely, a high acid strength and ease of reactant accessibility. The 3D open porous silica used was previously synthesized by Basset et al. [96], however, this material has not yet been examined in terms of catalysis and other various fields. The synthetic method for preparing 3D openporous silica was modified so as to be a more easy handling method in a hydrothermal reactor and for use as a support for the activecomponent, $H_3PW_{12}O_{40}$ (PW). In order to elucidate the effect of the 3D structure of pores, conventional mesoporous and microporoussilicas (SBA-15 and microrporous silica) were used for the support in a control experiment. Also, the effect of a porous structure on the dehydration of n-butanol was quantified by calculating the effectiveness factor using experimentally obtained kinetic data.

3.2 Experimental

3.2.1 Preparation of catalysts

To synthesize of the 3-dimentionally opened porous silica, we modified a previously reported synthetic method which uses a microwave reactor [96]. Echinometra-shaped Silica Spheres (ESS) were prepared by a water-in-oil microemulsion process in a hydrothermal reactor. 2.5 g of tetraethyl orthosilicate (TEOS) was dissolved in 30 mL of cyclohexane and 1.5 mL of pentanol. A solution of cetylpyridinium bromide (CPB; 1 g) and 0.6 g of urea in 30 mL of water was then added to the solution. The mixed solution was reacted at 393 K for 4 h in an autoclave with vigorous stirring. After the reaction, the suspension was slowly cooled to room temperature and the product was isolated by centrifugation. The resulting material was centrifuged with a mixture of D.I water and acetone (1:1 volume ratio) three times. The obtained precipitate was dried at room temperature for 24 h, and the dried material was calcined at 823 K (ramping rate of 1 K min^{-1}) for 6 h in the atmosphere of air. SBA-15 (SBA), comparison mesoporous silica, was prepared by the conventional method. Microporous silica(mi-S), another control sample, was made from kaolinite by heat treatment and a leaching process. Kaolinite was converted to meta kaolinite by a heat-treatment at 873 K for 24 h in air, and the calcined powder was then treated with the 2.5 M H_2SO_4 at 363 K for 5 h with vigorous stirring. It was then filtered and washed with 0.5 M H_2SO_4 solution and deionized water. Finally, the microporous silica was obtained after drying at 383 K over night [97]. 30 wt % of 12 tungstophosphoric acid n-hydrate ($H_3PW_{12}O_{40}$·n-H_2O, Junsei Chemical

Co. Ltd., GR) was supported on DSS, SBA-15 (SBA), and microporous silica (mi-S) by an incipient wetness impregnation method with water, and they were denoted as PW/DSS, PW/SBA and PW/mi-S, respectively.

3.2.2 Characterization

The pore structures of the prepared catalysts were observed by high-resolution transmission electron microscopy (HR-TEM, JEM-3010, JEOL), and the morphologies were examined by field-emission scanning electron microscopy (FE-SEM, Supra 55VP, CarlZeiss). The physical properties (pore size distribution, porosity, and BET surface area) of the porous supports were investigated by a N_2 adsorption−desorption technique using ASAP 2010 apparatus. The crystalline structure of the heteropoly acid supported onvarious silica supports were examined using an X-ray diffractometer (XRD, D-Max2500-PC, Rigaku) using Cu Ka source at 50 kV and 100 mA. In order to measure the amount of active sites of the acid catalysts, temperature-programmed desorption (TPD) experiment was performed using NH_3 gas with a mass spectrometer detector. TPD analyses were carried out in a flow reactor by pulse injection method using 0.05 g of catalyst in each measurement. Pre-treatment process was performed at 383 K in order to remove adsorbed water, and physically adsorbed NH_3 molecules were removed at 373 K before the TPD analysis. The temperature was increased up to 773 K at a rate of 5 K min^{-1}. The outlet gas was analyzed by an on-line mass spectrometer (VG Sensorlab). In order to avoid the peak from water fragmentation, the fragment with m/e = 16 was used for the ammonia desorption peak.

3.2.3 Catalytic activity

The liquid-phase dehydration of n-butanol to di-n-butyl ether (DNBE) was carried out over heteropolyacid ($H_3PW_{12}O_{40}$, PW) supported on various silicas in pyrex batch reactor, which was enclosed in an autoclave. In each reaction, 50 mL of n-butanol was used for the reactant with 0.1 g of powdered catalyst. The reactor was purged with nitrogen to remove residual oxygen, and the reaction was carried out at a pressure of 30 bar of nitrogen to prevent the vaporization of the reaction mixtures (at reaction temperatures, 453, 473 and 493 K). The product was analyzed by gas chromatography (GC, YL 6200, YoungLin Instrument) with a capillary column (HP-INNOWAX, 30 m × 320 mm × 0.5 lm) and flame ionization detector (FID).

3.3 Results and discussion

3.3.1 Catalyst morphology and pore structure

The 3D open-porous silica was synthesized by a hydrothermal reaction, which is more facile preparation compared to the microwave reaction reported in a previous study [96]. The pore structure and morphology of the prepared ESS were examined by HR-TEM and SEM, as shown in Figure 3-1. A TEM image showed well-oriented Echinometra-shaped porous silica spheres with a regular size of about 450−500 nm. The pores were well developed over the entire surface of the sphere and were three-dimensionally formed from the center to the edge, similar to a dendrimer. The size of the pores exposed on surface was larger (20−30 nm) than that of inner space (3−4 nm) of the material. Using the modified method, 3-dimentionally mesoporous silica spheres (ESS) were successfully prepared and resulted in the production of more uniformly sized nanoparticles compared with the reported method (in the range of size from 250 to 500 nm). For the control experiments, other silica supports, such as SBA-15 (SBA) and microporous silica (mi-S), were prepared by previously reported methods. Further investigations of the pore structure were carried out using a nitrogen adsorption−desorption technique, and the results of the pore size distribution and isotherms of the three samples (SBA, ESS and mi-S) are shown in Figure 3-2. The isotherm curve for SBA showed a hysteresis loop of type IV, characteristic of ordered mesoporous material. In the ESS results, a hysteresis loop was observed in two ranges (0.4−0.7 and 0.8−1.0) of relative P/P_0. These were caused by the developed mesoporosity and some parts of

the pores were formed from the textural porosity between the sphere particles, respectively. Microporous silica only showed textural porosity characteristics from the slit-shaped particles. As shown in Figure 3-2b, synthesized SBA and ESS had very uniform sized pores of 6.5 and 3 nm, respectively, and the pores of the mi-S were very small; below 1−2 nm. As shown in Table 3-1, the BET surface area of the ESS support (570 m^2 g^{-1}) was larger than that of mi-S (217 m^2 g^{-1}), but smaller than that of the SBA support (670 m^2 g^{-1}). The area developed from micro-sized pores of ESS was smaller than that of SBA. A significant microporosity was observed in mi-S supports, a factor that is related to the mass transport of reactants. The prepared SBA, DSS and mi-S materials were used as a support material in preparing $H_3PW_{12}O_{40}$ (PW) catalysts. Images of the PW catalysts supported on three different silica materials were obtained by HR-TEM and SEM. As shown in Figure 3-3, the supported PW catalysts showed different pore shapes, such as the long hexagonal shape (PW/SBA), 3-dimentionally-opened shape (PW/ESS) and a slab shape (PW/mi-S). The pores of the PW/SBA catalyst were well developed, and hexagonally shaped with average particle lengths of 1μm. The PW/mi-S showed a slit-like morphology and its pore structure was not clearly observed in TEM images due to the very small-sized pores (~ 2 nm) of the materials [97]. The image of the PW/ESS sample revealed that it had a three dimensional, Echinometra-shaped structure and that reactant, n-butanol, were readily able to access the pores. Importantly, the porous structures of prepared supports remained unchanged after impregnation with a heteropoly acid.

3.3.2 Crystalline structure and acidic properties

To investigate the crystalline structure of active material and support, we analyzed the X-ray diffraction of the samples and the results were represented in Figure 3-4. Three different silica supports were shown an amorphous structure, so there were no characteristic peaks for crystalline SiO_2. Characteristic peaks corresponding to active sites, heteropolyacid (PW), were not observed on the PW/SBA and PW/ESS samples, indicating that the PW was finely dispersed on the silica supports due to their large surface area. From the XRD patterns of the PW/mi-S sample, characteristic peaks corresponding to the presence of PW were observed. However the intensity was lower than that of the bulk PW, and the overall shape of patterns was looks like amorphous silica material [98, 99]. Therefore, we conclude that the active sites on the PW/mi-S catalyst were also well dispersed on the mi-S support. The amounts of active sites were evaluated by an ammonia temperature-programmed desorption (TPD) technique. As seen in Figure 3-5, three desorption peaks, corresponding to different acidic strengths, were observed in the supported PW on porous silica. On the porous silica support, the desorption temperature corresponding to three peaks of weak (~ 523 K), medium (573−673 K) and strong (over 673 K) acid sites were shifted to higher temperature, compared to a non-porous silica support. It is due to the interaction of heteropolyacid with porous silica, which is stronger than that of non-porous support through an extensive dispersion of PW with the large surface area of porous materials [100]. The strong acidic sites of the prepared catalysts had a positive effect on the dehydration of n-butanol [48]. Both the amount of acid site and acidic

strength were increased with increasing BET surface area (SBA >ESS > mi-S). The amount of adsorbed ammonia, calculated by a pulse injection technique in the TPD analysis was found tobe 3.23, 2.18 and 1.02 mmol on the surface of 1 g of the PW/SBA, PW/ESS, and PW/mi-S, samples, respectively.

3.3.3 Effect of porous structure on catalytic performance

To elucidate the effect of the porosity of the structure on the dehydration of n-butanol, we carried out the reaction in liquid phase using an autoclave batch reactor. The reaction was performed at 473 K and for 10 h and the results are shown in Figure 3-6. In view of acidic amount and strength, the PW/SBA was respected to show higher performance in dehydration of n-butanol than that of PW/ESS and PW/mi-S in Section 3.3.2. However, the PW/ESS catalyst showed the highest conversion for time-on-stream, and showed a better performance for the yield of DNBE than the PW/SBA and PW/mi-S (Yield of DNBE: 43%, 53%, and 36% over PW/SBA, PW/DSS and PW/mi-S, respectively). Non-catalytic reaction tests confirmed that this reaction can only proceed via catalysis, which means that the activity was completely dependent on the activity of the catalyst. Although the PW/SBA was shown to have a larger pore size and surface area than the PW/DSS catalyst, the conversion of n-butanol and the yield of DNBE were lower compared to the 3D open porous catalyst, PW/DSS. This can be attributed to the fact that the dehydration of n-butanol is diffusion limited in a porous catalyst [51]. Further investigations were carried out using kinetic study in order to elucidate the effect of porous materials on the dehydration of n-

butanol.

3.3.4 Kinetic study for internal mass transfer

The kinetics of the reaction have been investigated by many researchers [87, 101-103], and the Langmuir–Hinshelwood kinetic model appears to be an appropriate mathematical model for accomplishing this. However, if the adsorption of DNBE is not significant compared with n-butanol or water, the rate raw can be expressed by equation 1; where *k* is the reaction rate constant, *K* is the equilibrium constant, [C_4H_9OH] and [water] are the concentrations of the n-butanol and water, respectively [104].

$$-r = \frac{k[BuOH]}{1 + K[H_2O]} \qquad (1)$$

In order to obtain the kinetic parameters, *k* and *K*, Eq. (2) was derived by integrating Eq. (1). The parameters '*a*' and '*b*' were defined as the function of *k* and *K*, and '*t*' and '*X*' indicate the reaction time and the conversion of n-butanol, respectively.

$$t = a\ln(1 - X) - bX \qquad (2)$$

The activity tests were carried out at three temperatures of 453, 473 and 493 K to investigate the kinetic parameters based on Eq.(2), as shown in Figure 3-7. The conversion of n-butanol was increased with increasing temperature for all samples, and PW/ESS showed the highest conversion at

various reaction temperatures. Through curve fitting of conversion versus reaction time with a non-linear regression the parameters '*a*' and '*b*' were obtained, and the kinetic parameters *k* and *K* were then calculated using the corresponding definition. The results were listed in Table 3-2 and Figure 3-8 shows the results for the experimental and calculated curves for conversion versus time at 453, 473 and 493 K for the dehydration of n-butnaol for the three different catalysts. As shown in Table 3-2, the reaction rate constant *k* increased with increasing reaction temperature, and the value for *k* using the PW/ESS catalyst was the highest among the prepared catalysts. Figure 3-9 shows an Arrhenius plot of the rate constant *k* for the prepared heteropoly acid supported on different types of silica. The activation energy for the dehydration of n-butanol was determined from the slope of Arrhenius plots. The values for the activation energy of the PW/ESS, PW/SBA, and PW/mi-S were 24.4, 22.7, and 19.5 kcal mol^{-1}, respectively, as listed in Table 3-3. The value for the activation energy on PW/ESS is slightly higher than the values for the other samples. This can be attributed to the fact that the reaction rate constant increases rapidly with increasing reaction temperature. The increasing rate of the rate constant on the PW/ESS is also the largest among the prepared catalysts, as seen in Figure 3-10. As the temperature for the dehydration of n-butanol is increased, the ratio of various formed byproduct butenes increases. Makarova et al. [52, 105] reported that the activation energy for the formation of butenes is much higher (more than 1.5 times) than that of ethers. Therefore, on the PW/ESS, the reaction rate is accelerated for the production of both ether and butene, resulting in the higher activation energy in the range of reaction temperatures. The measured kinetic parameters were used to calculate the effectiveness factor (η) of the

various catalysts. The effectiveness factor was defined as the actual rate ofthe reaction (r_a) over the rate of reaction where the interior surface was exposed to the external surface conditions (r_{as}) [106, 107]. Based on the calculated effectiveness factor, it can be concluded that the actual reaction rate of the three different catalysts was decreased compared with theoretical reaction rate. This decrease was attributed by the internal mass transfer resistance in the dehydration of n-butanol. The term for the actual reaction rate in the equation of effectiveness factor was calculated using the data obtained for *k* and *K* at 493 K. The reason for the calculation using the data of the high temperature is the reaction rate was strongly dominated by mass transfer in the high temperature region [108]. The ideal term of reaction rate was obtained by theoretical calculation with the kinetic parameters at 453 and 473 K through the Arrhenius equation and Van't Hoff equations, assumed that the active site was exposed to only on the surface at 493 K, in defining the effectiveness factor. Firstly, in order to check the effect of external mass transfer on catalytic conversion, the activity test was carried out using different stirring speeds at 493 K for 4 h in the batch reactor. No significant effect of external diffusion was found for this stirring speed, as shown in Figure 3-11. As shown in Table 3-3, the effectiveness factors for the PW/SBA, PW/ESS and PW/mi-S catalysts were 0.63, 0.83 and 0.52, respectively. Among the catalysts examined, PW/ESS showed the highest value for the effectiveness factor, which means that the molecules in the pores of ESS were transferred more efficiently than the other porous catalysts. Compared to PW/SBA, PW/ESS showed a larger effectiveness factor above 30 %. This is the why the PW/ESS catalyst showed a better performance in the dehydration of n-butanol. The effectiveness factor for

PW/SBA was not significantly different compared with PW/mi-S, 0.63 and 0.52 respectively, although the pore size of PW/SBA (6.5 nm) was much larger than that of PW/mi-S (less than 2 nm). It is due to the length of the pores in the SBA catalyst is too long to approach of the molecules to the active sites. Thus, the performance of the PW/ESS catalyst, which has a three dimensional opened pore structure, was better in dehydration of n-butanol than a 2D hexagonal porous and microporous on slab structure, due to the increase in reactant transport by greater pore size or shorter diffusion length. Consequently, the catalyst with a 3D structure showed a dramatically enhanced accessibility because its structure facilitates the contact of molecules with the active sitein the pores. This suggests that the high accessibility of n-butanol to the active sites inside the catalyst is a key factor among other factors, such as the size or length of the pores as seen in Figure 3-12.

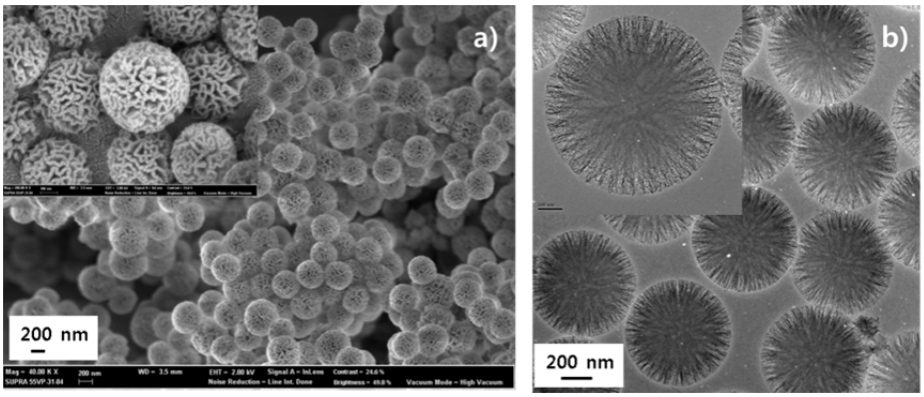

Figure 3-1. (a) FE-SEM and (b) HR-TEM images of prepared Echinometra silica sphere (ESS).

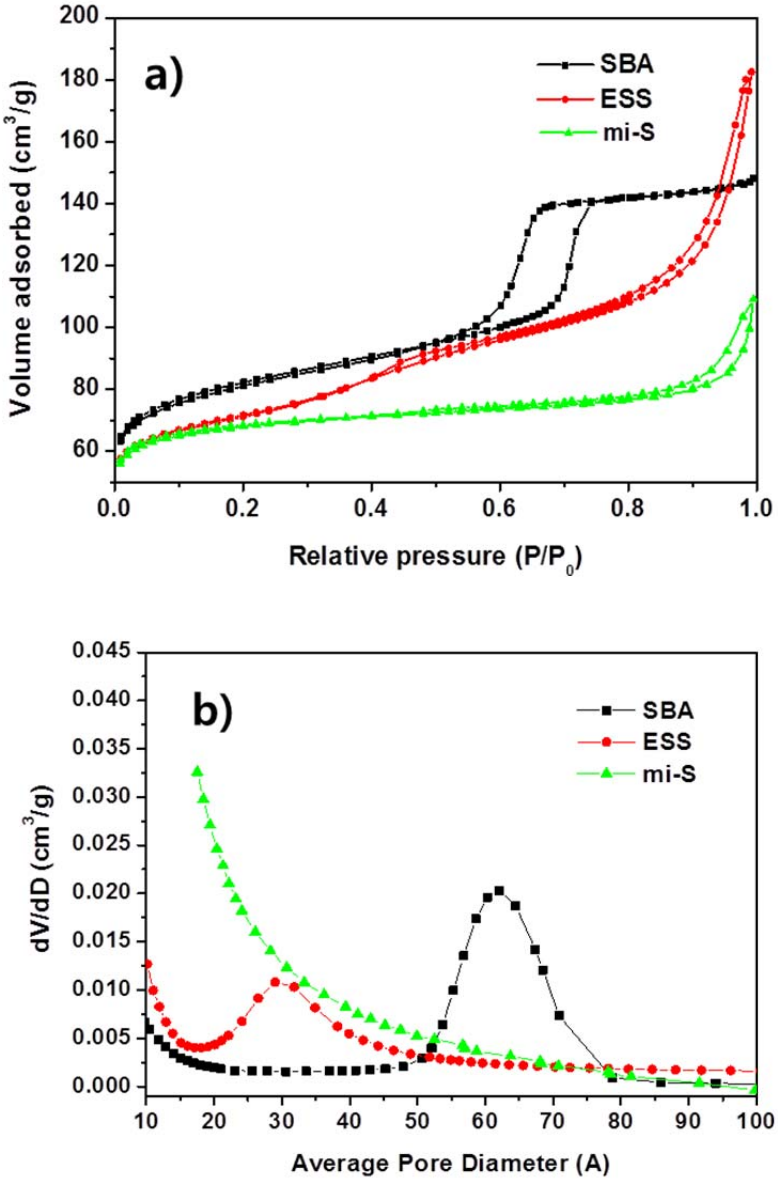

Figure 3-2. (a) N_2 adsorption−desorption isotherm curve and (b) pore size distribution of the prepared SBA, ESS, and microporous silica samples.

Table 3-1. BET surface area and porosity of the prepared SBA-15, ESS and microporous silica supports.

Catalysts	**BET Surface area (m^2/g)**	**Micropore area (m^2/g)**	**Micropore volume (cm^3/g)**	**Pore size (nm)**
SBA	679	97	0.029	6
ESS	570	25	0.013	3
mi-S	217	157	0.08	< 1~2

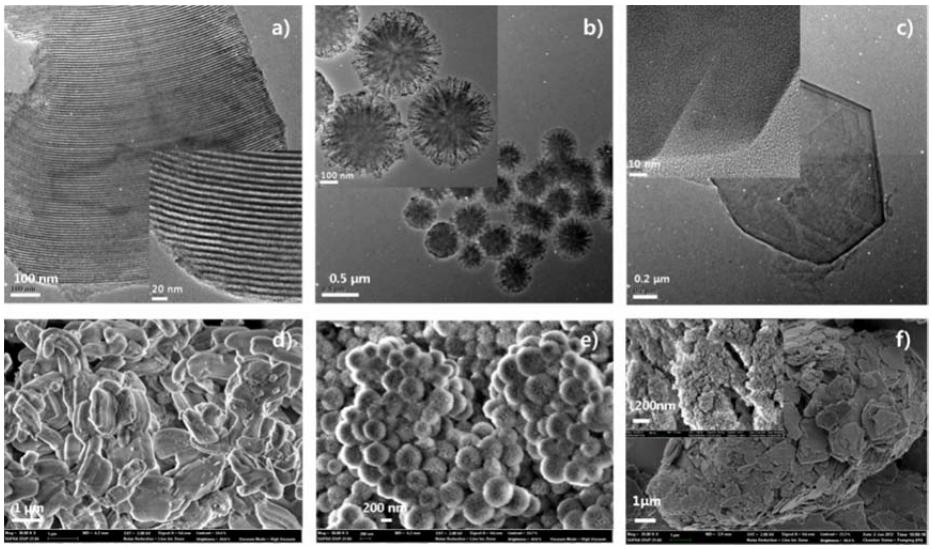

Figure 3-3. Morphologies of the different porous catalysts by HR-TEM and SEM images. (a) and (d) PW/SBA, (b) and (e) PW/ESS, (c) and (f) PW/mi-S.

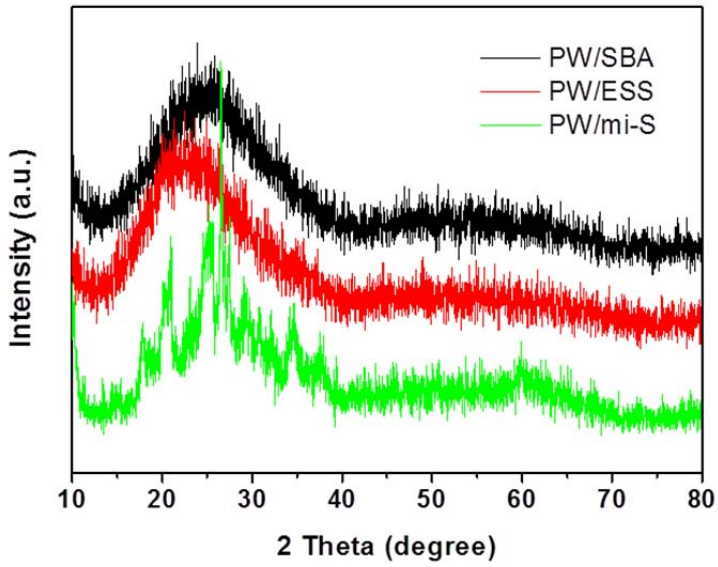

Figure 3-4. X-ray diffraction patterns of PW/SBA, PW/ESS and PW/mi-S.

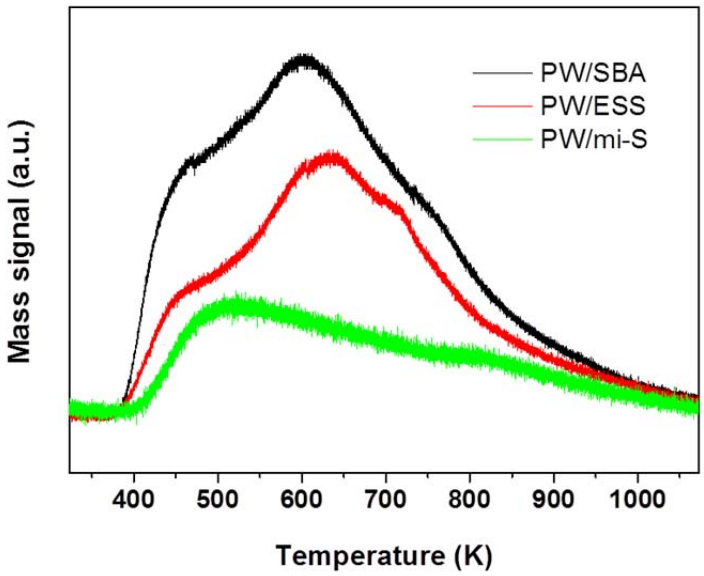

Figure 3-5. NH_3-TPD profiles of PW/SBA, PW/ESS and PW/mi-S.

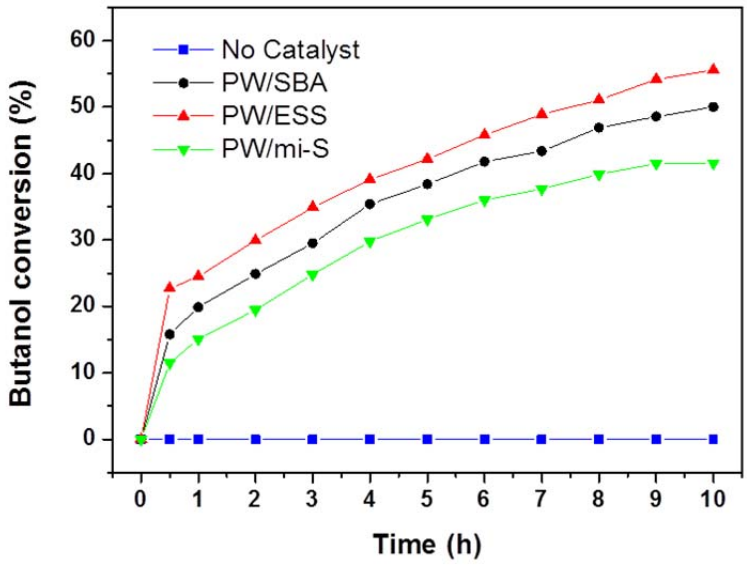

Figure 3-6. The conversion of n-butanol as a function of time-on-stream over PW/SBA, PW/ESS and PW/mi-S catalysts in the liquid-phase dehydration of n-butanol to di-n-butylether (DNBE). (Reaction conditions: 50 mL of n-butanol, 0.3 g of catalyst,473 K, 30 atm in nitrogen atmosphere, 400 rpm of stirring speed.)

Integration of the kinetic model

$2C_4H_{10}O \rightarrow C_8H_{18}O + H_2O$ <Stoichiometric equation>

$$-r = \frac{k[BuOH]}{1 + K[H_2O]}$$ <Rate raw>

(X : Butanol conversion, k : Reaction rate constant, K : Equilibrium constant, C_A : Butanol concentration at t, C_{A0} : Initial concentration of butanol)

➔ $$-\frac{dC_A}{dt} = \frac{kC_{A0}(1-X)}{1 + K\frac{1}{2}C_{A0}X} = C_{A0}\frac{dX}{dt}$$

➔ $$\int \frac{1 + K\frac{1}{2}C_{A0}X}{1-X} dX = \int k dt$$

➔ $$\int \left(\frac{1}{1-X} + \frac{1}{2}C_{A0}K\frac{X}{1-X} \right) dX = \int k dt$$

➔ $-\ln(1-X)-\frac{1}{2}C_{A0}K\left(X+\ln(1-X)\right)=kt$

➔ $-(1+\frac{1}{2}C_{A0}K)\ln(1-X)-\frac{1}{2}C_{A0}KX=kt$

➔ $t=-\frac{1}{k}(1+\frac{1}{2}C_{A0}K)\ln(1-X)-\frac{1}{2k}C_{A0}KX$

➔ $t=a\ln(1-X)-bX$ ---------- Equation 2

Where, $a=-\frac{1}{k}(1+\frac{1}{2}C_{A0}K), b=\frac{1}{2k}C_{A0}KX$ ----Equation S1

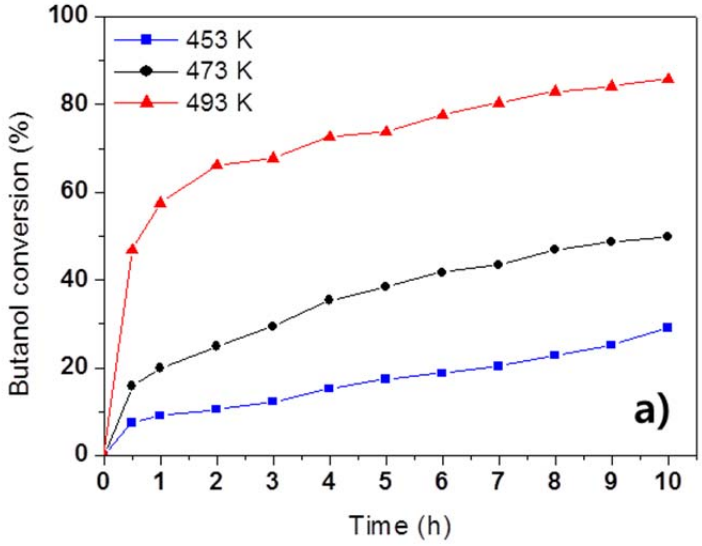
453 K
473 K
493 K
Butanol conversion (%)
Time (h)
a)

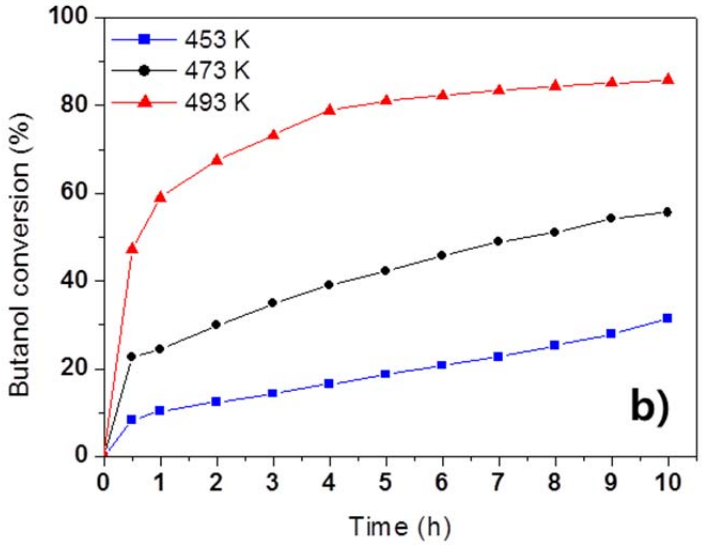
453 K
473 K
493 K
Butanol conversion (%)
Time (h)
b)

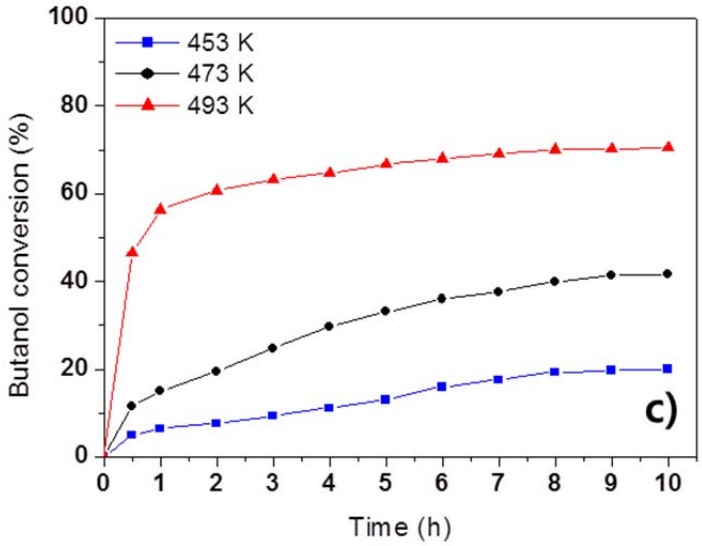

Figure 3-7. Conversions of the prepared catalysts at different temperatures in liquid phase n-butanol dehydration. (a) PW/SBA, (b) PW/ESS and (c) PW/mi-S. (Reactionconditions: 50 mL of n-butanol, 0.3 g of catalyst, 30 atm in nitrogen atmosphere,400 rpm of stirring speed, batch reactor.)

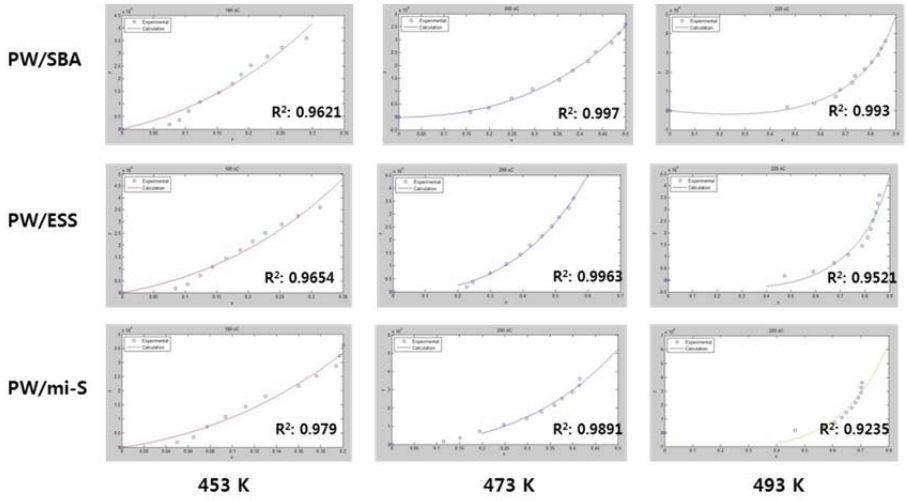

Figure 3-8. The regression results for the experimental and calculated curves for conversion (*x*-axis) versus time (*y*-axis) at 453, 473 and 493 K.

Table 3-2. Calculated kinetic parameters by non-linear curve fitting.

Catalysts	Temp. (K)	*a*	*b*	*k* (s^{-1})	*K* (g_{cat} mol^{-1})
PW/SBA	453	-429440	371080	0.00450	7065
	473	-185300	186630	0.00968	6561
	493	-43842	57746	0.03544	5683
PW/ESS	453	-392890	346230	0.00487	7001
	473	-151940	157050	0.01165	6476
	493	-42993	61432	0.04447	5421
PW/mi-S	453	-971200	917470	0.00191	6772
	473	-273680	274790	0.00656	6572
	493	-134910	191320	0.01104	5446

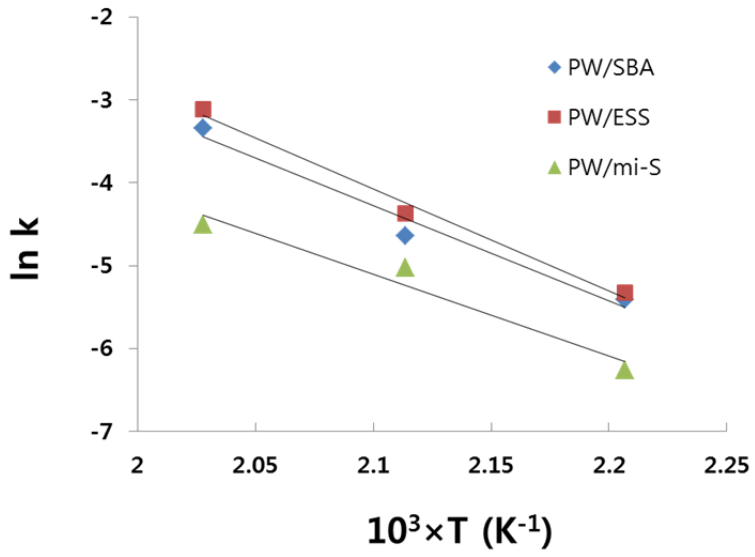

Figure 3-9. Arrhenius plots of constants *k* for the different catalysts.

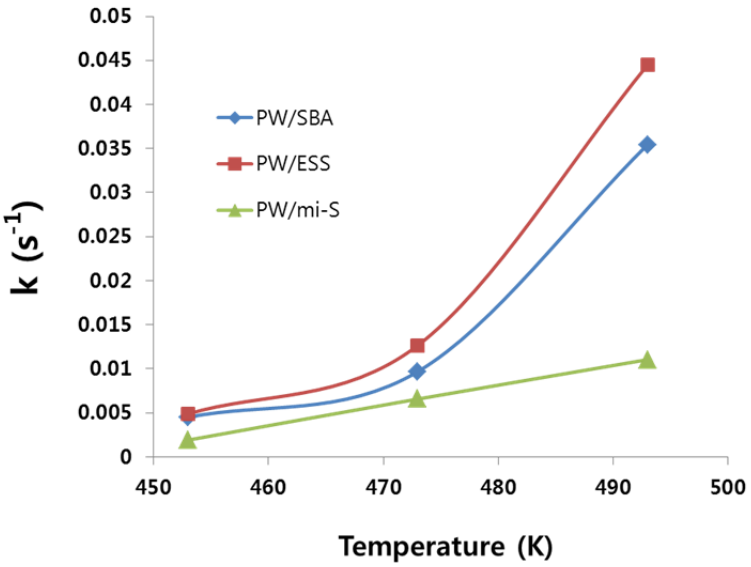

Figure 3-10. Rate constant as increasing a reaction temperature on the PW/ESS, PW/SBA, and PW/mi-S.

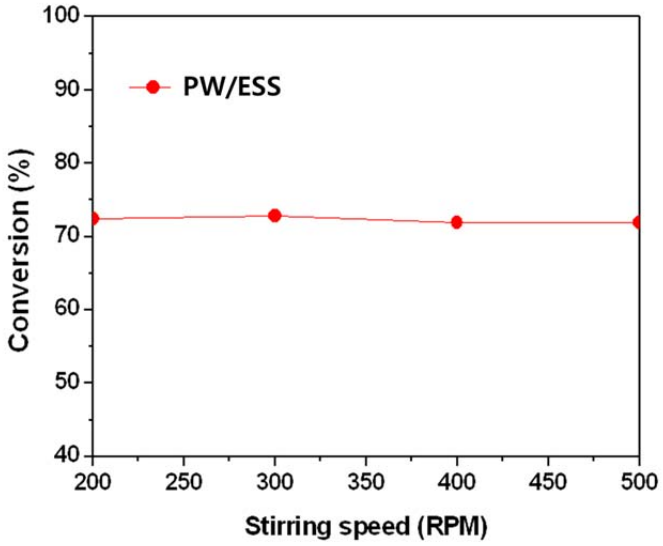

Figure 3-11. Conversion of the PW/ESS prepared at different stirring speeds from 200 to 500 rpm at 493 K for 4 h.

Table 3-3. Calculated various kinetic parameters and effectiveness factor of the PW/ESS, PW/SBA, and PW/mi-S catalysts.

Catalysts	k (h^{-1})	E_a (kcal mol^{-1})	$-r_{as}$ (mol s^{-1} gcat.$^{-1}$)	$-r_a$ (mol s^{-1} gcat.$^{-1}$)	η ($-r_a/-r_{as}$)
PW/DSS	0.0445	24.4	3.22	2.69	0.83
PW/SBA	0.0354	22.7	3.28	2.06	0.63
PW/mi-S	0.0110	19.5	3.28	1.69	0.52

Calculation of the rates (r_a (1) and r_{as} (2))

$$-r_a = \frac{k_{\exp} C_{A0}(1 - X_{\exp})}{1 + K\frac{1}{2}C_{A0}X_{\exp}} \text{ ---------- (1)}$$

Where $-r_a$ (1) indicates the actual rate of reaction

$k_{\exp}, X_{\exp}$ = Experimentally measured value

$$-r_{as} = \frac{k_{cal} C_{A0}(1 - X_{cal})}{1 + K\frac{1}{2}C_{A0}X_{cal}} \text{ ---------- (2)}$$

Where $-r_{as}$ (2) is the rate of reaction where the interior surface were exposed to the external surface conditions

k_{cal} = Calculated value using Arrhenius equation

X_{cal} = Calculated value (solve two equations between equation S1 and equation 2)

Equation S1 $\rightarrow$ $a = -\frac{1}{k_{cal}}(1 + \frac{1}{2}C_{A0}K), b = \frac{1}{2k_{cal}}C_{A0}KX_{cal}$

Equation 2 $\rightarrow$ $t = a\ln(1 - X_{cal}) - bX_{cal}$

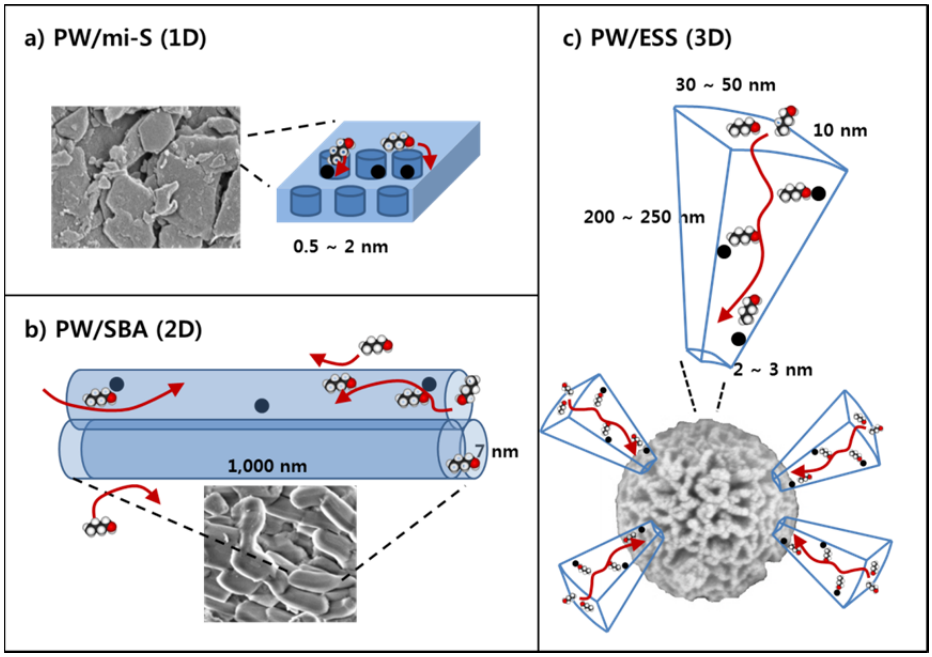

Figure 3-12. Suggested diffusion pathway of n-butanol on the different porous catalysts. (a) PW/mi-S, (b) PW/SBA and (c) PW/ESS.

Chapter 4. Preparation of 3D mesoporous carbon and its application fot the conversion of lignocellulose to sugar alcohols; Enhacing the accessibility to the catalyst

4.1 Introduction

The conversion of biomass, a promising alternative to fossil fuels, into value-added chemicals is an important technology in the renewable and sustainable chemical industry [109-111]. Lignocellulose, a component of wood, is the most abundant and non-digestible source of biomass and consists of cellulose, hemicellulose, and lignin. Cellulose, a major constituent of lignocellulose, is composed of glucose units linked by β-1,4-glycosidicbonds, which lead to a planar sheet arrangement that is held together by intermolecular hydrogen bonding or van der Waals forces between the glycosidic bonds. Owing to these structural characteristics, cellulose is not soluble in most conventional solvents, including water [112-116]. This is the major hindrance to the hydrolysis of cellulose on solid acid catalysts for the formation of soluble and lower molecular weight compounds, a primary step in preparing high-value chemicals. A breakthrough to resolving this issue is the use of ionic liquids as solvents; however, the extraction of products in ionic liquids is very difficult and ionic liquids are currently expensive to recover for reuse. Mesoporous carbon has

been recently widely explored as a candidate material in lignocellulosic biomass conversion since Y. Zhang and co-workers [117] reported the WC_x/MC catalyst and showed high yield of ethylene glycol (72.9 %) from cellulose conversion. Remarkable advances have been achieved in lignocellulosic biomass conversion through the use of carbon materials, because they are not only highly resistant to acidic media but also low cost. In addition, carbon has the excellent ability of adsorbing β-1,4 glucans via their OH groups and has a tendency to become hydrated in the presence of water [124-127]. Hara and co-workers [122, 123] improved the enhanced affinity between carbon materials and water insoluble cellulose by hydrogen−oxygen interactions. Since these findings, various carbon materials that are included in the class of mesoporous carbon have been used in the production of glucose or polyols.

We focused on the preparation of a new fibrous 3D carbon material, which mimics the shape of the sea urchin Echinometra mathae in an attempt to enhance the affinity of cellulose for the catalyst. The prepared material was used as a support for a Pt-based catalyst and was applied in the direct conversion of cellulose to a hexitol (sugar alcohol) which is one of the most attractive routes for the production of value-added building blocks. Since Fukuoka's [112] first investigation of the one-pot conversion of cellulose into hexitols over Pt/γ-Al_2O_3, interest has focused on designing bifunctional catalysts for both hydrolysis and hydrogenation [109, 110, 121]. Mechanistic studies indicated that metallic Pt performs not only hydrogenation but also the in situ generation of protons by H_2 dissociation or the splitting of water on the surface, resulting in the hydrolysis of cellulose [118-120]. During these investigations, several researchers developed dual-functionalized

catalysts, such as Ni–X (Pt, Ru, Rh) supported on mesoporous carbon (50~60 % yield of hexitol) or nitric acid treated Ni/CNF (76 % of yield of hexitol) [128-132]. Although they showed a relatively high performance, a major drawback was the need for an additional acid treatment of the catalyst for efficient hydrolysis of cellulose by H^+ species.

Herein, we report not only on the synthesis of a new 3D mesoporous carbon material, but also the design of a catalyst in which acid treatment is not needed for activity, resulting in a more facile and eco-friendly catalyst preparation. We showed that the Pt-based catalyst supported on 3D carbon was very active for the conversion of cellulose to hexitols (close to an 80 % yield) without the need for an additional acid treatment of the catalyst. The Pt-based catalyst with abundant oxygen functional groups on the fibrous 3D mesoporous carbon synthesized from a phenolic resin [39, 133] brings about an increased hydrogenutilization on the Pt metal by increasing the spillovereffect [134-136]. This leads to the formation of H^+ from the hydrogen sources on the Pt metal, resulting in a catalyst that can be applied in the hydrolysis of cellulose without the need for an acid treatment step. We investigated the two-step mechanisms on the mesoporous catalysts in the direct conversion of cellulose to hexitols by accessibility tests, H_2 uptake, and electrochemical lanalyses. The activity test for the direct conversion of hardwood powder suggests that the prepared 3D mesoporous carbon will perform remarkably in the conversion of lignocellulosic biomass materials.

4.2 Experimental

4.2.1 Preparation of catalysts

Carbon Nano Echinometramathae (CNE) was synthesized by a hard template method using phenol formaldehyde resin. The synthesis of phenolic resin was referred to the method of Yan Meng et al [39]. To synthesize of the 3-dimentionally opened porous silica, we modified a previously reported synthetic method which uses a microwave reactor. Echinometramathae shaped Silica Spheres (ESS) was prepared by a water-in-oil microemulsion process in a hydrothermal reactor. 2.5 g of tetraethyl orthosilicate (TEOS) was dissolved in 30 mL of cyclohexane and 1.5 mL of pentanol. A solution of cetylpyridinium bromide (CPB; 1 g) and 0.6 g of urea in 30 mL of water was then added to the solution. The mixed solution was reacted at 393 K for 4 h in an autoclave with vigorous stirring. After the reaction, the suspension was slowly cooled to room temperature and the product was isolated by centrifugation. The resulting material was centrifuged with a mixture of D.I water and acetone (1:1 volume ratio) three times. The obtained precipitate was dried at room temperature for 24 h, and the dried material was calcined at 823 K (ramping rate of 1 K min^{-1}) for 6 h in the atmosphere of air. Echinometra Mathae shaped silica (ESS) which was used as hard template and resol precursors were mixed and centrifuged at 10,000 rpm for 50 minutes. Excess resin was removed and the solid product was dried at room temperature in air. The resulting sample was aged at 373 K in air and carbonized at 1173 K for 3 h in the flow of N_2. The DSS-Carbon composite was etched for 24 h using HF, followed by filtering and drying at room

temperature in air.

An aqueous solution of $PtH_2Cl_6xH_2O$ (30 mL, 0.108 g) was added to a mixture of carbon 1 g and water 100 mL. Sodium hydroxide (0.1 M, 5-7 mL) was added dropwise to the solution until the pH 11 was almost. Sodium borohydride (0.1 M, 100 mL) was added and stirred for 3 h in order to reduce the Pt ion. After filtering and washing the mixture, we obtained Pt deposited on carbon [142].

4.2.2 Characterization

The transmission electron microscopy (TEM) and the scanning electron microscope (SEM) images were obtained on a JEOL JEM-3010 microscope operating at 300 kV and Carl Zeiss SUPRA 55VP field-emission scanning electron microscope respectively. In order to explore the element distribution mapping on the samples, an analytical high-angle annular dark-field scanning transmission electron microscope (HAADF-STEM, Tecnai F20-FEI, 200 kV) equipped with energy dispersive X-ray spectroscopy (EDS, Tecnai 136-5-EDAX) was used. X-ray powder diffraction (XRD) patterns of the catalysts were measured with a Rigaku D-MAX2500-PC powder X-ray diffractometer operating at 50 kV and 100 mA using Cu Kα radiation (1.5406 Å). Thermogravimetric analysis (TGA, SDT Q600, TA instruments) were performed under flux of air at a heating rate of 10 K min^{-1}.

The N_2 adsorption-desorption isotherms, the BET surface area and the external surface area were determined using an ASAP 2010 Micromeritics apparatus. The pore volume and diameter were examined using the method of Barrett–Joyner–Halenda (BJH) applied to the desorption branch of the

isotherm. The temperature-programmed desorption (TPD) profiles were measured on a MicromeriticsAutochemII chemisorption analyzer. In the case of NH_3-TPD, a 50 mg of sample loaded in a quartz reactor was pretreated in a He flow at 573 K for 3 h, and then cooled to room temperature. The samples were then exposed to a gas mixture and kept at 323 K for 2 h for adsorption. After removing the NH_3 by purging with He, NH_3-TPD profiles were obtained in a flow by heating up to 900 K at a rate of 10 K min-1. The outlet gas was analyzed by an on-line mass spectrometer (QGA, HIDEN ANALYTICAL). In order to avoid the peak from water fragmentation, the fragment with m/e = 16 was used for the ammonia desorption peak. For a H_2-TPD measurement, the temperature was ramped from 323 K to 1073 K at a rate of 10 K min^{-1} in 10 % H_2/Ar flow. Prior to obtain the profiles, the samples were pretreated at 453 K for 3 h in an Ar flow. The Platinum dispersion was calculated by pulse chemisorption method in H_2 using the Micromeritics ASAP 2920 instrument. X-ray photoelectron spectroscopic (XPS) technique was taken on a AXIS-HSi (KRATOS) instrument. The binding energy of each elements are calibrated by using carbon peak for standard (C 1s = 284.5 eV).

After the hydrolytic hydrogenation of cellulose, the leaching amount of platinum was analyzed by inductively coupled plasma-Mass (ICP-Mass) Spectrometer (PERKIN-ELMER SCIEX, ELAN 6100).

Electrochemical analyses were conducted using a standard three-electrode cell system with a platinum plate of 3 cm^2 (counterelectrode). A saturated Ag/AgCl electrode was used as the reference electrode. A working electrode was prepared by mixing 80 wt.% of the synthesized active material, 10 wt% Ketjen black, and 10 wt.% poly (tetrafluoroethylene) (PTFE, Sigma-Aldrich)

of the total electrode mass (ca. 7 mg). The three components were mixed with a few drops of 2-propanol (Sigma-Aldrich) to form a rubber-like paste. It was loaded on both sides of an SUS mesh (1 cm^2) and was compressed to prepare a pellet-type electrode. Cyclic voltammetry was carried out using a computer-controlled potentiostat (Iviumstat, Ivium). The electrochemical measurements were carried out in a 0.5 M H_2SO_4 solution at room temperature.

4.2.3 Catalytic activity

Hydrolytic hydrogenation was carried out in a Teflon-lined stainless steel autoclave reactor (Hanwoul Co., 100 mL). In each reaction, cellulose (0.4 g), pre-treated milled for 2 hours (HP-Ballmilling), catalyst (0.2 g), and distilled water (40 mL) were placed into the pyrex reactor (100 mL). Before the reaction, the reactor was purged 3 times with N_2, and filled with 50 bar of H_2 at room temperature. After the reaction, the products were separated by filtration and water-soluble products were analyzed by high-performance liquid chromatography (HPLC; Younglin Instrument, YL 9100, Metacarb 67C column, R.I. detector). The products were also analyzed by means of a GC-Mass system (Agilent Technologies, 7890 A) with Agilent Tech. 5975 C mass detector (HP-5MS capillary column). Cellulose conversion was determined by the weight difference of cellulose before and after the reaction. The yield of sugar alcohols was calculated using the following equation: yield (%) = (weight of sugar alcohol in the products) / (weight of cellulose put in to the reactor) × 100 %. To confirm mole of carbon in the charged cellulose, the conversion was also calculated by TOC (total organic carbon)

method using Total Organic Carbon Analyzer (Sievers 5310 C, GE) (Conversion (%) = TOC × 4250^{-1} × 100 %). The 4250 (ppm) represents to the carbon content of the cellulose in the reactor which was determined by elemental analysis.

4.3 Results and discussion

4.3.1 Preparation of the 3D mesoporous carbon

The EchinometraMathae-like mesoporous carbon (Carbon Nano-EchinometraMathae, CNE) was prepared by nanocasting a replica of a silica template. Such fibrous mesoporous silica spheres, such as KCC-1, have been exploitedin various research fieldsafter their first report in 2010 by Basset et al [137-140]. We modified the synthetic method for preparing KCC-1 by a hydrothermal reaction, and it was used as a hard template for preparing a uniquely structured carbon material. The structures of the 3D CNE were characterized by TEM and SEM, as shown in Figure 4-1.The TEM image of CNE is similar to the EcinometraMathae shown in Figure 4-1d and e. The CNE consists spherical shaped particles with diameters of 400 nm, smaller than that of the silica template (Figure 4-1a). This can be attributed to the opened structure in part of the edge that resembles the prickles of the spherical particle. The carbon precursor fills the pores from the inside to the edge excluding the very edge part as shown in Figures 4-1b and c. The overall shape and the pore wall were retained during the carbonization and the process of removing the template (Figure 4-1f and h). The carbon source, a polymerized phenol-formaldehyde resin, was extensively incorporated into the 3D interconnected pores, and the coherence was sufficient to retain the morphology by in-situ polymerization on the template. Unlike the replication process, the wall thickness of CNE was reduced compared with the thickness of the pores of the ESS template. This unusual process is due to the shrinkage of the phenolic resin after incorporation into the pores.Thus, the

CNE could be prepared with an exactly same morphology as that of the silica template. However, in the case where a sucrose-sulfuric acid solution was used as a carbon precursor, the pores with broad size were not uniformly filled, as shown in Figure 4-2. In situ polymerized phenol resin has the advantage that a broad size distribution of pores are incorporated and interconnected in the polymeric structure and the final product has sticky properties. As seen in the Figure 4-1g, in the cross section image of CNE, the pores inside of the CNE are partly developed by the removal of the fibrous silica template and have a pseudo hollow structure. Developed pores were formed three-dimentionally from the center with small sized pores on the surface of the sphere, along with some relatively large sized pores. For this reason the surface area of the CNE increased substantially from an ESS template. As evidenced by N_2 adsorption-desorption isotherms (Figure 4-3), the particles had a uniform pore size of 3 nm and a large surface area of 1570 $m^2 g^{-1}$ with a mesoporous area of 1340 $m^2 g^{-1}$. Above 80 % of the surface area consists of meso-sized pores, such a high ratio of the mesoporosity facilitates the accessibility of the large molecules to the pores. Hysteresis loops were found in two ranges (0.4~0.7 and 0.8~1.0) of relative P/P_0. These were caused by mesoporosity (hysteresis loop of type H3 in IUPAC regulation [141]) and the textural porosity of the sphere particles, respectively. We confirmed that the carbon had the characteristics of a conventional amorphous carbon material as evidenced by XRD patterns and TGA analysis (Figure 4-3c and d).

4.3.2 Characterization of the Pt supported on various carbons

The 3D mesoporous CNE provides the multi-sized and three dimensionally opened pores. This unique structure is particularly favorable for the conversion of biomass comprised of relatively large molecules. Therefore, we applied this material to the hydrolytic hydrogenation of cellulose. For the direct conversion of cellulose through hydrolytic hydrogenation, the catalyst needs to contain not only the acidic sites, but also a metal for catalyzing the subsequent hydrogenation. We choose the Pt metal for the hydrogenation in order to induce the development of acidic properties by Pt-hydrogen interactions. Pt nanoparticles are attractive in terms of the hydrogen and the spillover effect, which permits only the characteristics of the CNE excluding the catalytic intrinsic effect to be investigated. The Pt/CNE catalyst was prepared by anelectroless deposition method [142, 143], and the microscopic images are shown in Figure 4-4. The Pt nanoparticles were well dispersed on CNE, dominantly on the edge of the sphere particle as shown in Figure 4-4a. The distance of the lattice was assigned to the simple (111) phase with d-spacing = 1.19 Å. From the STEM image (Figure 4-4c), it is clear that the Pt nanoparticles were dispersed on the 3D CNE sphere particle in a three-dimensional manner, which enhances the accessibility to the active sites on the catalyst. As evidenced by 2-D atomic mapping by a STEM analyzer, the carbon, oxygenated functional group and the Pt nanoparticles were evenly distributed on the 3D particle.

We prepared a series of Pt catalysts supported on carbon materials, such as activated carbon (AC), CNT, MWCNT, CMK-3 (CMK), graphene oxide(GO) and prepared CNE to investigate the effect of 3D mesoporous CNE. As shown in Figure 4-5, on the AC, CMK, and CNE carbon supports, the Pt particles were highly dispersed with 3-4 nm size of nanoparticles due to their

large surface area (larger than 1,000 m^2 g^{-1}, in Table 4-1). However, the Pt/CNT, MWCNT and GO samples showed the lower dispersion than on the amorphous carbon based Pt catalysts. The Pt particles were supported on these supports in which the size range of the Pt particles was 7.5-10 nm, relatively larger than that of amorphous carbons, as evidenced from TEM image and Scherrer equation using XRD patterns (Figure 4-6a). It is because of the low surface area of the carbons and no acidic treatment on CNT, MWCNT, and GO in the preparation process. In electroless deposition method, the Pt ions are easily exchanged in carboxylic group on the surface of carbon materials. On the surface of CNT, MWCNT, and GO, the hydroxyl groups are abundant, but not carboxylic groups, thus additional acid-treated process is required in preparation procedures [142, 143].

From the XRD results (Figure 4-6a), we confirmed that the activated carbon, CMK-3 and CNE had an amorphous structure, and diffraction peaks at 26.5 and 43.16 ^{o} were found for the CNT and MWCNT samples, corresponding to crystalline carbon. An NH_3-TPD analysis was carried out to measure the acidity of the prepared Pt/C catalysts and showed in Figure 4-6b. (Acidity; Pt/GO > Pt/CMK > Pt/CNE > Pt/AC > Pt/CNT > Pt/MWCNT, see the Table 4-1) The Pt/GO catalyst contained a relatively large amount of acidic sites, compared with the other carbon based catalysts because of the large number of acidic sites as the result of having the largest surface area. Many surface functional groups of the carbon material, such as hydroxyl (OH-) groups, which can be useful for the hydrolysis of cellulose to glucose, which proceeds via protonation of the β-1,4-glycosidic bond [122, 123]. The results of N_2 adsorption-desorption of the various prepared Pt/C catalysts are represented in Figure 4-7. The pore diameters of Pt/CMK and Pt/CNE were

3-4 nm and Pt/AC was about 1 nm, which were not changed for each support before Pt immobilization. In the Langmuir isotherm curves, the Pt/CMK and Pt/CNE catalysts showed a similar hysteresis loop which is related to the characteristic of the mesoporous structure of the materials [141].

4.3.3 Hydrolytic hydrogenation

The hydrolytic hydrogenation of cellulose was carried out as a model reaction on the prepared Pt/C catalysts in order to investigate the effect of the carbon materials on catalytic performance. Table 4-2 shows the results for the hydrolytic hydrogenation of cellulose over Pt supported on various carbon materials in a batch reactor. The products, cello-oligomers, glucose and fructose, are produced by the hydrolysis of cellulose, and EG and hexitol are competitively produced by additional hydrogenation after the hydrolysis of the cellulose [144-146]. Without a catalyst, the rate of hydrolysis was minimal, resulting in an approximate yield of 15 % (Entry 1) because of the in-situ produced protons from water at thereaction temperature used [147]. The Pt catalysts supported on mesoporous carbon, Pt/CMK-3 and Pt/CNE (Entry 5 and 7), showed a good selectivity for hexitol (sorbitol + mannitol) against ethylene glycol compared with the AC or CNT supports. This can be attributed to the high utilization of hydrogen, which is also evidenced from the lower yield of the product produced by only catalytic hydrolysis [146]. When the prepared 3D porous catalyst, Pt/CNE, was evaluated, a large amount of hexitol was produced in 60 % yield with a selectivity of 68 % (Entry 7). On the other hand, the use of Pt/AC (Entry 2) and Pt/GO (Entry 6) resulted in a relatively high yield of glucose and fructose. The Pt/CNT and

Pt/MWCNT catalysts resulted in a very low yield for hydrolytic hydrogenation of cellulose. These results suggest that the Pt/mesoporous carbon is a good candidate for use as a catalyst in the hydrolytic hydrogenation of cellulose, and that hydrogen utilization is a very important factor in the selectivity of the catalyst for hexitol. The conversion of cellulose increased with increasing an acidity and with hydrogen pressure (Table 4-1). We also carried out the hydrolytic hydrogenation of cellulose on the sucrose-based Pt/CNE catalyst (Pt/CNE-S) for the comparison to the Pt/CNE synthesized from phenol-aldehyde resin (Pt/CNE-P). As shown in Figure 4-8a and c, the average particle size of Pt on Pt/CNE-S was larger than that of Pt/CNE-P. This is due to the fact that the sucrose sources were not extensively incorporated into the 3D interconnected pores, resulting in poorly developed 3D mesoporous carbon. The cellulose conversion and the yield of hexitols were lower over Pt/CNE-S sample compared to Pt/CNE-P, but the yield of ethylene glycol was slightly higher than Pt/CNE-P (Figure 4-8c). As described above, the amount of surface oxygen groups were increased when the phenol-aldehyde resin was used as a carbon source. Consequently, the phenol-aldehyde resin was a relevant carbon source compared to conventional sucrose source in order to obtain a high yield of hexitols and ordered 3D mesoporous carbon from ESS template.

We carried out activity tests under different reaction conditions, i.e., hydrogen pressure. The yield of hexitol over the Pt/CNE catalyst at 50 bar of H_2 was about 80 % which is the highest performance among the reported catalysts (Entry 9). As the hydrogen pressure is increased, cellulose conversion and the yield of hexitol also increased, however the yields of ethylene glycol, glucose and fructose were lower. This indicates that the

hydrogen capability of the catalyst is highly dependent on the initial pressure of hydrogen.

The prepared Pt/CNE catalyst exhibited a good stability in recycling tests at 453 K in 50 bar of H_2. We confirmed that a leaching of Pt ions nearly never occurred during the reaction from the result of ICP-Mass analysis (0.121 ppb of Pt in aqueous phase products). After the first recycle test, changes in the values of the cellulose conversion and the yield of hexitol were negligible (Entry 10). But the values (cellulose conversion and yield of hexitols) gradually became lower after the 2nd recycling test of Pt/CNE (Entry 11). From the results of the 3rd recycling test, the Pt/CNE catalyst showed cellulose conversion of 91.6 % and a 66 % yield of hexitols, and the selectivity for hexitols was 10 % lower than that for the fresh Pt/CNE catalyst. As seen in Figure 4-9, the particle size of Pt nanoparticle was not changed after 3 times recycling tests, however, the opened 3D mesoporous morphology of Pt/CNE was slightly collapsed, significantly on the edge shape.Therefore, on the inside pores the hydrogenation activity ofsoluble oligomers to sugar alcohols was deactivated, resulting in a decrease in the yield of sugar alcohols. However, the conversion of non-soluble cellulose was slightly lower over used Pt/CNE catalyst because the cellulose was adsorbed and converted on only external surface of catalyst. This conclusion is also verified on the next section through the mechanism study by the control activity tests of cellulose and cellobiose.

4.3.4 Mechanistic study over Pt supported on carbon

To clarify the effect of mesopore-structures on the transport of large

molecules, such as cellulose, we carried out the activity test using different crystalline indexed-cellulose samples as the reactant. Park et al. [148] reported that the accessibility of cellulose is affected by its crystallinity in a water-based medium [148, 149]. We prepared different crystalline cellulose samples by ball-milling cellulose samples under different conditions, and their XRD patterns are represented in Figure 4-10. Pt catalysts supported on amorphous carbons, Pt/AC, Pt/CMK-3 and Pt/CNE, were used in this control activity test to avoid other intrinsic characteristics of carbon materials. As shown in Figure 4-11, the conversion over the mesoporous carbon, using catalysts such as Pt/CMK-3 and Pt/CNE, was lower than that for Pt over activated carbon. However, the yield of sorbitol was higher on the mesoporous carbon based Pt catalysts. The hydrolysis of cellulose involves the protonationof the glycosidic O atom on an acid catalyst. In our Pt/CNE catalytic system, the hydrolytic activity is ascribed to the in-situ formation of H^+ and the functional groups on the carbon support. From this result, it appears the polymerized cellulose is first decomposed to water-soluble oligomers by H^+ ions on the external surface of the carbon support, whereby smaller soluble intermediates are converted into glucose or sorbitol on the inside of the pores [109]. For further investigations of the pore effect, the hydrolysis of cellobiose to glucose was carried out on metal-free carbon supports. Cellobiose is a water-soluble disaccharide consisting of di-glucose and is produced from polymerized cellulose. As seen in Figure 4-11b, the conversion and product yield were rapidly increased on the mesoporous carbon. These results provide sufficient evidence for the mechanism of direct conversion of cellulose to sugar alcohol over a mesoporous carbon based metal catalyst [109, 110].

The Pt in the catalyst not only plays a key role in the hydrogenation of glucose to a hexitol, but also induces hydrolysis through in-situ formation of H^+ by the splitting of hydrogen or water [117-121]. We investigated hydrogen dissociation and the splitting of water on the amorphous carbon supported Pt by the temperature-programmed desorption of H_2 and electro-chemical experiment. In Figure 4-12a, the dissociatively adsorbed hydrogen molecules were desorbed at 300-360 ^oC over the Pt metal supported on amorphous carbon. Among the six Pt/C catalysts, Pt/CNE had the largest amount of desorbed hydrogen (0.342 mmol/g). (See the Table 4-1) The high level of hydrogen desorption is because of the well-dispersed Pt on the three-dimensional CNE structure and the spillover effect on the sufficient oxygen groups on carbon. As seen in the Table 4-1, the dispersion percentage of Pt on CNE was about 35 %, and it is a significantly high value compared to other carbon materials. During electroless deposition where Pt was randomly dispersed and reduced onto the carbon support, ionic exchange occurs between hydroxyl group and Pt ion and the three dimensionally structured open pores and large surface area of CNE seemed to supply a sufficient sites for the exchange. The adsorbed hydrogen on the metal surface can migrate in a form of atomic H onto the carbon support via surface diffusion, and the migrated atomic H is to stable on oxygen functional group with electron in the surface of the support [134]. This phenomenon, called hydrogen spillover, was significantly enhanced on the CNE support because of the presence of numerous oxygen groups on the surface (Figure 4-12c), a deliberate enhancement by utilizing phenolic resin for the oxygen-linked carbon source in synthesis [134-136]. This results in maximizing the spillover effect and increasing the selectivity (above 80% in Table 4-2) for hexitol production

[146]. The H^+ can also be in-situ generated through the electrolysis of H_2O. We also investigated the effect of our catalytic system using electrochemical linear sweep voltammetry as suggested by Koper's group [150], designed in order to apply the cellobiose hydrolysis through generated H^+ from water. From the Figure 4-12b, the oxidation current peak identically begins from 1.0 V in the electrodes prepared with the three catalysts. The current density on Pt/CNE catalyst was higher than that of Pt/AC and Pt/CMK. The result means the oxidation on the anode composed of Pt/CNE is faster compared to other catalysts, although the amount of Pt loaded was almost exactly equal on each carbon support. (Figure 4-10b) From these results, we confirmed the Pt/CNE is also good candidate for the production of H^+ from electrolysis of water.

To elucidate the effect of the hydrogen and the Pt metal, the other control activity test was carried out of CNE and Pt/CNE catalysts with and without hydrogen pressures (Figure 4-13). A small amount of cello-oligomer and glucose could be produced on the CNE in a condition of absence of hydrogen pressure. It is due to the hydrolysis by acidic functional groups (OH- or COOH-) on the surface of CNE and the slightly generated H^+ by water spillover. After addition of hydrogen, the yield of cellooligomer by hydrolysis of cellulose was increased to 27 %. On Pt/CNE samples the hydrolytic hydrogenation was effectively not occurred without hydrogen, however, in the condition of hydrogen atmosphere, the sequential reaction was effectively performed. This result indicates that the Pt/CNE catalyst shows the bifunctional charateristics on the carbonand the Pt metal which role to the hydrolysis and the hydrogenation, respectively [112, 117]. (Figure 4-14)

4.3.5 Lignocellulose conversion using hard wood powder

To investigate the catalytic performance of Pt/CNE in the direct conversion of woody lignocellulose, we carried out the hydrolytic hydrogenation of raw hardwood material (from oak wood consisted in 15.2 % of hemicellulose and 52.9 % of cellulose determined by Wise method [151, 152]), and the results were represented in Table 4-3. The Pt/CNE showed the 53 % of wood conversion, the 12.7 % of pentitols (C5 sugar alcohols) and 12.1 % of hexitols yields. After a ball-milling of the wood powder, the activity was increased about 9 % of the conversion and 6 % of the hexitols yield. However, the yield of pentitols was not increased, after pre-treatment of wood powder by ball-milling. It should be noted that pentitols were mainly produced from hemicellulose (C5 carbons) which is more reactive than cellulose in moderate conditions. Compared to the result for un-milled Avicel PH-101 (cellulose), the selectivity for sugar alcohols was significantly decreased due to the existence of hemicellulose and lignin in hardwood feedstock [153, 154]. In Figure 4-15 and 16, in case of the wood powder was used for the feedstock, the various sugar alcohols, such as, d-glycerol-d-galacto-heptose, 6-Desoxy-l-gulitol, and arabinitol,were produced as different from the results that mostly produced sorbitol in using the Avicel PH-101. Showing a Figure 4-15a, we can find that the product was mostly derived from C6 oligomers, except for the arabinitol, C5 sugar alcohol, in cellulose conversion. However, various C2~C7 acids and alcohols were produced in wood conversion (Figure 4-15b). From the hemicellulose, acetic acid (present on 7 in every 10 sugar units in oak wood hemicellulose), 1,2-propanediol and 1,2-pentanediol were produced by severe heating and the

ring-opening of furan rings. The arabinitol, C5 sugar alcohol, was derived from the arabinose (sugars in hemicellulose) by hydrogenation on noble metal. Meanwhile, from the lignin in lignocellulose, the only vanillic acids were produced in this reaction conditions. Vanillic acids can be released by relatively gentle heat or mild acidic conditions from syringyl structures in lignin [155, 156]. (See the Figure 4-17) These results indicate that an appropriate reaction temperature and hydrogen pressure are required to selectively produce sugar alcohols from lignocellulosic materials. To inhibit the production of C_2~C_4 acids or linear diols from hemicellulose, a non-noble metal catalyst is required for the direct conversion of lignocellulose to sugar alcohols. At moderate reaction temperatures and hydrogen pressures (below 453 K and 50 bar of hydrogen), it is likely that extensively hydrogenated alcohols, such as d-glycerol-d-galacto-heptose, 1,2,6-hexanetriol, and 6-desoxy-l-gulitol would be produced in lower yields from cellulose and hemicellulose, and would also prevent the production of lignin derived chemicals. Although a number of byproducts are produced on Pt/CNE in the hydrolytic hydrogenation of hardwood powder, the 3D mesoporous CNE performed efficiently in terms of the conversion of lignocellulosic biomass materials.

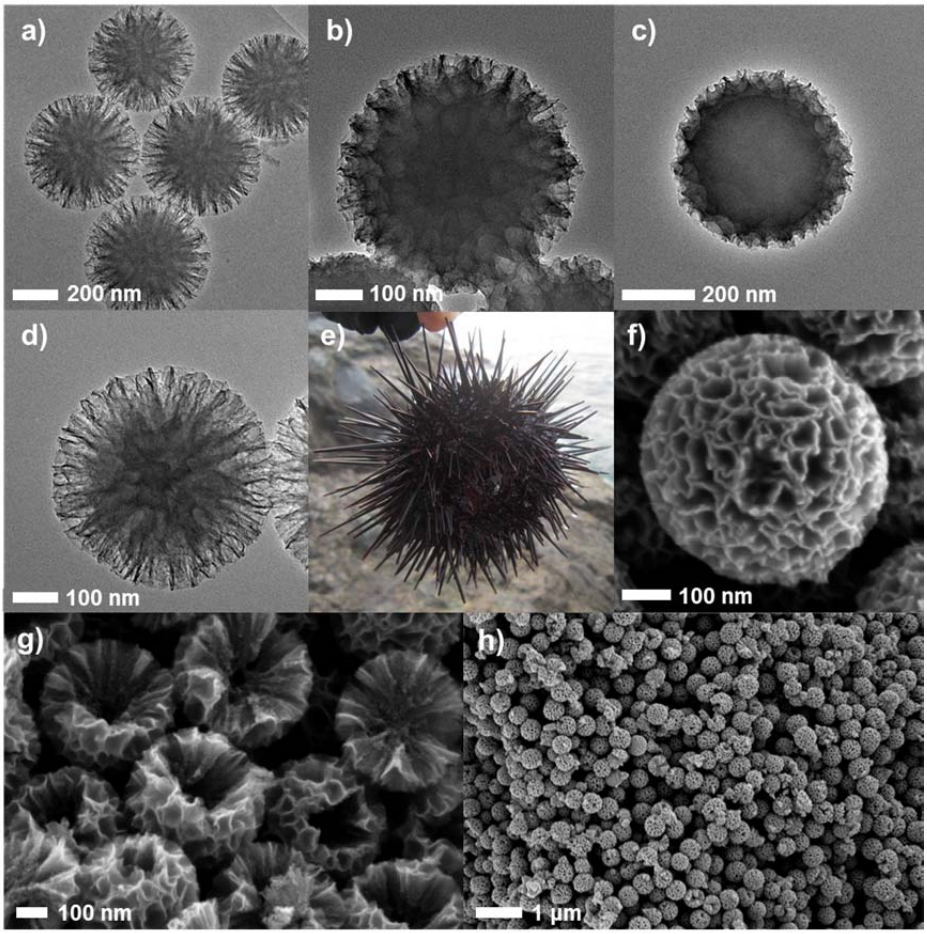

Figure 4-1. HR-TEM images of a) ESS silica template, b) ESS–carbon composite after drying, c) ESS–carbon composite after aging, d) CNE, e) Image of actual Echinometra mathae. SEM images of: f) a particle of CNE, g) cross-section of CNE, and h) prepared CNE particles in a large-scale view.

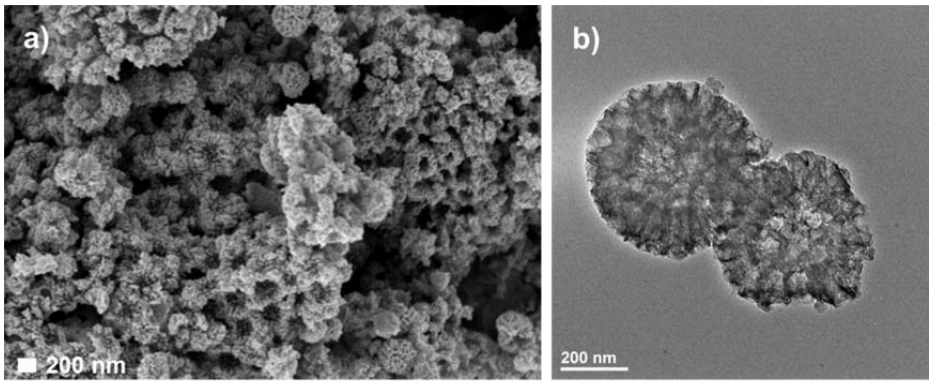

Figure 4-2. a) SEM and b) TEM images of carbon material using an ESS hard template with sucrose sulfuric acid as the carbon source.

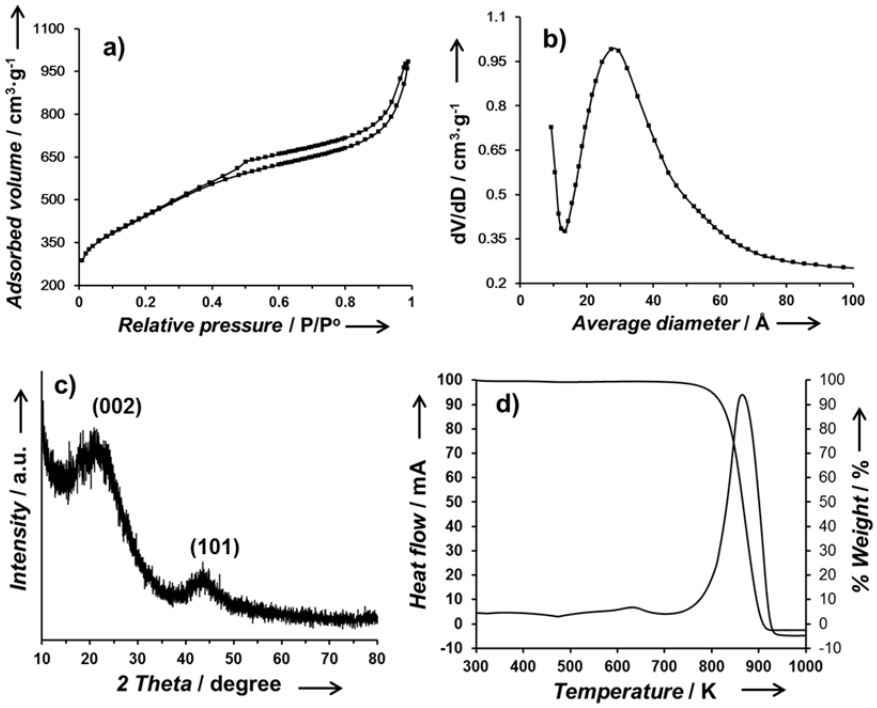

Figure 4-3. a) Nitrogen adsorption–desorption isotherm, b) pore-size distribution, c) XRD patterns, and d) TGA–DTA results: weight percent and heat flow changes during oxidation in an oxygen flow of amorphous CNE.

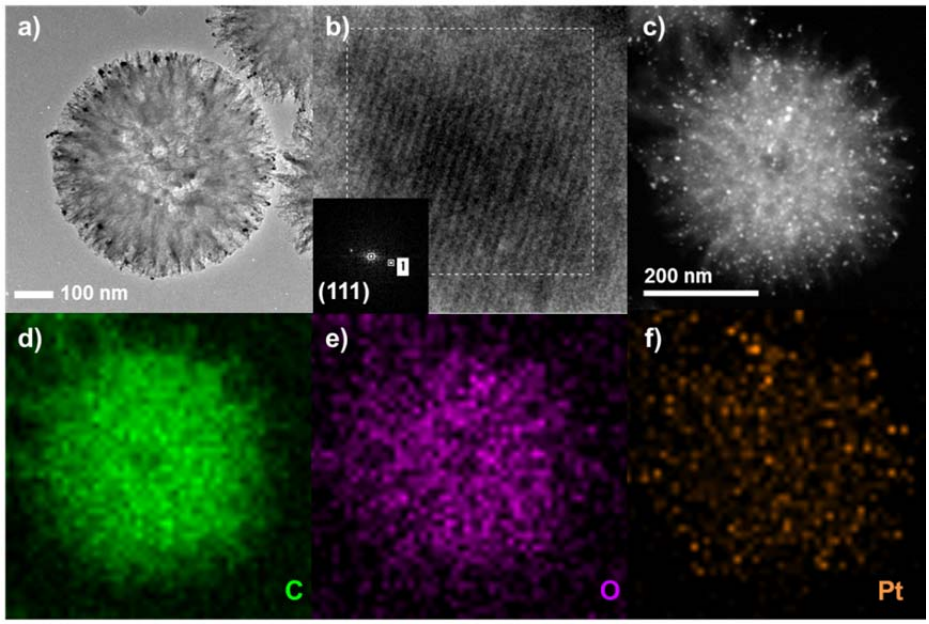

Figure 4-4. a) HR-TEM image of Pt/CNE, b) lattice image of Pt nanoparticle and electron diffraction pattern, c) STEM image of 5Pt/CNE, 2D atomic mapping using analytical STEM equipped with EDS: (g) C, (h) O, and (i) Pt.

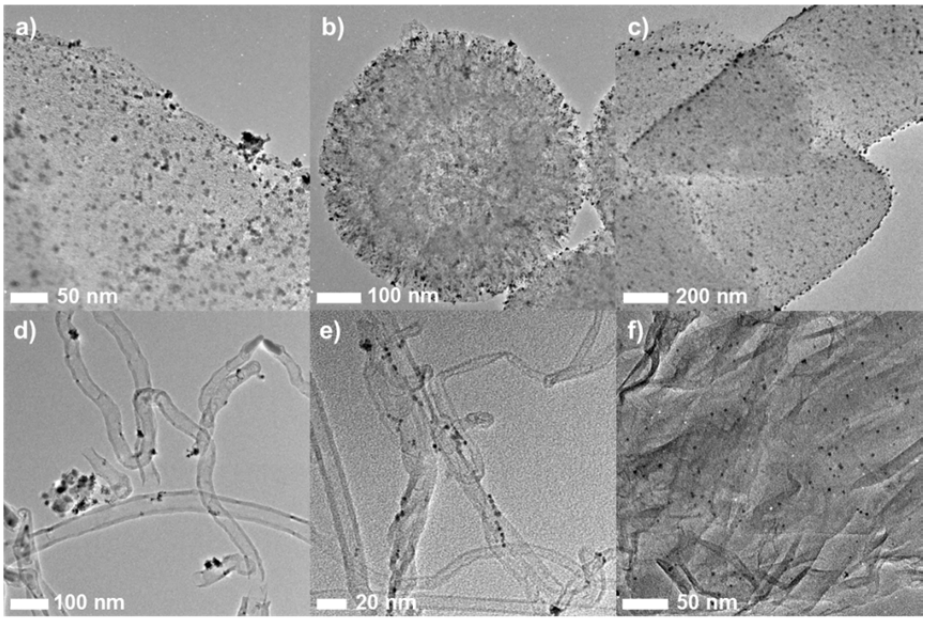

Figure 4-5. TEM images of Pt catalysts supported on various carbon supports: a) activated carbon, b) CNE, c) CMK-3, d) CNT, e) MWCNT, and f) grapheneoxide.

Table 4-1. Physicochemical properties of the prepared Pt over various carbon supports (surface area, porevolume, pore size, acidity, Pt dispersion, and H_2 uptake).

Catalyst	BET area (m^2)	S_{meso} (m^2)	V (m^3g^{-1})	D_p (nm)	NH_3 uptake (mmol g^{-1})	Pt dispersion (%)[a]	H_2 uptake (mmol g^{-1})[b]
Pt/AC	1923.7	383.2	0.94	1.7	0.21	10.2	0.275
Pt/CNE	1036.8	779.0	1.29	4.5	0.24	34.8	0.342
Pt/CNT	187.6	8.1	1.27	-	0.06	3.1	0.069
Pt/MWCNT	102.3	88.7	0.40	-	0.05	5.4	0.079
Pt/CMK	1450.5	929.0	1.40	3.1	0.25	15.0	0.257
Pt/GO	31.2	11.3	0.03	-	0.55	0.4	0.257

[a] Pulse chemisorption. [b] Hydrogen-TPD technique.

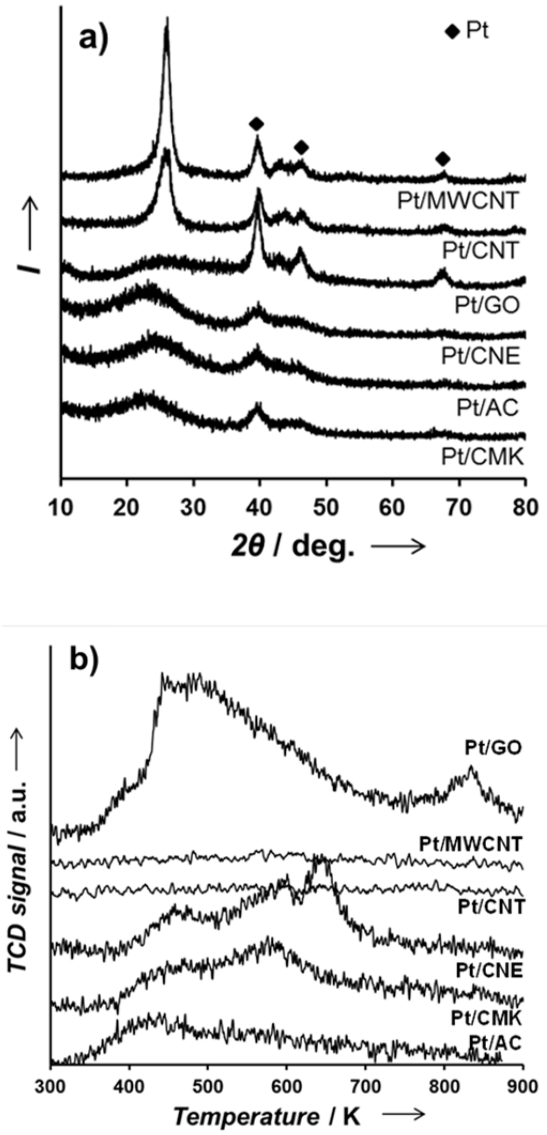

Figure 4-6. a) XRD patterns and NH_3-TPD profiles of the prepared Pt/C catalysts.

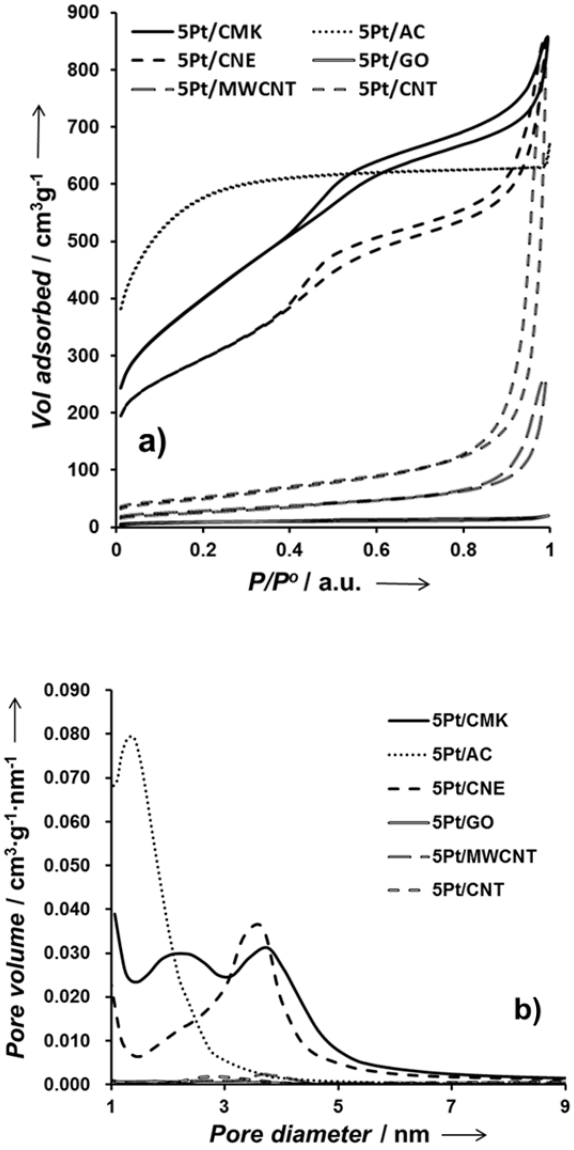

Figure 4-7. a) Isotherm curves and b) pore size distribution of the prepared Pt/C catalysts based on nitrogen adsorption-desoprtion.

Table 4-2. Degree of cellulose conversion and yield of glucose and polyols over different catalysts. (453 K, 30 bar H_2 (r.t.), 24 hours, 40 mL D.I. water, 0.4 g high power ball milled cellulose and 0.2 g catalyst)

Entry	Catalyst[a]	Conversion (%)[b]	Yield (%)[d]							Hexitol selectivity (%)
			Oligomer	Glucose	Fructose	EG	Mannitol	Sorbitol	Hexitol	
1	w/o cat.	-	11.4	2.1	2.2	0.0	0.0	0.0	0.0	0.0
2	Pt/AC	80.9 (80.6)[c]	0.0	0.8	15.5	15.6	5.7	15.1	20.9	25.8
3	Pt/CNT	77.5 (65.9)[c]	3.5	0.0	0.1	4.3	2.3	1.1	3.4	4.3
4	Pt/MWCNT	70.6 (60.8)[c]	1.9	0.0	0.1	1.9	8.3	0.0	8.2	11.6
5	Pt/CMK	83.0 (77.5)[c]	0.0	0.0	2.1	0.0	12.5	23.9	36.4	43.8
6	Pt/GO	100 (88.4)[c]	28.0	0.0	3.7	10.9	6.9	0.4	7.2	7.2
7	Pt/CNE	88.1 (87.4)[c]	0.24	1.3	4.75	20.9	10.4	50.1	60.5	68.6
8	Pt/CNE (40 bar)	90.9	0.0	0.0	1.7	18.9	7.7	61.3	69.0	75.9
9	Pt/CNE (50 bar)	95.9	1.4	0.0	0.0	0.0	12.4	67.1	79.5	82.9
10	Pt/CNE-recy.1[e]	92.7	1.6	0.0	3.6	3.9	15.4	62.7	78.1	84.2
11	Pt/CNE-recy.2[e]	91.5	1.1	0.3	3.6	0.0	14.3	57.4	71.7	78.4
12	Pt/CNE-recy.3[e]	91.6	0.4	0.0	6.9	0.0	10.6	56.0	66.6	72.7

[a] The loading amount of metal was 5 wt.%.

[b] The conversion was calculated by the weight difference of cellulose before and after reaction (uncertainty of ± 3%).

[c] The conversion in the parenthesis was calculated based on the TOC (total organic carbons) analysis of the liquid product. (Conv = TOC×4250^{-1}×100%)

[d] The yield of sugar alcohols was calculated by the equation: yield (%) = (weight of sugar alcohol in the products) / (weight of cellulose put in the reactor) ×100%.

[e] The recycle test was carried out at 453 K, 50 bar H_2(r.t.), 24 hours.

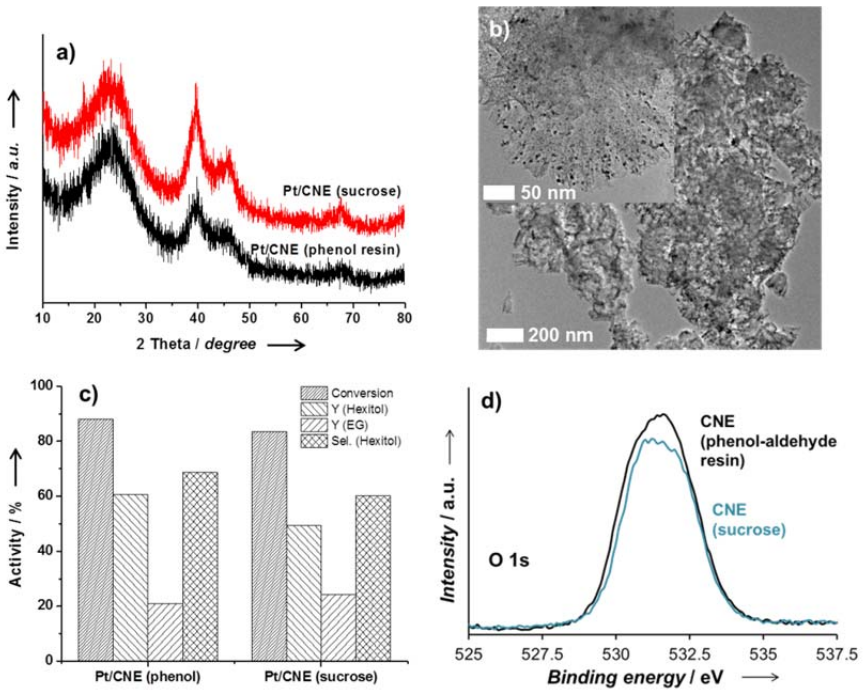

Figure 4-8. a) XRD patterns, c) catalytic activity test, d) XPS profile on O 1s of the Pt/CNE-S and Pt/CNE-P catalysts and b) HR-TEM images of Pt/CNE-S.

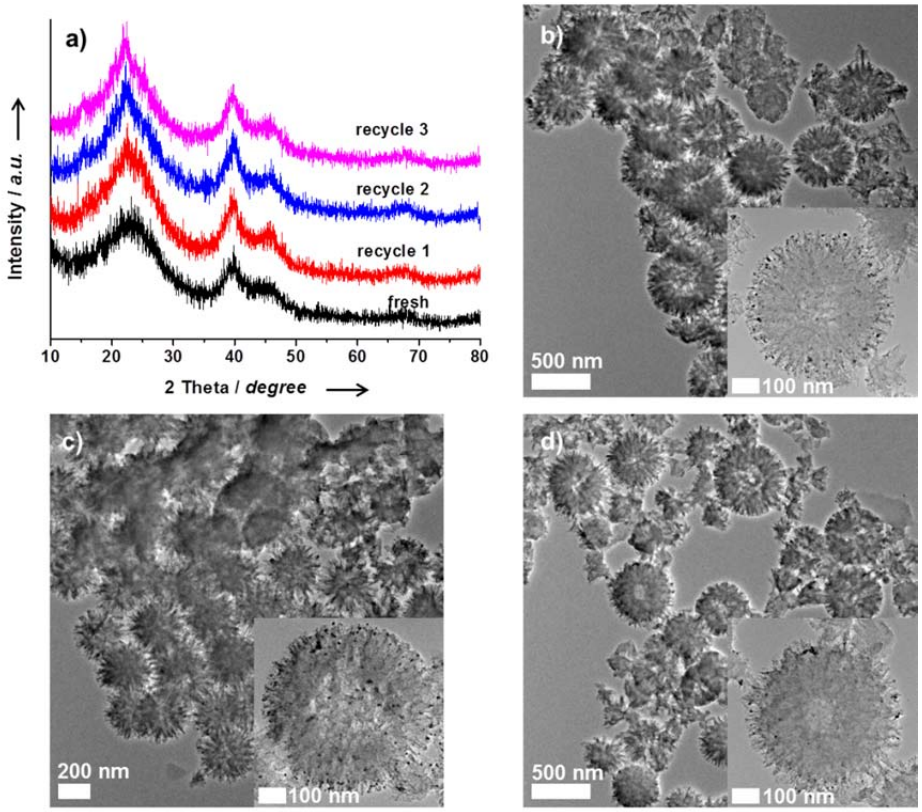

Figure 4-9. a) XRD pattens for fresh and used Pt/CNE catalysts, HR-TEM images of used Pt/CNE catalyst sample before the b) 1st recycling test, c) 2nd recyceling test, and d) 3rd recycling test.

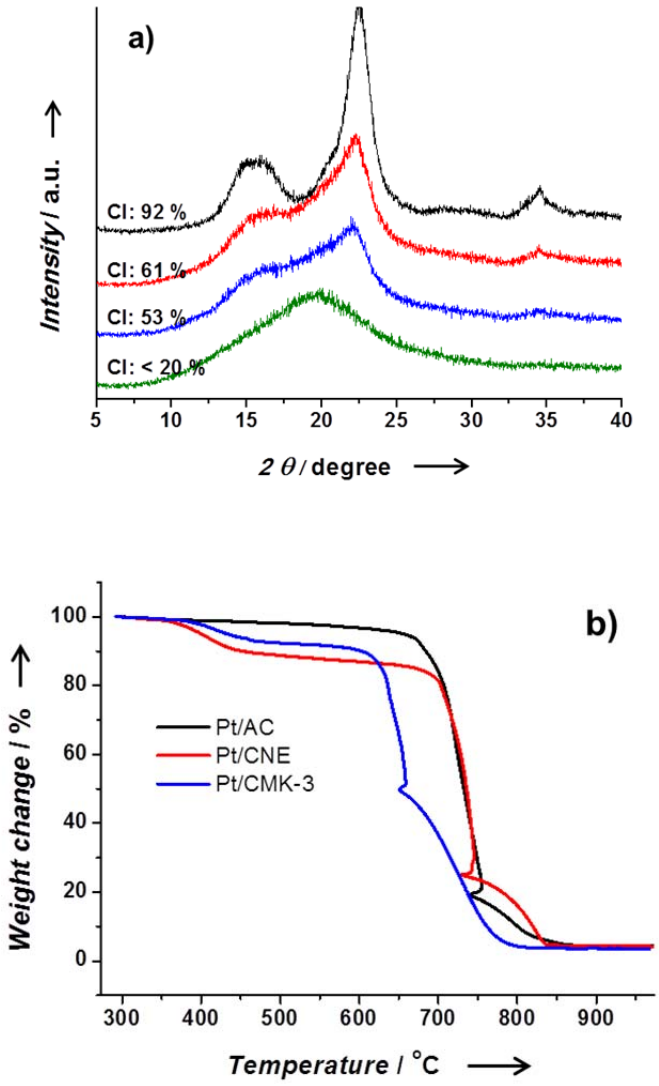

Figure 4-10. a) XRD patterns of different CI (crystalline index; (%) = $I_{002}/(I_{002}+I_{AM})\times100$) cellulose prepared by ball-milling, b) amount of Pt metal loaded on the AC, CND, and CMK-3 by TGA analysis.

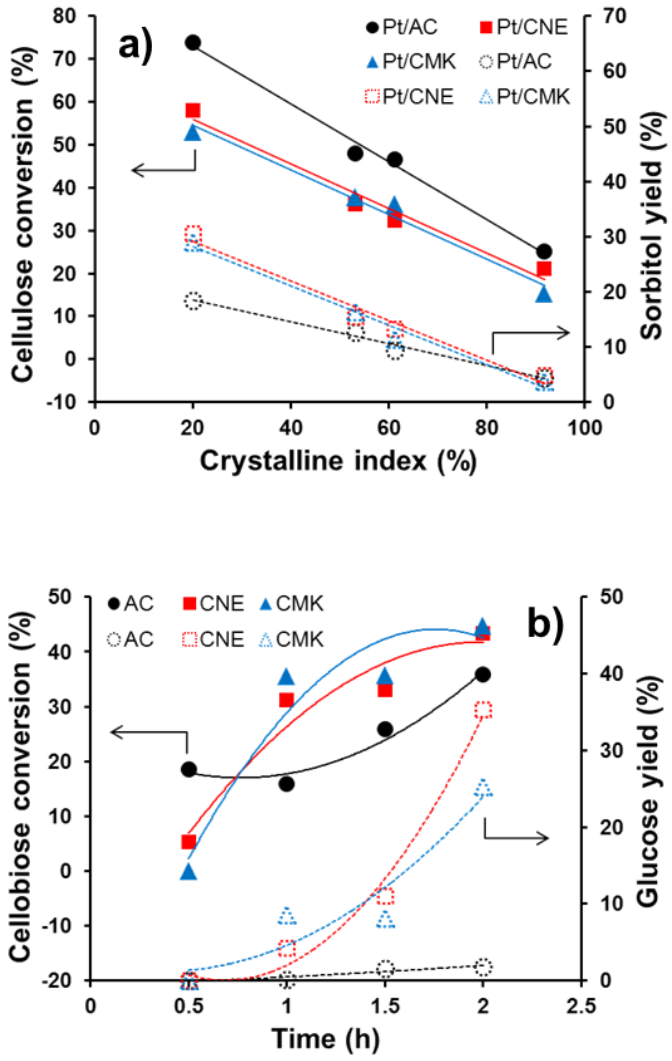

Figure 4-11. a) Cellulose conversion and sorbitol yield for different crystalline-indexed (peak height method [125]) cellulose samples (453 K, 30 bar, 0.4 g of reactantin 40 mL of water, 0.1 g of cat., 3 h), b) cellobiose conversion and glucose yield as function of time on stream (0.03 M of cellobiose, 40 mL of reactant,453 K, 0.1 g of cat.).

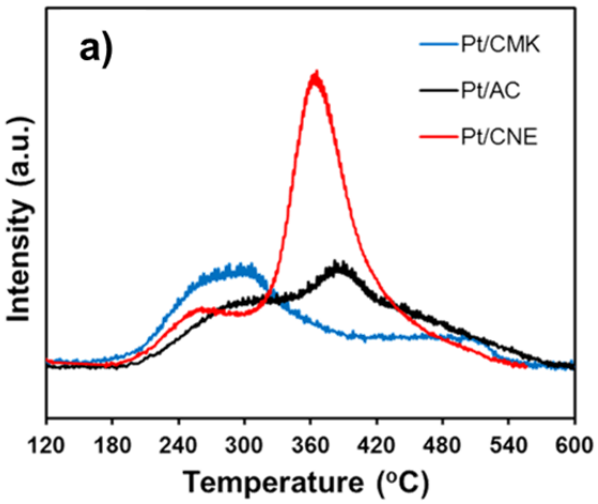
a)
Pt/CMK
Pt/AC
Pt/CNE
Intensity (a.u.)
120
180
240
300
360
420
480
540
600
Temperature (°C)

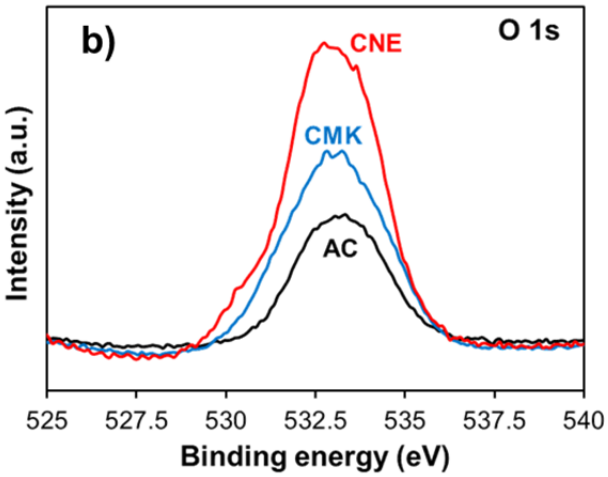
b)
O 1s
CNE
CMK
AC
Intensity (a.u.)
525
527.5
530
532.5
535
537.5
540
Binding energy (eV)

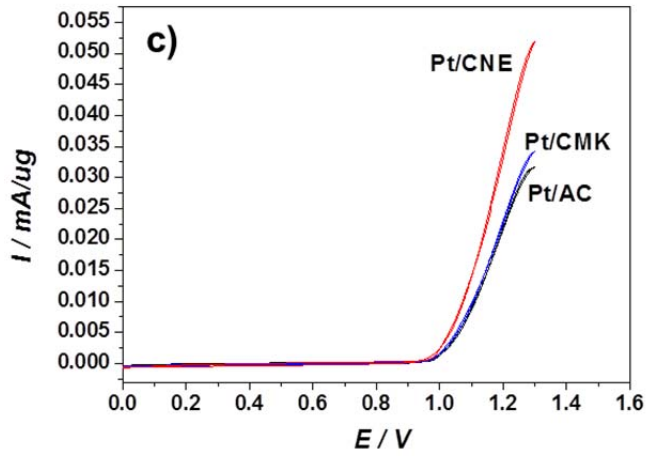

Figure 4-12. a) H_2-TPD profiles, b) XPS spectra on O (1s) of AC, CNE, and CMK-3 , and c) current density during linear sweep voltammetry with a scan rate of 10 mVs^{-1} in 0.5 M H_2SO_4 [anode (oxidation): $2H_2O(l) \rightarrow O_2(g) + 4H^+(aq) + 4e^-$; overall reaction: $2H_2O(l) \rightarrow O_2(g) + 2H_2(g)$].

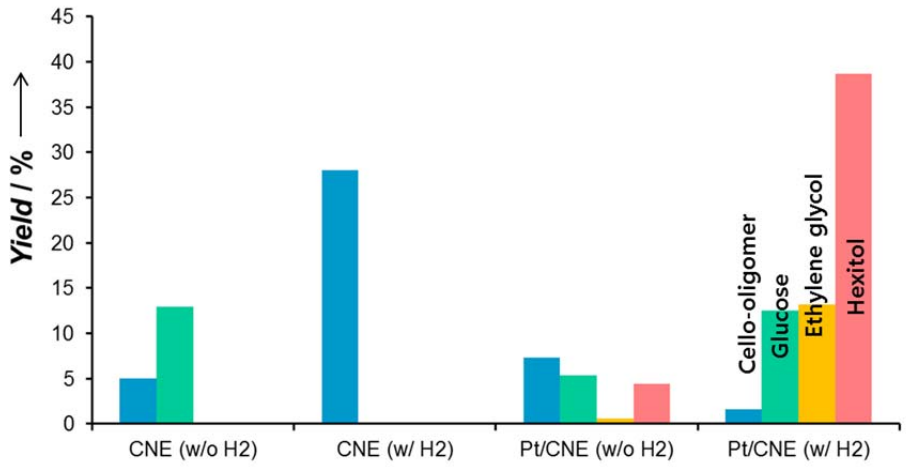

Figure 4-13. Catalytic activity of CNE and Pt/CNE catalysts for conversion of cellulose with (w/) and without (w/o) hydrogen gas (reaction conditions: 453 K, 0.1 g cat., 0.4 g cellulose, 40 mL of water, time: 3 h, 30 bar of H_2).

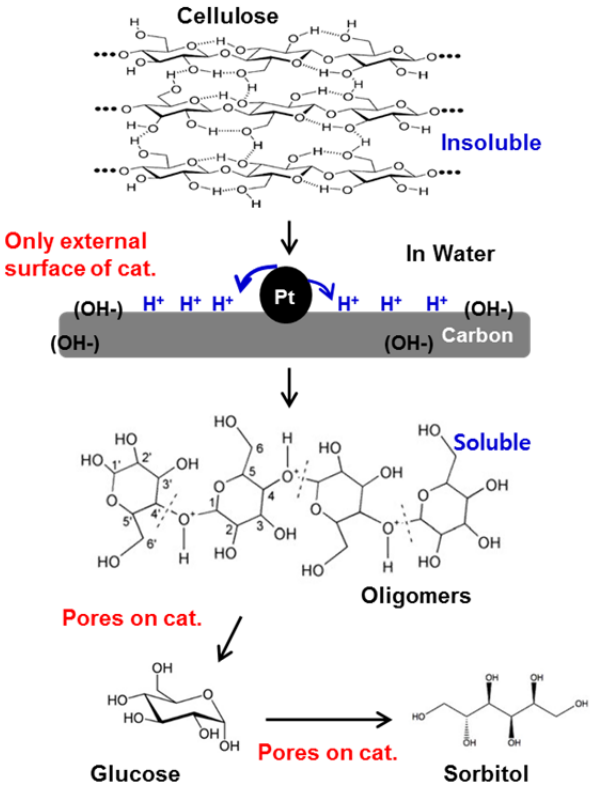

Figure 4-14. Proposed mechanism over Pt supported on mesoporous carbon in hydrolytic hydrogenation of cellulose to soluble oligomers and sorbitol.

Table 4-3. Hydrolytic hydrogenation of lignocellulose to sugar alcohols (453 K, 50 bar H_2 (RT), 24 h, 40 mL deionized water, 0.4 g feedstock, and 0.2 g catalyst).

ntry	Feedstocks	Conversion (%)	Sugar alcohols yield (%)		Selectivity [%]
			Pentitols	Hexitols	
1	Avicel PH-101	61.2	0	41.3	67.5
2	Wood powder[a]	53.4	12.7	12.1	57.3
3	Wood powder[b]	62.5	12.4	18.9	68.2

[a] Contents of wood powder: hemicellulose (15.2 %), cellulose (52.9 %) and lignin (31.9 %) determined by Wise and TAPPI methods [128, 129]

[b] Ball-milled wood powder

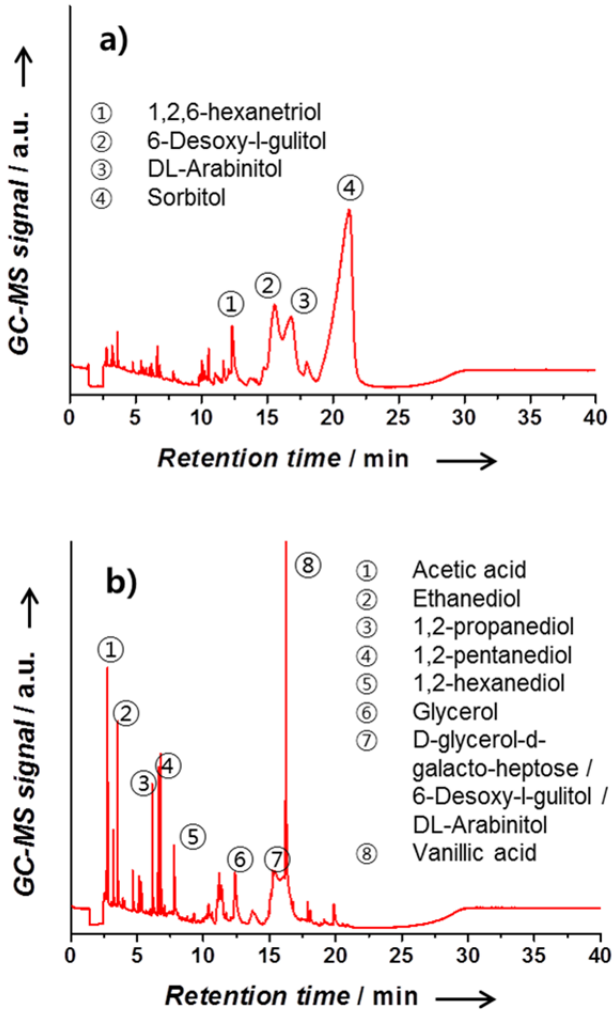

Figure 4-15. GC-MS profiles of the product in hydrolytic hydrogenation of a) ball-milled Avicel PH-101 (cellulose) and b) ball-milled hardwood powder (lignocellulose).

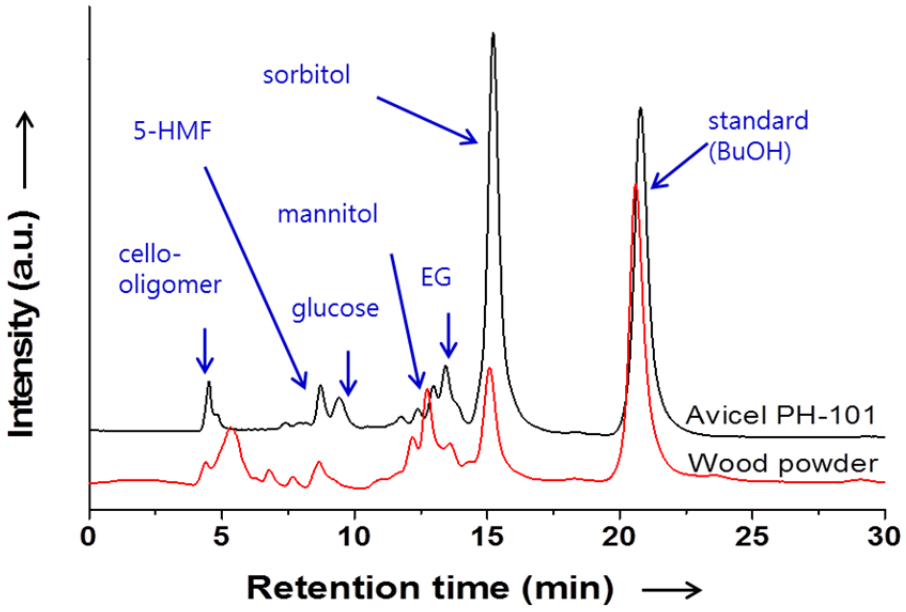

Figure 4-16. LC profiles of liquid products after the conversion of cellulose (Avicel PH-101) and woodpowder to sorbitol.

1,2,6-hexanetriol	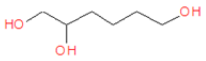	Arabinitol	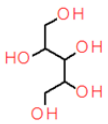
6-desoxy-l-gulitol	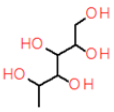	Sorbitol	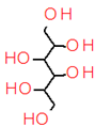
Acetic acid	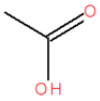	1,2-hexanediol	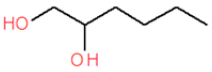
Ethanediol	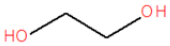	Glycerol	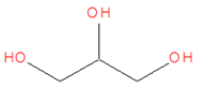
1,2-propanediol	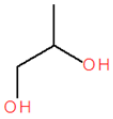	D-glycerol-d-galacto-heptose	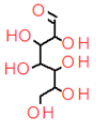
1,2-pentanediol	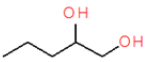	Vanillic acid	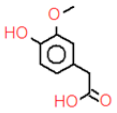

Figure 4-17. The various products in the hydrolytic hydrogenation of lignocellulose (oak wood powder) over Pt/CNE.

Chapter 5. Summary and Conclusions

The novel designed 3D mesoporous catalysts was successfully prepared to apply for the catalytic conversion of biomass derived feedstocks. Through the several reactions, such as dehydration in gas- and liquid pahse, and hydrolytic hydrogenations, the suggested 3D porous catalyst is deeply investigated to show good catalytic stability and enhancing the accessibility.

Fistly, we demonstrated the effect of coke-capturing in a Pd lattice on coking resistance in heteropoly acid catalysts. During a reaction, the coke produced from the intermediates diffused into the Pd lattice. It leads to a lattice-expansion through the formation of a Pd–coke precursor phase that was assisted by the carbon support. After the reaction, the active sites on PWC were efficiently maintained and the amount of coke on the catalyst had decreased owing to the addition of Pd. The catalytic stability of PWC also increased, owing to the inhibition of coke deposition on the active sites of the catalyst. A synergetic effect between Pd and the support was only observed in the case of the carbon support. Although palladium produced coke precursors from the hydrocarbon reactants, based on its dehydrogenation activity, the catalytic activity of Pd-PWC was enhanced. Therefore, the capture effect of Pd played an important role with carbon support in this reaction. Moreover, on the PW supported on 3D mesoporous carbon catalyst (PW/CNE), the pore plugging by coke is significantly reduced on inside the pores. For this reason, the catalyst showed a good catalytic stability even though a large amount of coke deposited on catalyst during a reaction.

Secondly, a 3D open-porous silica support (ESS) with a very uniform pore size was prepared in a hydrothermal reactor for use in the dehydration of n-butanol to di-n-butyl ether (DNBE) which is known to proceed in a diffusion limited manner. The heteropolyacid, PW, supported on DSS showed a higher conversion and yield (57 % of conversion and 53 % of yield) than PW supported on SBA-15 (50 % of conversion and 43 % of yield) or microporous silica (45 % of conversion and 36 % of yield) in liquid-phase dehydration of n-butanol to di-n-butyl ether. The extent of diffusion enhancement over the 3D porous catalyst was quantified by calculating the effectiveness factor (η) using data obtained from a kinetic study. The transport of molecules increases with increasing pore size, shorter pore length, and the catalyst with a 3D structure shows an enhanced accessibility of n-butanol.

Finally, the prepared 3D mesoporous carbon, CNE, was used to the catalyst with platinum nanoparticle for the conversion of cellulose into hexitols. The Pt/CNE catalyst showed a high performance for the conversion of cellulose and for sorbitol selectivity. The fibrous porous structure of Pt/CNE enhanced the affinity of cellulose for the catalyst, and the mesoporosity induced a high selectivity for soluble oligomers or target chemicals. On the surface of Pt metal the spillover effect increased due to presence of abundant oxygen groups on the CNE and a high dispersion, resulting in efficiently supplying the in-situ generated H^+ for the hydrolysis step. On the mesoporous catalysts, cellulose can be directly converted glucose or other target chemicals through two-step mechanisms. Firstly, hydrolysis of cellulose proceeds on the H^+ species released by the surface of the carbon or formed in the medium. In a second step, soluble and smaller

oligomers enough to access the pores are reacted to another oligomers and chemicals on the catalytic sites of the carbon-based catalysts. In our prepared catalyst, even though no additional acid treated-process of the catalyst, the catalyst shows the highest performance for this reaction (with yields approaching 80 %). To our best knowledge, this is the best performance over solid bifunctional catalysts ever reported for the production of hexitols from cellulose. Through the direct conversion of the hardwood material, it is confirmed that the CNE material would be applied for the various catalytic transformation of lignocellulosic biomass.

Chapter 6. Recommendations for Further Research

The recommendations for further research are summarized as follows;

1) It is generally known that Brønsted acid sites are good for the selective conversion of glycerol to acrolein. And a decrease of the ratio of Lewis (L) acid sites over Brønsted (B) acid sites leads to prevent a production of coke precursors from various undesired reactions. On the conventional oxide catalysts, both B and L acid sites are distributed on the suface of catalyst, and the B acid sites are reversibility changed to the L acid sites during a reaction. We studied the deactivation by coking in dehydration of glycerol with respect to the only structural aspect of the support. To develop a more stable catalyst, it should be considered of not only the catalyst structure but also the precise control of active sites.

2) The hydrogen spillover is still a controvercial topic. For detailed investigation of the reaction pathway, the hydrogen spillover is certainly proved experimentally and theoretically on the Pt supported on mesoporous carbon with hydrogen gas. The 3D mesoporous carbon, CNE, showed good performance in conversion of lignocellulosic biomass. However, the fibrous structure of the CNE is a weak to an acidic medium. The production of glucose from hydrolysis of cellulose is a primary step to produce the various valuable building blocks by sequential reaction. Unfortunately, for the hydrolysis of cellulose, the catalyst has to resistant to the acidic chemicals. Therefore, the carbon material should be strongly improved in order to apply for the various reactions from lignocellulosic biomass.

3) To investigate the effect of 3D structured-catalyst on a mass transfer-

limited reaction, another reactions from high-branched compounds in biomass will be tested as a control test, for instance, the dehydration of 5-HMF to levulinic acid and hydrolysis of cello-oligomers to glucose.

Bibliography

[1] J. Goldemberg, *Science*, 2007, **315**, 808-810.

[2] N. Armaroli, V. Balzani, *Angew. Chem. Int. Ed.,* 2007, **46**, 52-66.

[3] D. Mohan, C. U. Pittman, P. H. Steele, *Energy Fuels*, 2006, **20**, 848-889.

[4] J. O. Metzger, *Angew. Chem. Int. Ed.*, 2006, **45**, 696-698.

[5] M. Stöcker, *Angew. Chem. Int. Ed.*, 2008, **47**, 9200-9211.

[6] P. Gallezot, *Chem. Soc. Rev.*, 2012, **41**, 1538-1558.

[7] C.-H. Zhou, X. Xia, C.-X. Lin, D.-S. Tong, J. Beltramini, *Chem. Soc. Rev.*, 2011, **40**, 5587-5617.

[8] Y.-C. Lin, G. W. Huber, *Energy Environ. Sci.*, 2009, **2**, 68-80.

[9] J. N. Chheda, G. W. Huber, J. A. Dumesic, *Angew. Chem. Int. Ed.*, 2007, **46**, 7164-7183.

[10] C. E. Wyman, *Bioresour. Technol.*, 1994, **50**, 3-15

[11] E. V. Sagadeev and V. P. Barabanov, Russ. *J. Phys. Chem.*, 2006, **80**, S152-S162.

[12] R. Rinaldi, F. Schüth, *Energy Environ. Sci.*, 2009, **2**, 610-626.

[13] P. Gallezot, *Green Chem.*, 2007, **9**, 295-302.

[14] A. Corma, S. Iborra, A. Velty, *Chem. Rev.*, 2007, **107**, 2411-2502.

[15] G. W. Huber, S. Iborra, A. Corma, *Chem. Rev.*, 2006, **106**, 4044-4098.

[16] P. Mäki-Arvela, B. Holmbom, T. Salmi, D. Y. Murzin, *Catal. Rev.*, 2007, **49**, 197-340.

[17] J. H. Clark, F. E. I. Deswarte, T. J. Farmer, *Biofuels, Bioprod. Bioref.*, 2009, **3**, 72-90.

[18] J.-P. Lange, *Biofuels, Bioprod. Bioref.*, 2007, **1**, 39-48.

[19] D. J. Cole-Hamilton, *Science*, 2003, **299**, 1702-1706.

[20] A. Corma, H. Garcia, *Adv. Synth. Catal.*, 2006, **348**, 1391-1412.

[21] W. Tischer, F. Wedekind, *Top. Curr. Chem.*, 1999, **200**, 95-126.

[22] P. Calvini, *Cellulose*, 2005, **12**, 445-447.

[23] C. Li, Z. K. Zhao, *Adv. Synth. Catal.*, 2007, **349**, 1847-1850.

[24] C. Li, Q. Wang, Z. K. Zhao, *Green Chem.*, 2008, **10**, 177-182.

[25] R. Rinaldi, R. Palkovits, F. Schüth, *Angew. Chem. Int. Ed.*, 2008, **47**, 8047-8050.

[26] Q. Liu, M. H. A. Janssen, F. Rantwijk, R. A. Sheldon, *Green Chem.*, 2005, **7**, 39-42.

[27] M. Gamba, A. A. M. Lapis, J. Dupont, *Adv. Synth. Catal.*, 2008, **350**, 160-164.

[28] Q. Wu, H. Chen, M. Han, D. Wang, J. Wang, *Ind. Eng. Chem. Res.*, 2007, **46**, 7955-7960.

[29] A. P. Abbott, P. M. Cullis, M. J. Gibson, R. C. Harris, E. Raven, *Green Chem.*, 2007, **9**, 868-872.

[30] S. M. Csicsery, *Zeolites*, 1984, **4**, 202-213.

[31] L. P. Ramos, *Quim. Nova*, 2003, **26**, 863.

[32] A. Taguchi, F. Schüuth, *Microporous Mesoporous Mater.*, 2005, **77**, 1-45.

[33] T. J. Barton, L. M. Bull, W. G. Klemperer, D. A. Loy, B. McEnaney, M. Misono, P. A. Monson, G. Pez, G. W. Scherer, J. C. Vartuli, O. M. Yaghi, *Chem. Mater.*, 1999, **11**, 2633-2656.

[34] F. Schüth, in Handbook of Porous Solids, ed. F. Schüth, K. S. W. Sing, J. Weitkamp, Weinheim, vol. 1, 2002, pp. 535.

[35] F. Schüth, W. Schmidt, *Adv. Mater.*, 2002, **14**, 629-638.

[36] Y. Wan, H. F. Yang, D. Y. Zhao, *Acc. Chem. Res.*, 2006, **39**, 423-432.

[37] Y. Wan, Y. F. Shi, D. Y. Zhao, *Chem. Mater.*, 2008, **20**, 932-945.

[38] C. Liang, Z. Li, S. Dai, *Angew. Chem. Int. Ed.*, 2008, **47**, 3696-3717.

[39] Y. Meng, D. Gu, F. Q. Zhang, Y. F. Shi, L. Cheng, D. Feng, Z. X. Wu, Z. X. Chen, Y. Wan, A. Stein, D. Y. Zhao, *Chem. Mater.*, 2006, **18**, 4447-4464.

[40] W.-C. Li, A.-H. Lu, F. Schüth, *Chem. Mater.*, 2005, **17**, 3620-3626.

[41] C. Liang, Z. Li, S. Dai, *Angew. Chem. Int. Ed.*, 2008, **47**, 3696-3717.

[42] D. T. Johnson, K. A. Taconi, *Environmental Progress,* 2007, **26**, 338-348.

[43] T. Werpy, G. Petersen, *Top Value Added Chemicals from Biomass, vol. 1, Results of Screening for Potential Candidates from Sugars and Synthesis Gas*, US DOE Report, 2004.

[44] M. Pagliaro, R. Ciriminna, H. Kimura, M. Rossi, C. D. Pina, *Angew. Chem. Int. Ed.,* 2007, **46**, 4434-4440.

[45] B. Katryniok, S. Paul, V. Belliere-Baca, P. Rey, F. Dumeignil, *Green Chem.,* 2010, **12**, 2079-2098.

[46] B. Katryniok, S. Paul, M. Capron, F. Dumeignil, *ChemSusChem,* 2009, **2**, 719-730.

[47] S.H. Chai, H. P. Wang, Y. Liang, B. Q. Xu, *Green Chem.,* 2007, **9**, 1130-1136.

[48] J.H. Choi, J.K. Kim, D.R. Park, S. Park, J. Yi, I.K. Song, Etherification of n-butanol to di-n-butyl ether over $H_3PMo_{12-x}W_xO_{40}$ (x=0, 3, 6, 9, 12) Keggin and $H_6P_2Mo_{18-x}W_xO_{62}$

(x=0, 3, 9, 15, 18) Wells–Dawson heteropolyacid catalysts, *Catal. Comm.*, 2011, **14**, 48-51.

[49] R. Patrini, M. Marchionna, US Patent 0159341 (2003).

[50] F.E.M. Alaoui, E.A. Montero, J.-P. Bazile, F. Aguilar, C. Boned, Liquid Density of Biofuel Additives: 1-Butoxybutane at Pressures up to 140 MPa and from (293.15 to 393.15) K, *J. Chem. Eng. Data*, 2011, **56**, 595-600.

[51] R. Bringué, J. Tejero, M. Iborra, J.F. Izquierdo, C. Fité, F. Cunill, Supported Nafion catalyst for 1-pentanol dehydration reaction in liquid phase, *Chem. Eng. J.*, 2008, **145**, 135-141.

[52] M.A. Makarova, E.A. Paukshtis, J.M. Thomas, C. Williams, K.I. Zamaraev, Dehydration of n-Butanol on Zeolite H-ZSM-5 and Amorphous Aluminosilicate: Detailed Mechanistic Study and the Effect of Pore Confinement, *J. Catal.*, 1994, **149**, 36-51.

[53] A. T. Okuhara, *Chem. Rev.*, 2002, **102**, 3641-3666.

[54] L. Ott, M. Bicker, H. Vogel, *Green Chem.*, 2006, **8**, 214- 220.

[55] G. Yaluris, R. B. Larson, J. M. Kobe, M. R. Gonzalez, K. B. Fogash, J. A. Dumesic, *J. Catal.*, 1996, **158**, 336- 342.

[56] S. van Donk, J. H. Bitter, K. P. Jong, *Appl. Catal. A*, 2001, **212**, 97-116.

[57] S.-H. Chai, H.-P. Wang, Y. Liang, B.-Q. Xu, *Green Chem.*, 2008, **10**, 1087 -1093.

[58] S. Chai, H. Wang, Y. Liang, B. Xu, *J. Catal.*, 2007, **250**, 342-349.

[59] W. Suprun, M. Lutecki, T. Haber, H. J. Papp, *J. Mol. Catal. A,* 2009, **309**, 71-78.

[60] C. H. Bartholomew, *Appl. Catal. A*, 2001, **212**, 17-60.

[61] A. Alhanash, E. F. Kozhevnikova, I. V. Kozhevnikov, *Appl. Catal. A*, 2010, **378**, 11-18.

[62] H. Atia, U. Armbruster, A. Martin, *J. Catal.*, 2008, **258**, 71-82.

[63] Y. Arita, H. Kasuga, M. Kirishiki, JP pat. 2008110298, 2008.

[64] B. Katryniok, S. Paul, M. Capron, C. Lancelot, V. Belliere-Baca, P. Rey, F. Dumeignil, *Green Chem.*, 2010, **12**, 1922 -1925.

[65] S. B. Ziemecki, G. A. Jones, D. G. Swartzfager, R. L. Harlow, *J. Am. Chem. Soc.*, 1985, **107**, 4547 -4548.

[66] R. Lamber, G. Schulz-Ekloff, *Surf. Sci.*, 1990, **227**, 15-23.

[67] B. Ingham, M. F. Toney, S. C. Hendy, T. Cox, D. D. Fong, J. A. Eastman, P. H. Fuoss, K. J. Stevens, A. Lassesson, S. A. Brown, M. P. Ryan, *Phys. Rev. B*, 2008, **78**, 245408.

[68] R. Lamber, S. Wetjen, N. I. Jaeger, *Phys. Rev. B*, 1995, **51**, 10968-10971.

[69] S. B. Ziemecki, G. A. Jones, *J. Catal.*, 1985, **95**, 621-622.

[70] K. M. Neyman, S. Schauermann, *Angew. Chem.* 2010, **122**, 4851-4854; *Angew. Chem. Int. Ed.*, 2010, **49**, 4743-4746.

[71] N. Seriani, F. Mittendorfer, G. Kresse, *J. Chem. Phys.*, 2010, **132**, 024711.

[72] D. Teschner, Z. Revay, J. Borsodi, M. Havecker, A. Knop-Gericke, R. Schlogl, D. Milroy, S. D. Jackson, D. Torres, P. Sautet, *Angew. Chem.*, 2008, **120**, 9414-9418; *Angew. Chem. Int. Ed.*, 2008, **47**, 9274 – 9278.

[73] Z. Bastl, O. Pribyl, P. Mikusik, *J. Phys. B*, 1984, **34**, 981-988.

[74] H. Gabasch, W. Unterberger, K. Hayek, B. Klotzer, E. Kleimenov, D. Teschner, S. Zafeiratos, M. Havecker, A. Knop-Gericke, R.

Schlogl, J. Han, F. H. Ribeiro, B. Aszalos-Kiss, T. Curtin, D. Zemlyanov, *Surf. Sci.*, 2006, **600**, 2980-2989.

[75] P. A. Jalil, M. Faiz, N. Tabet, N. M. Hamdan, Z. Hussain, *J. Catal.*, 2003, **217**, 292-297.

[76] G. Ranga Rao, T. Rajkumar, *Catal. Lett.*, 2008, **120**, 261- 273.

[77] J. Wang, Z. Lin, S.-Y. Han, M. Eum, C. W. Lee, *J. Ind. Eng. Chem.*, 2003, **9**, 281- 286.

[78] I. V. Kozhevnikov, S. Holmes, M. R. H. Siddiqui, *Appl. Catal. A*, 2001, **214**, 47-58.

[79] F. Wang, J.-L. Dubois, W. Ueda, *J. Catal.*, 2009, **268**, 260– 267.

[80] A. Corma, G. W. Huver, L. Sauvanaud, P. O'Connor, *J. Catal.*, 2008, **257**, 163-171.

[81] P. M. Rao, A. Wolfson, S. Kababya, S. Vega, M. V. Landau, *J. Catal.*, 2005, **232**, 210-225.

[82] L. R. Pizzio, C. V. Caceres, M. N. Blanco, *Appl. Catal. A*, 1998, **167**, 283-294.

[83] G. I. Kapustin, T. R. Brueva, A. L. Klyachko, M. N. Timofeeva, S. M. Kulikov, I. V. Kozhevnikov, *Kinet. Katal.*, 1990, **31**, 1017.

[84] H. S. Cerqueira, P. Ayrault, J. Datka, M. Guisnet, *Microporous Mesoporous Mater.*, 2000, **38**, 197-205.

[85] G. Baronetti, H. Thomas, C. A. Querini, *Appl. Catal. A*, 2001, **217**, 131-141.

[86] J. Tejero, C. Fité, M. Iborra, J.F. Izquierdo, F. Cunill, R. Bringué, *Microporous Mesoporous Mater.,* 2009, **117**, 650-660.

[87] G. A. Olah, T. Shamma, G. K. S. Prakash, *Catal. Lett*., 1997, **46**, 1-4.

[88] W. J. Piel, R. X. Thomas, Hydrocarbon Processing, 1990, 68-73.

[89] P. Chu, G. H. Kuhl, *Ind. Eng. Chem. Res.*, 1987, **26**, 365-369.

[90] G. A. Olah, US Patent 5,520,710 (1996).

[91] R. Patrini, M. Marchinonna, US Patent 6218583 (2001).

[92] Y. Zhang, A. Wang, T. Zhang, *Chem. Commun.*, 2010, **46**, 862-864.

[93] H. Oveisi, C. Anand, A. Mano, S.S. Al-Deyab, P. Kalita, A. Beitollahi, A. Vinu, *J. Mater. Chem.*, 2010, **20**, 10120-10129.

[94] C. H. Christensen, K. Johannsen, E. Törnqvist, I. Schmidt, H. Topsøe, C.H. Christensen, *Catal. Today*, 2007, **128**, 117-122.

[95] C. Sun, S. Rajasekhara, J.B. Goodenough, F. Zhou, *J. Am. Chem. Soc.*, 2011, **133**, 2132-2135.

[96] V. Polshettiwar, D. Cha, X. Zhang, J. M. Basset, *Angew. Chem*., 2010, **122**, 9846-9850.

[97] K. Okada, A. Shimai, T. Takei, S. Hayashi, A. Yasumori, K.J.D. MacKenzie, *Microporous and Mesoporous Materials*, 1998, **21**, 289-296.

[98] H. Atia, U. Armbruster, A. Martin, *J. Catal.*, 2008, **258**, 71-82.

[99] A. Ciftci, D. Varisli, K. C. Tokay, N. A. Sezgi, T. Dogu, *Chem. Eng. J.*, 2012, **207-208**, 85-93.

[100] D. S. Park, B. K. Kwak, N. D. Kim, J. R. Park, J.-H. Cho, S. Oh, J. Yi, *ChemCatChem*, 2012, **4**, 836-843.

[101] B. Shi, B. H. Davis, *J. Catal.*, 1995, **157**, 359-367.

[102] Y.-S. Hsu, Y.-L. Wang, A.-N. Ko, *J. Chinese Chem. Soc.*, 2009, **56**, 314-322.

[103] I. B. Ju, H.-W. Lim, W. Jeon, D. J. Suh, M.-J. Park, Y.-W. Suh, *Chem. Eng. J.*, 2011, **168**, 293-302.

[104] B. Sow, *Microporous and Mesoporous Materials*, 2005, **79**, 129-136.

[105] M. A. Makarova, C. Williams, J. M. Thomas, *Catalysis Letters*, 1990, **4**, 261-264.

[106] C. N. Satterfield, Mass Transfer in Heterogeneous Catalysis, M.I.T. PRESS, Cambridge, Massachusetts, London, 1970, pp. 1-41.

[107] G. W. Roberts, C. N. Satterfield, *I&EC Fundamentals*, 1965, **4**, 288-293.

[108] J. K. Lee, J. B. Ko, D. H. Kim, *Appl. Catal. A*, 2004, **278**, 25-35.

[109] P. L. Dhepe, A. Fukuoka, *ChemSusChem,* 2008, **1**, 969-975.

[110] S. V. Vyver, J. Geboers, P. A. Jacobs, B. F. Sels, *ChemCatChem,* 2011, **3**, 82-94.

[111] R. Rinaldi, F. Schüth, *ChemSusChem,* 2009, **2**, 1096-1107.

[112] A. Fukuoka, P. L. Dhepe, *Angew. Chem. Int. Ed.,* 2006, **45**, 5161-5163.

[113] L. Ding, A. Wang, M. Zheng, T. Zhang, *ChemSusChem,* 2010, **3**, 818-821.

[114] W. Deng, X. Tan, W. Fang, Q. Zhang, Y. Wang, *Catal Lett.,* 2009, **133**, 167-174.

[115] J. W. Han, H. Lee, *Catal. Commun.,* 2012, **19**, 115-118.

[116] G. Liang, H. Cheng, W. Li, L. He, Y. Yu, F. Zhao, *Green Chem.,* 2012, **14**, 2146-2149.

[117] Y. Zhang, A. Wang, T. Zhang, *Chem. Commun.,* 2010, **46**, 862-864.

[118] V. Jollet, F. Chambon, F. Rataboul, A. Cabiac, C. Pinel, E. Guillon, N. Essayem, *Green Chem.,* 2009, **11**, 2052-2060.

[119] V. Jollet, F. Chambon, F. Rataboul, A. Cabiac, C. Pinel, E. Guillon,

N. Essayem, *Top Catal.,* 2010, **53**, 1254-1257.

[120] W. Deng, Y. Wang, Q. Zhang, Y. Wang, *Catal. Surv. Asia,* 2012, **16**, 91-105.

[121] H. Kobayashi, H. Ohta, A. Fukuoka, *Catal. Sci. Technol.,* 2012, **2**, 869-883.

[122] S. Suganuma, K. Nakajima, M. Kitano, D. Yamaguchi, H. Kato, S. Hayashi, M. Hara, *J. Am. Chem. Soc.,* 2008, **130**, 12787-12793.

[123] M. Kitano, D. Yamaguchi, S. Suganuma, K. Nakajima, H. Kato, S. Hayashi, M. Hara, *Langmuir,* 2009, **25**, 5068-5075.

[124] H. Kobayashi, T. Komanoya, Ke. Hara, A. Fukuoka, *ChemSusChem,* 2010, **3**, 440-443.

[125] A. Onda, T. Ochi, K. Yanagisawa, *Green Chem.,* 2008, **10**, 1033-1037.

[126] J. Pang, A. Wang, M. Zheng, T. Zhang, *Chem. Commun.,* 2010, **46**, 6935-6937.

[127] S. Suganuma, K. Nakajima, M. Kitano, S. Hayashi, M. Hara, *ChemSusChem,* 2012, **5**, 1841-1846.

[128] J. Pang, A. Wang, M. Zheng, Y. Zhang, Y. Huang, X. Chen, T. Zhang, *Green Chem.,* 2012, **14**, 614-617.

[129] J. Geboers, S. V. Vyver, K. Carpentier, K. Blochouse, P. Jacobs, B. Sels, *Chem. Commun.,* 2010, **46**, 3577-3579.

[130] C. Luo, S. Wang, H. Liu, *Angew. Chem. Int. Ed.,* 2007, **46**, 7636-7639.

[131] S. V. Vyver, J. Geboers, W. Schutyser, M. Dusselier, P. Eloy, E. Dornez, J. W. Seo, C. M. Courtin, E. M. Gaigneaux, P. A. Jacobs, B. F. Sels, *ChemSusChem,* 2012, **5**, 1549-1558.

[132] A. Shrotri, A. Tanksale, J. N. Beltramini, H. Gurav, S. V. Chilukuri, *Catal. Sci. Technol.,* 2012, **2**, 1852-1858.

[133] M. Kruk, B. Dufour, E. B. Celer, T. Kowalewski, M. Jaroniec, K. Matyjaszewski, *J. Phys. Chem. B,* 2005, **109**, 9216-9225.

[134] H. Chen, R. T. Yang, *Langmuir,* 2010, **26**, 15394-15398.

[135] Q. Li, A. D. Lueking, *J. Phys. Chem. C,* 2011, **115**, 4273-4282.

[136] D. E. Demirocak, M. K. Ram, S. S. Srinivasan, A. Kumar, D. Y. Goswami, E. K. Stefanakos, *Int. J. Hydrogen. Energ.,* 2012, **37**, 12402-12410.

[137] V. Polshettiwar, D. Cha, X. Zhang, J. M. Basset, *Angew. Chem. Int. Ed.,* 2010, **49**, 9652-9656.

[138] V. Polshettiwar, J. Thivolle-Cazat, M. Taoufik, F. Stoffelbach, S. Norsic, J. M. Basset, *Angew. Chem. Int. Ed.,* 2011, **50**, 2747-2751.

[139] A. Fihri, D. Cha, M. Bouhrara, N. Almana, V. Polshettiwar, *ChemSusChem,* 2012, **5**, 85-89.

[140] D. Moon, J. Lee, *Langmuir,* 2012, **28**, 12341-12347.

[141] K. Sing, D. Everett, R. Haul, L. Moscou, R. Pierotti, J. Rouquerol, T. Siemieniewska, *Pure Appl. Chem.,* 1985, **57**, 603-619.

[142] K. Lee, J. Zhang, H. Wang, D. P. Wilkinson, *J. Appl. Electrochem.,* 2006, **36**, 507-522.

[143] L. Zhao, L. Gao, *Carbon,* 2004, **42**, 423-460.

[144] N. Ji, T. Zhang, M. Zheng, A. Wang, H. Wang, X. Wang, J. G. Chen, *Angew. Chem. Int. Ed.,* 2008, **47**, 8510-8513.

[145] Y. Liu, C. Luo, H. Liu, *Angew. Chem. Int. Ed.,* 2012, **51**, 3249-3253.

[146] J. Zhang, L. Lin, J. Zhang, J. Shi, *Carbohyd. Res.,* 2011, **346**, 1327-1332.

[147] H. Hattori, T. Shishido, *Catal. Surv. Jpn.,* 1997, **1**, 205-213.

[148] S. Park, J. O. Baker, M. E. Himmel, P. A. Parilla, D. K. Johnson, *Biotechnology for biofuels,* 2010, **3,** 10.

[149] D. N.-S. Hon, H. Yan, *J. Appl. Polym. Sci.,* 2001, **81**, 2649-2655.

[150] Y. Kwon, S. E. F. Kleijn, K. J. P. Schouten, M. T. M. Koper, *ChemSusChem,* 2012, **5**, 1935-1943.

[151] A. Sluiter, B. Hames, R. Ruiz, C. Scarlata, J. Sluiter, D. Templeton, *Determination of ash in biomass*. Laboratory Analytical Procedures, National Renewable Research Laboratory, Technical Report TP-510-42622, Golden, Co. 2008.

[152] A. Sluiter, B. Hames, R. Ruiz, C. Scarlata, J. Sluiter, D. Templeton, *Determination of structural carbohydrates and lignin in biomass*. Laboratory Analytical Procedure. 2008.

[153] R. C. Pettersen, in *The Chemistry of Solid Wood* (Eds.: R. Rowell), Am. Chem. Soc., Washington D.C., 1984.

[154] M. V. Ramiah, *Appl. Polymer Science,* 1970, **14**, 1323.

[155] R. Sahu, P. L. Dhepe, *ChemSusChem,* 2012, **5**, 751-761.

[156] J. Zakzeski, A. L. Jongerius, P. C. A. Bruijnincx, B. M. Weckhuysen, *ChemSusChem,* 2012, **5**, 1602-1609.

요약(국문초록)

바이오매스 원료는 탄소 연료를 지속적이고 재생적으로 공급하여 연료 및 화합물을 생산할 수 있기에, 화석연료를 대체할 수 있는 중요한 에너지원이 될 수 있다. 바이오매스는 식물, 목재 등에 함유된 매우 풍부한 에너지원임과 동시에 이를 이용한 에너지원 생산은 화석연료 대비 이산화탄소 배출을 줄일 수 있는 장점이 있다. 촉매공정을 이용한 바이오매스 유래 화합물의 전환 공정은 기존의 석유화학 공정의 촉매반응과 크게 다르지 않다. 하지만 바이오매스 내에 함유된 다른 탄소-산소-수소의 비율 및 그 구조적 특징으로 인해 기존의 촉매공정에서 사용되는 촉매가 아닌 새로운 맞춤형 고체 촉매의 개발이 필요하다. 이 학위논문은 바이오매스에서 유래된 원료의 전환에 널리 이용가능한 촉매로서 3차원적으로 열린 기공구조를 갖는 촉매를 제조 및 제안하였다. 3차원 구조 촉매가 바이오매스 전환에서 보이는 효과를 기상, 액상 탈수반응 및 가수분해-수소화반응이 동시에 일어나는 반응 등을 통해 집중적으로 연구하였다. 먼저 3차원 탄소 담체를 이용한 촉매를 개발하여 글리세롤의 탈수반응에서 중요한 도전과제인 코크침적으로 인한 심한 비활성화 문제를 해결하고자 하였다. 또한 이러한 3차원 중형기공 탄소에 백금을 담지한 촉매를 개발하여 리그노셀룰로오즈로부터 소비톨을 고효율로 생산할 수 있었고 이를 통해 큰 분자체로 이루어진 바이오매스 화합물의 촉매로의 접근성을 해결할 수 있었다. 마지막으로 3차원 구조가 갖는 최대 장점인 내부물질전달의 효과를 정량화 하기 위하여 노말 부탄올의 액상 탈수반응을 통한 다이-엔-부틸에테르 생산 반응에 응용하였고, 속도론적 해석을 이용하여 내부유효인자를 직접적으로 계산하였다. 자세한 내용은 다음과 같다.

헤테로폴리산 촉매는 글리세롤의 탈수반응을 통한 아크롤레인 생산 반응에 매우 높은 활성을 보이고 현재 많은 연구가 진행되고 있다. 하지만 코크 침적으로 인한 촉매의 심한 비활성화 문제는 여전히 해결해야할 과제로 남아있다. 우리는 먼저 팔라듐과 탄소담체를 동시에 사용하여 팔라

듐 격자 안으로 생성된 코크 전구체를 삽입하여 비활성화 문제를 해결하고자 하였다. 팔라듐이 첨가된 $H_3PW_{12}O_{40}$/C 촉매는 첨가되지 않을 때와 비교하여 약 40 %의 코크가 활성 촉매에서 감소함을 확인하였다. 이는 팔라듐 금속과 탄소담체가 만나 비교적 낮은 반응온도 범위에서도 팔라듐 격자를 쉽게 느슨하게 만들어 Pd_6C의 구조로 코크를 가두는 효과를 이루어 내었기 때문이다. 이러한 탄소담체의 효과는 실리카 담체에서는 확인되지 않았다. 또한 3차원으로 기공이 발달된 탄소담체를 개발하여 반응에 응용한 결과 코크의 양이 감소하지 않았음에도 기공막힘 현상을 방지하여 활성점을 유지하는 결과를 보였고 이는 더 높은 촉매의 안정성을 가져올 수 있었다.

3차원 구조 촉매가 큰 기공 내에서의 반응물의 접근성 및 물질전달을 원활하게 하는 효과를 정량적으로 증명하기 위하여 노말 부탄올의 탈수반응을 통한 다이-엔-부틸에테르 생산 반응에 응용해 보았다. 2차원 기공구조를 갖는 촉매 및 1차원 구조의 미세기공을 갖는 촉매를 추가로 제조하여 비교실험한 결과 3차원 구조촉매가 가장 우수한 전환율 및 수율을 보임을 확인하였다. 또한 속도론적 해석을 위한 실험을 통해 활성화에너지 및 속도상수를 계산하였고, 이를 내부물질전달의 척도를 알 수 있는 내부유효인자를 계산하는데 이용하였다. 그 결과 3차원 구조, 2차원 구조, 1차원 구조의 기공성 촉매에서 각각 0.83, 0.63, 0.52의 값을 나타내는 것을 확인하였고 이를 통해 실질적으로 기공내에서의 반응물의 전달에 매우 우수함을 입증하였다.

리그노셀룰로오즈의 전환은 매우 풍부한 자원이고 비식용 자원이기 때문에 매우 각광받는 연구 분야이다. 하지만 큰 고분자성 구조 및 일반적인 용매에 녹지 않는 특성 때문에 불균일 촉매인 고체 촉매로의 접근이 용이하지 않아 반응이 매우 힘들다고 알려져 있다. 이러한 문제를 해결하고자 3차원 열린기공구조를 갖는 탄소를 제조하여 탄소표면의 풍부한 수산화기 및 큰 기공구조를 통해 셀룰로오즈의 촉매로의 접근성을 용이하게 하고자 하였다. 성게모양을 갖는 중형기공성 탄소 (CNE)를 담체로 사용하여 백금금속을 활물질로 하는 촉매를 제조하였고 이를 셀룰로오즈로부터 소비톨을 생산하는 2단계 (가수분해 – 수소화반응) 반응에 응용

하였다. 촉매 표면의 풍부한 수산화기는 셀룰로오즈 분자의 촉매 외부표면으로의 접근성을 증가시켰고, 셀룰로오즈 전환 후 물에 녹는 셀로올리고머를 생성한 후에는 큰 기공 내에서 원활하게 원하는 물질인 소피톨을 생산할 수 있었다. 또한 산처리 공정을 거치지 않고도 백금과 넓은 표면적의 기공성 탄소 촉매위에서 수소 스필오버 현상을 일으켜 효율적으로 산촉매적 기능을 발현할 수 있었다. 개발된 Pt/CNE 촉매는 약 80 %의 소비톨 생산 수율을 보여 지금까지 보고된 촉매 중 가장 우수한 활성을 보이는 것을 확인하였다. 또한 오크나무 가루를 직접 반응물로 사용하여 리그노셀룰로오즈를 전환시킨 결과 약 23 %의 당알코올류의 생산 수율을 보여 향후 리그노셀룰로오즈 관련 촉매반응에 CNE 탄소가 매우 널리 사용될 수 있음을 보였다.

주요어: 3차원 다공성 물질, 글리세롤, 리그노셀룰로오즈, 백금, 헤테로폴리산, 물질전달
학번: 2010-30805

List of publications

International Published Papers (First author)

1. Y. S. Yun[*], **D. S. Park[*]**, and J. Yi, "Effect of nickel on catalytic behaviour of bimetallic Cu-Ni catalyst supported on mesoporous alumina for the hydrogenolysis of glycerol to 1,2-propanediol" *Catal. Sci. & Technol.,* (2014), published online. **doi**: 10.1039/c4cy00320a. ([*]co-first author)
2. **D. S. Park[*]**, D. Yun[*], T. Y. Kim, J. Baek, Y. S. Yun, and J. Yi, "A Mesoporous Carbon-Supported Pt Nanocatalyst for the Conversion of Lignocellulose to Sugar Alcohols" *ChemSusChem*, **6** (2013), 2281–2289. ([*]co-first author)
3. **D. S. Park**, D. Yun, Y. Choi, T. Y. Kim, S. Oh, J.-H. Cho, and J. Yi, "Effect of 3D open-pores on the dehydration of n-butanol to di-n-butylether (DNBE) over a supported heteropolyacid catalyst" *Chemical Engineering Journal*, **228** (2013), 889–895.
4. **D. S. Park**, B. K. Kwak, N. D. Kim, J. R. Park, J.-H. Cho, S. Oh, and J. Yi, "Capturing Coke Precursors in a Pd Lattice: A Carbon-Supported Heteropoly Acid Catalyst for the Dehydration of Glycerol into Acrolein" *ChemCatChem*, **4** (2012), 836–843.

International Published Papers (co-author)

1. D. Yun[*], T. Y. Kim[*], **D. S. Park**, Y. S. Yun, J. W. Han and J. Yi, "A Tailored Catalyst for the Sustainable Conversion of Glycerol to Acrolein: Mechanistic Aspect of Sequential Dehydration" *ChemSusChem*, (2014), published online. **doi**: 10.1002/cssc.201402057. ([*]co-first author)
2. Y. Choi[*], Y. S. Yun[*], H. Park, **D. S. Park**, D. Yun, and J. Yi, "A facile approach for preparation of tunable acid nanocatalyst with hierarchically mesoporous structure" *Chem. Commun.*, **50** (2014), 7652-7655. ([*]co-first author)
3. Y. Choi, **D. S. Park**, H. J. Yun, J. Baek, D. Yun, and J. Yi, "Mesoporous Siliconiobium

Phosphate as a Pure BrønstedAcid Catalyst with Excellent Performance for the Dehydration of Glycerol to Acrolein" *ChemSusChem*, **5** (2012), 2460–2468.

4. J. R. Park, B. K. Kwak, **D. S. Park**, T. Y. Kim, Y. S. Yun, and J. Yi, "Effect of acid type in WO_X clusters on the esterification of ethanol with acetic acid" *Korean J. Chem. Eng.*, **29** (2012), 1695-1699.
5. N. D. Kim*, J. R. Park*, **D. S. Park**, B. K. Kwak and J. Yi, "Promoter effect of Pd in $CuCr_2O_4$ catalysts on the hydrogenolysis of glycerolto 1,2-propanediol" *Green Chem.*, **14** (2012), 2638–2646. (*co-first author)
6. B. K. Kwak, **D. S. Park**, Y. S. Yun, and J. Yi, "Preparation and characterization of nanocrystalline $CuAl_2O_4$ spinel catalysts by sol–gel method for the hydrogenolysis of glycerol" *Catalysis Communications*, **24** (2012) 90–95.
7. T. Y. Kim, **D. S. Park**, Y. Choi, J. Baek, J. R. Park and J. Yi, "Preparation and characterization of mesoporous Zr-WO_x/SiO_2 catalysts forthe esterification of 1-butanol with acetic acid" *J. Mater. Chem.*, **22** (2012), 10021–10028.

Patent applications

1. 이종협, **박대성**, 곽병규, 오석일, 조정희, "열린 기공구조를 갖는 구형의 실리카에 담지된 헤테로폴리산 촉매 및 이를 이용한 아크롤레인 제조방법", 대한민국특허 **등록** 10-1369924 (2014.02.26).
2. 이종협, **박대성**, 박재률, 김남동, 오석일, 조정희, "귀금속이 도입된 구리-크롬촉매 및 이를 이용한 1,2-프로판디올의 제조방법", 대한민국특허 **등록** 10-1369921 (2014.02.26).
3. 이종협, **박대성**, 곽병규, 오석일, 조정희, "글리세롤의 탈수반응을 통한 아크롤레인 생산반응용 촉매 및 그 제조방법", 대한민국특허 **등록** 10-1322678 (2013.10.22).
4. 이종협, **박대성**, 곽병규, 오석일, 조정희, "글리세롤의 탈수반응을 통한 아크롤레인 생산반응용 촉매 및 그 제조방법", 대한민국특허 **등록** 10-1268461 (2013.05.22).
5. 이종협, **박대성**, 박재률, 오석일, 조정희, "글리세롤의 탈수반응을 통한

아크롤레인 생산반응용 촉매 및 그 제조방법", 대한민국특허 **등록** 10-1268459 (2013.05.22).

6. 이종협, **박대성**, 윤다님, 윤양식, 박홍석, "금속이 분산된 열린기공구조를 가지는 탄소촉매 및 이를 이용한 소르비톨의 생산방법", 대한민국특허 **출원** 10-2014-0001636 (2014.01.07).
7. 이종협, 김태용, **박대성**, 최영보, 백자연, 박재률, "균일한 중형기공을 갖는 복합산화물촉매, 그 제조방법 및 상기촉매를 이용하여 에스테르화합물을 제조하는방법", 대한민국특허 **출원** 10-2012-0053823 (2012.05.21).

International Conference (First author)

1. **D. S. Park**, D. Yun, Y. S. Yun, H. Park, T. Y. Kim, J. Baek, and J. Yi, "Direct conversion of lignocellulose to sugar alcohols over Pt supported on a new 3D mesoporous carbon", *247th American Chemical Society National Meeting & Exposition*, Dallas, Texas, USA, March 16-20 (2014)
2. **D. S. Park**, D. Yun, Y. Choi, T. Y. Kim, S. Oh, J.-H. Cho, and J. Yi, "Enhancement of Mass Transport over 3D Open-porous Dandelion-like Catalyst in Liquid-phase Heterogeneous Catalysis", *9th World Congress of Chemical Engineering*, Seoul, Korea, August 18-23 (2013)
3. **D. S. Park**, Y. S. Yun, D. Yun, S. Oh, Y. A. Shin, and J. Yi, "The hydrogenolysis of glycerol on CuNi bimetallic catalyst supported on mesoporous alumina", *The 14th Japan-Korea Symposium on Catalysis*, Nagoya, Japan, July 1-3 (2013)
4. **D. S. Park**, B. K. Kwak, J.-H. Cho, S. Oh, and J. Yi, "Stability enhancement of heteropoly acid catalyst supported on carbon for dehydration of glycerol to acrolein", *15th International Congress on Catalysis*, Munich, Germany, July 1-6 (2012)
5. **D. S. Park**, B. K. Kwak, Y. S. Yun, and J. Yi, "Synthesis of nanocrystalline copper aluminate ($CuAl_2O_4$) by sol-gel technique and its application to the to the glycerol hydrogenolysis", *Asian Crystallization Technology Symposium*, Seoul, Korea, May 23-25 (2012)

International Conference (co-author)

1. Y. S. Yun, Y. Choi, H. Park, D. Yun, **D. S. Park**, and J. Yi, "Preparation of 3D Open-Porous Acidic Heterogeneous Catalysts for the Chemical Production", *2013 MRS Fall Meeting Program & Exhibit*, Boston, Massachusetts, USA, December 1-6 (2013)
2. D. Yun, **D. S. Park**, T. Y. Kim, S. Oh, Y. A. Shin, and J. Yi, "Preparation of DSS-SO3H Catalyst for Stable Production of Acrolein from Glycerol", *The 14th Japan-Korea Symposium on Catalysis*, Nagoya, Japan, July 1-3 (2013)
3. Y. Choi, **D. S. Park**, J. Yeo, and J. Yi, "Design and application of catalysts for value-added chemical productions from biomass resources", *244th American Chemical Society National Meeting & Exposition*, Philadelphia, Pennsylvania, USA, August 19-23 (2012)
4. N. D. Kim, H. J. Yun, B. K. Kwak, **D. S. Park**, I. Nam, J. R. Park, I. K. Song, J. R. Yoon, and J. Yi, "Simple preparation method of nanostructured Mn oxide-doped carbon nanotubes for pseudocapacitor", *218th ECS Meeting*, Las Vegas, Nevada, USA, October 10-15 (2010)

Domestic Conferences

1. **박대성**, 윤다님, 오석일, 신용안, 이종협, "3차원 구조의 중형기공 탄소물질의 제조 및 리그노셀룰로오스 직접전환을 통한 당알코올 생산에의 응용", 한국화학공학회 2014년도 봄 총회 및 학술대회, 창원컨벤션센터, 4. 23-25 (2014)
2. 윤다님, 김태용, **박대성**, 윤양식, 한정우, 오석일, 신용안, 이종협, "글리세롤로부터 아크롤레인을 안정적으로 생산하기 위한 맞춤형 촉매개발", 한국화학공학회 2014년도 봄 총회 및 학술대회, 창원컨벤션센터, 4. 23-25 (2014)
3. 백자연, 김태용, **박대성**, 박홍석, 송찬경, 이경록, 이종협, "글루코오스 발효액으로부터의 1,3-부타디엔 생성", 한국화학공학회 2014년도 봄 총회 및

학술대회, 창원컨벤션센터, 4. 23-25 (2014)

4. 윤양식, 박홍석, 윤다님, **박대성**, 김태용, 백자연, 이경록, 이종협, “계층구조를 갖는 나노크기의 고체산 촉매제조 및 응용”, 2014년 한국청정기술학회 춘계학술발표회, 여수경도리조트, 3. 27-28 (2014)
5. 윤다님, 김태용, **박대성**, 윤양식, 한정우, 이종협, “열린 기공구조를 갖는 브뢴스테드 산촉매의제조 및 글리세롤 탈수반응에의적용”, 2014년 한국청정기술학회 춘계학술발표회, 여수경도리조트, 3. 27-28 (2014)
6. **박대성**, 윤다님, 윤양식, 김우식, 이종협, “3차원 중형기공 탄소물질의 개발 및 목질계 바이오매스 전환을 통한 당알코올 생산기술에의응용”, 2014년 한국 청정기술학회 춘계학술발표회, 여수경도리조트, 3. 27-28 (2014)
7. 김태용, 백자연, 송찬경, 윤양식, **박대성**, 한정우, 이종협, “바이오매스 유래물질의 맞춤형 탈수반응을 위한 비시널디올로부터 에폭사이드 유래물질생성”, 2014년 한국 청정기술학회 춘계학술발표회, 여수경도리조트, 3. 27-28 (2014)
8. 백자연, 송현돈, 김태용, **박대성**, 윤다님, 윤양식, 박홍석, 이종협, “금나노입자의 암모니아 보란을이용한 4-니트로페놀 환원반응에서의 실시간 전자이동관찰”, 2013년 한국 청정기술학회 추계학술발표회, 제주 한화리조트, 9. 25-27 (2013)
9. 윤양식, **박대성**, 윤다님, 김태용, 오석일, 이종협, “무수소 조건에서의 글리세롤의 가수소분해반응을 위한 중형기공 알루미나에 담지된 구리-니켈이 중금속촉매의 제조 및 적용”, 2013년 한국 청정기술학회 춘계학술발표회, 여수경도리조트, 3. 28-29 (2013)
10. **박대성**, 윤다님, 오석일, 신용안, 이종협, “3차원 다공성 촉매를 이용한 n-butanol의 탈수반응 및 속도론적 해석을 통한 내부확산의영향”, 2013년 한국청정기술학회 춘계학술발표회, 여수경도리조트, 3. 28-29 (2013)
11. **박대성**, 윤다님, 오석일, 조정희, 이종협, “바이오매스 유래 글리세롤의 고부가가치용 촉매공정개발 2. Coking 최소화 촉매개발”, 2012년 추계 한국청정기술학회, 영남대학교, 11. 16 (2012)
12. 김태용, **박대성**, 백자연, 최영보, 김영훈, 이종협, “바이오매스 유래 알코올과 유기산의 고부가가치용 촉매개발 연구”, 2012년 추계 한국청정기술학회,

영남대학교, 11. 16 (2012)

13. 최영보, **박대성**, 백자연, 윤다님, 이종협, “바이오매스 유래 글리세롤의 고부가가치용 촉매개발 1. 고효율 촉매설계 및 제조”, 2012년 추계 한국청정기술학회, 영남대학교, 11. 16 (2012)
14. 오석일, 조정희, **박대성**, 이종협, “글리세롤로부터 1,2-프로판디올 생산을 위한 촉매개선 및 연속공정 Scale-up”, 한국화학공학회 2012년 가을학술대회, 부산 BEXCO, 10. 24-26 (2012)
15. **박대성**, 김남동, 오석일, 조정희, 이종협, “바이오매스 유래 화합물인 글리세롤 전환반응용 Pd-PW12O40/C 촉매의개발”, 춘계한국청정기술학회, 연세대학교, 5.25 (2012)
16. 김태용, **박대성**, 최영보, 백자연, 이종협, “바이오매스로부터 고부가가치 화학물질 제조와 중형기공성 Zr-WOx/SiO_2 촉매의 개발”, 춘계 한국청정기술학회, 연세대학교, 5.25 (2012)
17. 오석일, 장준호, 전영선, 조정희, 이종협, **박대성**, “Effects of co-catalysts supported on Cu-based catalyst for the reaction of glycerol to 1,2-propanediol”, 한국화학공학회 봄 총회 및 학술대회, 제주국제컨벤션센터, 4.25-27 (2012)
18. 김태용, **박대성**, 최영보, 백자연, 박재률, 이종협, “부탄올 에스테르화 반응을위한 중형기공의 Zr-WO_x/SiO_2 촉매의 제조 및 특성분석”, 한국화학공학회 봄 총회 및 학술대회, 제주국제컨벤션센터, 4.25-27 (2012)
19. 박재률, 김남동, 곽병규, **박대성**, 오석일, 조정희, 이종협, “귀금속을 포함하는 copper chromite 촉매를 이용한 glycerol로부터 1,2-propandiol의 제조에 관한 연구”, 추계한국화학공학회, 송도컨벤시아, 10. 26-28 (2011)
20. 오석일, 장준호, 전영선, **박대성**, 이종협, 조정희, “글리세롤로부터 1,2-프로판디올 생산을 위한 촉매개발 및 연속공정적용”, 추계 한국화학공학회, 송도컨벤시아, 10. 26-28 (2011)
21. **박대성**, 곽병규, 김태용, 박재률, 윤양식, 이종협, “다공성구형 실리카에 담지된 헤테로폴리산촉매의 제조 및 불균일 촉매반응에의 적용”, 추계 한국화학공학회, 송도컨벤시아, 10. 26-28 (2011)
22. 곽병규, **박대성**, 박재률, 윤양식, 김태용, 이종협, “폐글리세롤 수소첨가분해반응용 $CuCr_2O_4$ 촉매에서 조촉매의효과”, 추계 한국화학공학회,

송도컨벤시아, 10. 26-28 (2011)

23. 최영보, **박대성**, 윤형진, 백자연, 윤다님, 이종협, “새로운 산촉매 개발과 글리세롤 탈수반응에의 적용”, 추계한국화학공학회, 송도컨벤시아, 10. 26-28 (2011)
24. 오석일, 장준호, 전영선, 조정희, 이종협, **박대성**, “Catalytic Conversion of Glycerol to 1,2-Propanediol by Copper-based Catalyst with co-catalysts”, 춘계화학공학회, 창원컨벤션센터, 4. 27-29 (2011)
25. 장준호, 오석일, 전영선, **박대성**, 이종협, 조정희, “촉매반응성개선을위한 Crude Glycerin 전처리공정개발”, 춘계화학공학회, 창원컨벤션센터, 4. 27-29 (2011)
26. 오석일, 장준호, 전영선, **박대성**, 이종협, 조정희, “글리세롤로부터 1,2-Propanediol 생산을위한 Ru기반 촉매의 담체효과”, 추계한국공업화학회, 대전컨벤션센터, 10. 27-29 (2010)
27. 박재률, **박대성**, 곽병규, 이종협, “헤테로폴리산을 이용한 아세테이트 생산공정의 기초연구”, 추계화학공학회, 대전컨벤션센터, 10. 20-22 (2010)
28. 장준호, 전영선, 오석일, **박대성**, 이종협, 조정희, “Crude Glycerin 촉매반응성개선”, 추계화학공학회, 대전컨벤션센터, 10. 20-22 (2010)
29. **박대성**, 곽병규, 김남동, 박재률, 오석일, 조정희, 이종협, “Carbon 및 silica에 담지된 헤테로폴리산 촉매에 Pd 첨가가 coking 저항성에미치는영향”, 추계화학공학회, 대전컨벤션센터, 10. 20-22 (2010)
30. 곽병규, 김남동, **박대성**, 박재률, 이종협, “폐글리세롤의 전환반응을 위한 다공성구조의 알루미나 담지촉매의 제조”, 춘계 환경공학회, 제주국제컨벤션센터, 5. 6-7 (2010)
31. 곽병규, 김남동, **박대성**, 백자연, 최영보, 박재률, 김우영, 이종협, “Organosilicate를 이용한 균일한 크기의 중형기공 탄소체의 합성”, 춘계화학공학회, 대구 EXCO, 4. 21-23 (2010)